University of Alberta

THE ROLE OF FIRST ORDER SURFACE EFFECTS IN LINEAR ELASTIC FRACTURE MECHANICS

by

CHUN IL KIM

A thesis submitted to the Faculty of Graduate Studies and Research
in partial fulfillment of the requirements for the degree of

Doctor of Philosophy

Department of Mechanical Engineering

Fall 2012
Edmonton, Alberta

This dissertation is dedicated to my wife, ***Hyejeong Yang*** *and to the memory of my grand mother,* ***Gyeseon Son (9125 ~ 2010).***

ABSTRACT

Structures at relatively small scales (e.g. nano/micro scale) behave differently in comparison to those examined at the macro scale. This is mainly because a high surface area to volume ratio is present at this scale making physical factors such as surface stress/energy and electromagnetic forces much more significant. In particular, 'surface effects' induced by a local environmental change of the region near the surface of solids, greatly influence the general behavior of the corresponding bulk material especially when the scale of materials become compatible with the nano/micro scale. This in turn, suggest that a more accurate and comprehensive description of the general behavior of an elastic solid with one or more surfaces can be achieved by incorporating a description of the separate surface mechanics near each surface of the solid.

In the dissertation, we examine the effects of first-order surface elasticity in linear elastic fracture mechanics. A complete analysis has been performed for both plane and anti-plane deformations and for cases in which cracks are present in a homogeneous material and subsequently in the interface between two dissimilar elastic materials. It is shown that the introduction of the effects of first-order surface elasticity results in, in most cases, the reduction of the stress singularity at the crack tip from the classical strong square root singularity to a weaker logarithmic singularity. In particular, the refined model (with first-order surface effects integrated) predicts a more realistic description of size-dependent stress distributions commonly existing at the small scale structures. In the case of an interface crack arising in the interfacial region between two dissimilar materials, the refined model removes the classical oscillatory behaviors of the corresponding stress distributions leading again to size-dependent and stable stresses in the vicinity of the crack.

ACKNOWLEDGEMENTS

I would like to extend my deepest gratitude to Dr. Peter Schiavone and Chong-Qing Ru for their invaluable guidance, support and kind understanding, as a result of which this dissertation has been accomplished.

I am also grateful to all my friends and staffs in the department for their everlasting encouragement and supports. Special thanks to my family for their consistence love, support and encouragement throughout my studies.

CHUN IL KIM
Edmonton, AB
April 2012

TABLE OF CONTENTS

LIST OF FIGURES

CHAPTER 1

INTRODUCTION

1.1 SURFACES OF MATERIALS

For the purposes of mathematical modeling, engineering materials can be regarded as continuous elastic media (i.e. continua) with certain characteristic properties (much like spring constants) from which the responses of materials can be described. Over the years, classical continuum-based prediction models have been used successfully in the study of the general behavior of various engineering materials such as beams, shells and plates (see, for example, [1–6]). With recent advances in nanoscience and nanotechnology, there is increasing demand for the modeling and analysis of structures at the nano/micro scale. In this regard, the classical continuum theories are again adopted. However, predictions from the classical prediction models often produce results inconsistent with those of experimental studies (see, for example, [7–11]). This can be attributed to the fact that, perhaps, there exist some unknown properties and/or phenomena which are neglected at the macro scale, yet become significant as the scale of systems become compatible with the nano/micro scale. The analogy can be further established, a priori, that the unknown properties must heavily rely on the size of material (i.e. extensive quantity) not just sorely be intrinsic properties of material (i.e. intensive quantity). With that being said, the best candidates, as far as engineering analyses are concerned, would include some quantities associated with surface and/or volumes of materials, for example, surface tension/stress, surface material properties and

mass of materials which are entirely extensive properties and/or extensive-related intrinsic properties.

In fact, it is widely accepted that surfaces of materials and/or interfaces between pairs of solids display properties quite different from those associated with their interiors. This is mainly due to the fact that atoms of a solid material experience local environmental differences such as changes in lattice spacing and number of bonded legs (see Fig.1) as they approach the boundaries of a bulk material [12,13]. Recent studies reveal that these surfaces (the domain responsible for local changes) have actually non-vanishing thickness (see, for example, [14, 15]). In addition, authors in [16–18] provide quantitative measurements of surface properties for some engineering materials used in the manufacture of nano/micro scale structures (e.g. nanowires, microcantilevers and nanobeams.).

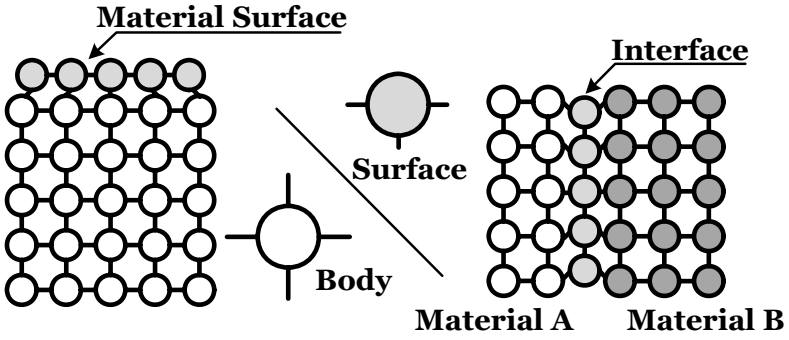

Figure 1: *Examples of molecular bonding on surfaces/interfaces*

The forgoing observations [12–18] seem to suggest that surfaces of solid materials may actually influence the general behavior of adhering bulk materials rather than just serve as "physical boundaries" of materials. The following question then arises naturally: how were the conventional theories able to produce satisfactory results in many engineering problems without considering the role of surfaces (sur-

face effects)? This can be explained by recognizing the fact that the surface effects are extensive properties rather than intensive properties. More precisely, it can be seen from Fig. 2 that surface to volume ratio of macro scale structures is much smaller than those of sufficiently small scale structures. This further implies that surface effects are negligibly insignificant for macro scale structures and therefore, the classical continuum theories (where surface effects are neglected) still provide quite successful predictions in the analysis of behavior of typical engineering materials at the macro scale.

However, the role of surfaces must be considerable in sufficiently small scale structures in which case, surfaces (with associated properties) make a non-trivial contribution to the general behavior of adhering bulk materials. Further, the intensity of the effects of surfaces significantly increases as the size of structures converges to the length scale compatible with nano/micro meters. In other words, structures at this scale behave differently in comparison to those examined at the macro scale and the corresponding elastic responses can be size dependent. In fact, experimental results in [17, 19–23] demonstrate that the elastic modulus of small structures changes as the diameter of for example, the beam or thickness of the plate varies, providing direct evidence of the size dependency of elastic properties at the nano/micro scale. It is therefore, quite natural that the classical continuum theories often fail to predict behaviors of structures at the nano/micro scale, since the classical assumptions do not include the contribution of the surface effects. This, in turn, suggests that a more accurate and comprehensive analysis can be achieved by incorporating the effect of surface mechanics on the structural boundaries of the solid in an attempt to account for the increasing surface area to

volume ratio of structures, especially those at the nano/micro scale.

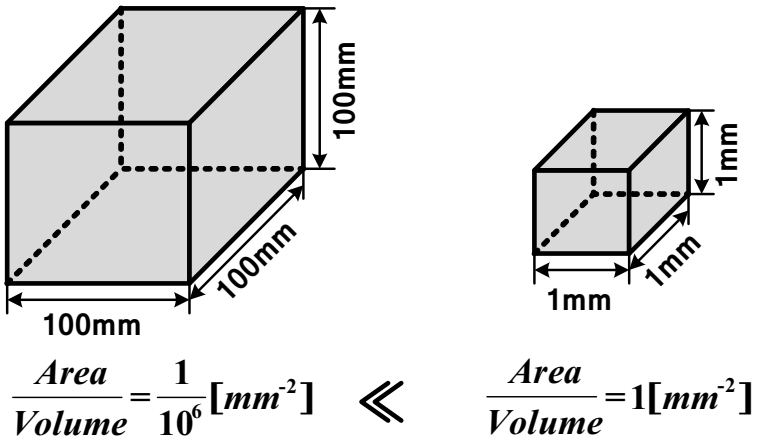

Figure 2: *Surface to volume ratios of two different cubes*

1.2 THE INCORPORATION OF SURFACE ELASTICITY

The incorporation of surface mechanics into mechanical models describing deformation of various elastic structures has drawn an increasing amount of attention in the literature [24–35]. Especially, with recent advances in nano/micro technology, the incorporation of surface mechanics into analytical models has provided a continuum based approach to a class of problems of great interest to theoreticians and practitioners alike. The concept is significant in a range of engineering problems, in particular, when the high surface area to volume ratio, present at the small scale, mean that the effects of the surface can no longer be neglected.

Currently, the two fundamental approaches used in the modeling of the deformation of solids at the small scale (nano/micro) involve either atomistic models or

refined continuum models. The former rely on massive atomistic simulation (e.g. molecular dynamic (MD) simulation), which most often require extensive computational resources. Nonetheless, these models were used successfully to investigate problems arising in nanomechanics (see, for example, [36–39]). Refined continuum models offer the advantages of the continuum setting and associated mathematical framework. This "refinement" of classical continuum theories to provide a more accurate and comprehensive analysis of solids with high surface to volume ratio can be achieved by employing a description of the separate surface mechanics on the structural boundaries (surfaces) of the solid. Experiments on various elastic structures (e.g. beams, plates and shells) indicated that predictions from these continuum models had good agreement with corresponding results obtained from the atomistic simulations (see, for example, [17,40]). An elastic deformable surface, in general, can be described by considering surface tension (pre-stress) applied on the membrane and the variation of surface free energy as the surface deforms (see Fig. 3). There are three different categories of continuum based models available in the literature within this subject and we shall briefly mention these surface models here for the purpose of the present study.

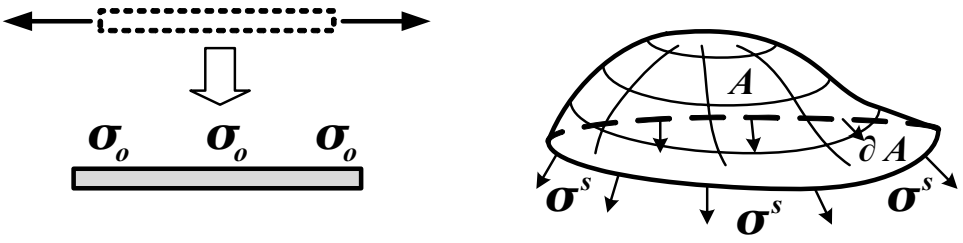

(a) Surface tension **(b) Deformation of an elastic surface**

Figure 3: *Schematics of an elastic deformable surface (R. Thomson et. al. Acta Metall. (1986))*

1.2.1 Surface Strain Independent Surface Model

This simplified model considers only the surface tension (excluding possibilities of surface dependency on stresses) leading to resulting models of the corresponding solid which are mathematically tractable (see Fig. 4(a)). The role of the surface can then be implemented with minimum modification of classical continuum theory: the "refinement" most often achieved by replacing surface tension by the equivalent resultant force acting on boundaries (and/or some part of boundaries) of the corresponding system (see, for example, [41–43]). In this case, classical constitutive relations still remain valid, yet balance equations change upon the introduction of surface effects. Although, this model leads itself to relatively simple analysis and thus can accommodate various situations arising in engineering problems, the assumption sacrifices the rigor and accuracy of a more comprehensive theory. Consequently, the model often fails to predict some crucial phenomena such as size-dependent characteristics arising in nano/micro structures (see, for example, [19–21, 44, 45]).

1.2.2 Surface Strain Dependent Surface Model

The surface strain dependent surface model, often referred as Gurtin-Murdoch surface elasticity model followed by Gurtin and co-workers' early contributions in this subject (see [26, 27, 34]), is, perhaps, one of the most important and accessible refined continuum models. In this model, a surface is regarded as a negligibly thin elastic membrane adhering to the bulk solid without slipping. The additional surface stress contributed by the surface strains (see Fig. 4(b)) leads, in most cases, to highly unusual and nonstandard boundary conditions on the surfaces of

the bulk solid. Consequently, the corresponding boundary value problems are not accommodated by existing classical theories and pose challenges not encountered previously in similar mathematical analysis. Nonetheless, the Gurtin-Murdoch assumptions were used successfully in a number of studies. For example, authors in [44,45] employed this model in the study of nanoscale inhomogeneity-matrix systems and showed the size-dependent elastic fields of the corresponding system. Zhi and Liying [46] examined piezoelectric nanowires using this model and found that bending behaviors and stiffness of nanobeams exhibit strong dependency on their size. Currently, several different versions of the Gurtin-Murdoch model are available in literatures (see, Ru [47] and the bibliographies contained therein) depending on their particular purpose of study. Regardless of the choice of each different version, the Gurtin-Murdoch surface elasticity model, overall, has produced satisfactory results in the analysis of the behavior of small structures, for example, in studies of the mechanics of nanocomposites (see, for example, [16,17,31,44,45,48]).

1.2.3 Comprehensive Surface Model (bending rigidity incorporated)

The model, in which the bending rigidity is supplemented on top of the previously mentioned contributions of the surface effects (see Fig. 4(c)), provides the most comprehensive description of an elastic deformable surface. The framework of the model has been suggested and further developed by Steigmann and Ogden [32,33]. Applications can be found, for example, in [49] where authors employed a complete version of the model and examined finite deformations of a pressurized circular annulus. Schiavone and Ru [50] adopted a linearized version of the model in the study of boundary reinforcement problems arising in plane elasticity. Although the comprehensive model provides more realistic descriptions of an elastic deformable

surface compared to other existing models, only a limited number of studies has been done in this regards (see, for example, [51,52]) due to the intrinsic complexity of the model: the contribution of additional bending effects most often leads to a system of fourth-order partial differential equations together with the combined boundary conditions which is even more complicated than the Gurtin-Murdoch surface elasticity model case. In addition, the bending rigidity of an infinitely thin elastic membrane is, in most cases, negligibly insignificant, especially those on the boundaries of nano/micro scaled structures where the thickness of surface layers usually converges to length scale compatible to the order of a few nanometers. Consequently, the comprehensive model is more or less unfavorable as long as actual analyses are concerned. However, we note here that this is an interesting area for future study, particularly when considering a system in which the bending rigidity of material surfaces is of significant and/or dominant.

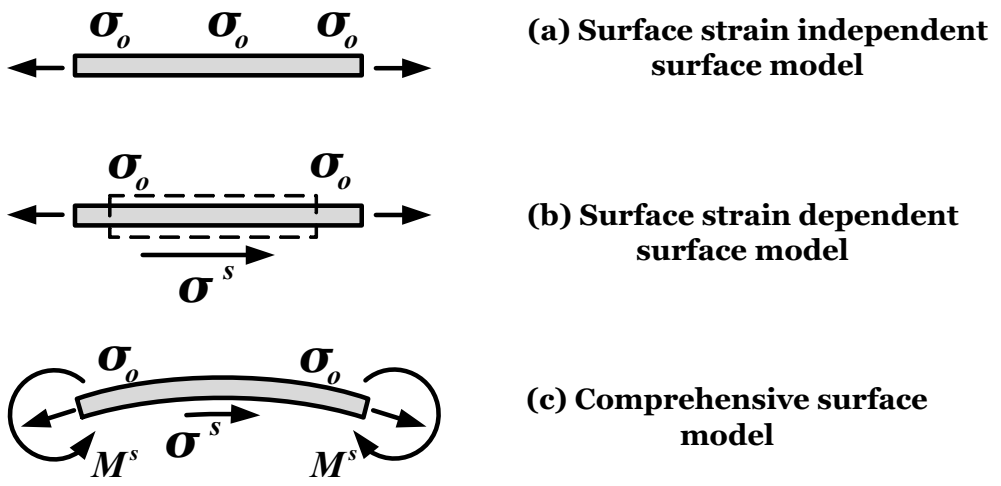

Figure 4: *Schematics of suggested surface models*

1.3 INTERFACE CONDITIONS

In the previous sections, we discussed the role of surface mechanics for small scale structures and feasible ways of incorporating the surface effects into models describing the general behavior of an elastic solid (i.e. different versions of refined continuum models in the description of an elastic deformable surface). Within the prescription of the continuum-based surface elasticity model, the general deformations of an elastic solid now involve the simultaneous responses of two different elastic media (i.e. a bulk solid and an adhering surface layer). This further requires, as far as engineering analysis is concerned, the transmission of displacement and/or stress related information from the bulk solid to the adjoining surface through an 'interface' and/or 'interfacial zone' between two distinctive bonded media. Here, we refer to an interface as a limiting case of the interfacial zone as its thickness tends to zero. In the physical sense, an interface can be regarded as a two dimensional boundary (a curved plane) across which material properties experience sudden change. Extensive research has been done in the field of micromechanics, chemistry and material sciences on the interface and various approximation models have been proposed in an attempt to characterize the complex behavior of the interface, mainly focusing on their role in the means of transmission of physical information (see, for example, [53–57]). Nevertheless, due to its intrinsic complexity in forming, it is extremely challenging to provide an accurate mathematical description of the behavior of the interface (interfacial zone). For the purpose of the present study, we briefly review some examples of interface models most often adopted in the literature.

A state of coherent interface (also referred as a perfectly bonded interface) assumes that there is perfect lattice matching between two phases (see Fig.5 (a)). This is often achieved through the introduction of coherency of tangential strain

in one or both of the phases. In general, coherent interface assumption is rather conventional, yet studies reveals that [58, 59] the model shows satisfactory physical correspondence in many cases. There are other categories of interface models available in literature, for example, an 'imperfect interface model'. The fundamental premise for the imperfect interface model is that there exists partial or complete lattice mismatching between two phases, namely; semi-coherent and incoherent interface condition, respectively. In these interface models, dislocations are formed at the interface to offset some of the coherency of tangential strain required to maintain the matching elsewhere (see Fig.5 (b)), otherwise there is no lattice matching (coherency in strain) available in between (see Fig.5 (c)).

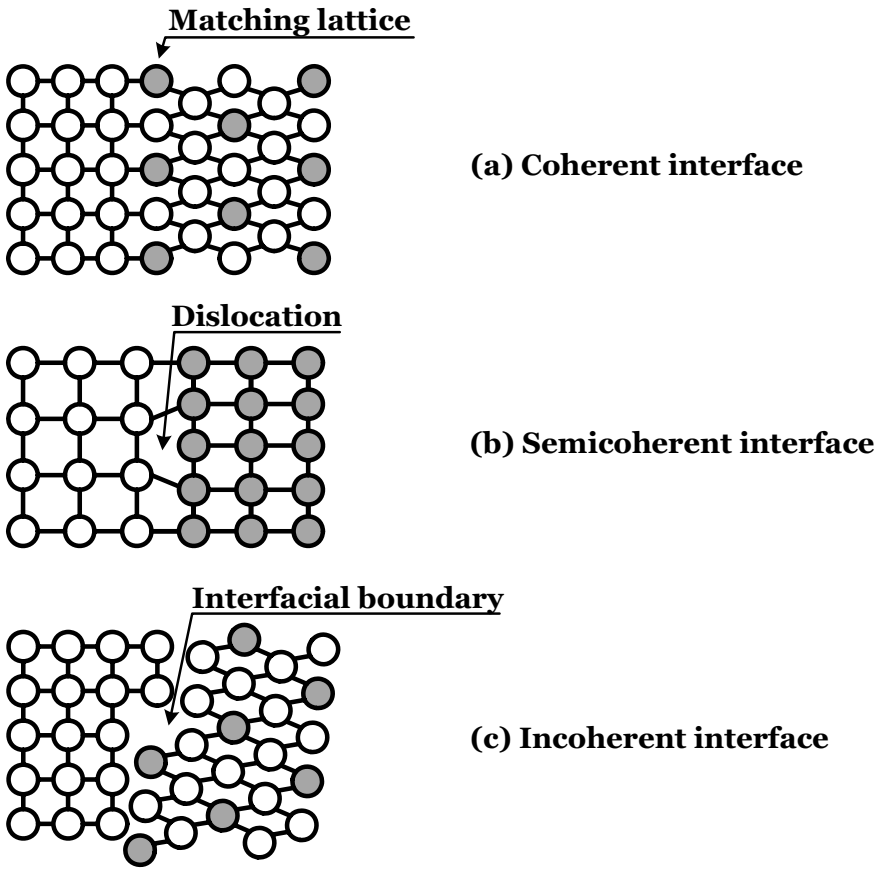

Figure 5: *Examples of interfaces*

Various different scenarios are possible in the description of an imperfect interface. For example, the imperfect interface can be regarded as an elastic spring-type interface in which the tangential strains/displacements jump across the interface, yet the amount of jump is directly proportional to their respective interface traction components (see, for example, [60–62]). This is probably the simplest assumption in capturing the complex nature of an imperfect interface, yet in reality, the conditions would be much more complicated. For interfaces in solids within the description of the continuum-based surface elasticity model, a coherent interface condition means that the equal amount of tangential strains are projected from the bulk solid to the abutting surface layer, where no atomic bonds break in the interfacial plane. An imperfect interface condition is related to a deformation with different tangential strains between the bulk solid and the surface layer [34, 63]], where atomic bonds may break in between. In the present study, we assume that the state of interface condition between bulk solid and adhering surface is coherent, since coherent interfaces commonly exist in materials, and they often remain coherent under a wide range of conditions [64].

1.4 CRACK PROBLEMS IN THE PRESENCE OF SURFACE MECHANICS

The analysis of stresses in an elastic solid incorporating a crack is of fundamental importance in the understanding of failure and in the general deformation analysis of engineering materials. In the Linear Elastic Fracture Mechanics (LEFM), due

to the high stress concentration ratio at crack tip regions (including at the tips themselves), even for cracks in sufficiently small length scales are well capable of initiating system failures. Failure often initiates (provided that there exists evidence of cracks in some regions of a material) at loading levels much lower than a material service load and/or yielding point. Therefore, it is extremely important to understand the general behavior of crack tip regions as well as the system containing one or multiple cracks. Depending on the types of applied loadings on the boundaries of a solid containing a crack, linear elastic crack problems fall generally into three different categories, namely; Mode-I, Mode-II and Mode-III crack problems. Mode-I and Mode-II cracks arise in plane-deformations of a solid containing a crack subjected to remote tension and in-plane shear, respectively (see Fig. 5(a)-(b)), whereas a Mode-III crack problem concerns anti-plane deformations where the system experiences out-of-plane remote shear loading (see Fig. 5(c)). Extensive studies have been done in the literature in regard to each category of crack problems in the context of the LEFM theory including those covering the non-linear regime (see, for example, [65–69]). The early solutions of such crack problems obtained from the theory of LEFM showed that the stresses at the crack tip are found to be infinite reflecting the fact that the crack front is usually taken to be perfectly sharp, yet in reality, most crack tips are, in fact, blunt with a radius of convergence of the order compatible with the nanoscale. In the case of an interface crack problem where a crack initiates on interfaces between two dissimilar materials, the classical LEFM theory predicts rapid oscillation in both the stress and displacement fields leading to the possibilities of material interpenetration between two bonded dissimilar materials. (see, for example, [66, 70]). The aforementioned results exhibit an apparent discrepancy with real world phenomena and can be attributed to the fact that the classical continuum models produce rather insufficient

and/or inappropriate descriptions of the behaviors of structures at the sufficiently small scale (see the discussions in sections 1.2-3).

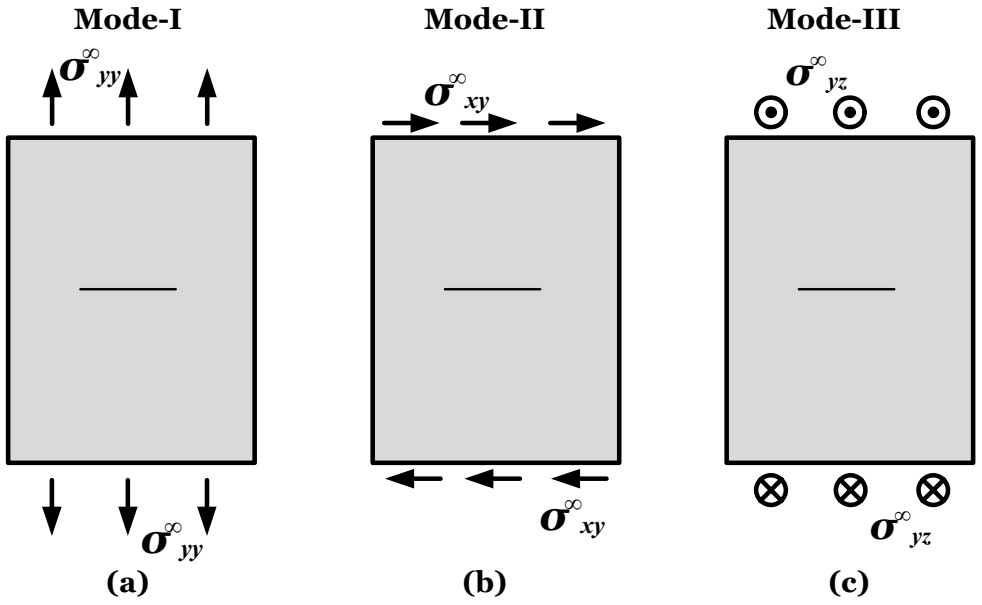

Figure 6: *Schematics of crack problems:* Mode-I, Mode-II and Mode-III crack

The size of cracks usually run from a few tenths of a micrometer to a few millimeters. In addition, recent experimental results have claimed that there exists evidence of cracks at the nanoscale (see Fig. 7). Therefore, it is reasonable to conclude, based on the developments in the previous sections, that the effects of surface mechanics can be quite significant on the crack face as well as in the vicinity of the crack. In fact, it was shown using atomistic models that the surface energy has non-negligible influences in the vicinity of the crack tip [71]. With that being said, it can be suggested that a more accurate and comprehensive analysis would include the surface effects corresponding to the either side of crack surfaces (faces). Indeed, a range of problems from the LEFM theory has been recently revisited in light of the recognition of the role of surface mechanics (see, for exam-

ple, [42, 43, 72–74]). Wu [42] incorporated the surface effects in the study of plane strain crack problems and found that surface stress can effectively strengthen a Griffith crack. In [73], the author examined surface grooves with high curvature with renewed realization of the role of surface mechanics. The corresponding results indicate that the stress concentration factor at the base of surface grooves can be improved with the introduction of the surface stress. However, in most of these published analyses, the incorporation of surface mechanics is oversimplified in an effort to make the ensuing models of deformation tractable. For example, surface conditions are limited only to the case when the surface energy is independent of the corresponding surface elastic strains (see section 1.2.1). To this end, authors in [74] examined the contribution of surface effects on the near-tip stresses of a Mode-III crack using the Gurtin-Murdoch theory (see section 1.2.2) under several simplifying assumptions including the assumption that the crack tip is blunt with a radius of convergence of the order compatible with the nanoscale. Approximated numerical results are presented using asymptotic and finite element methods. These results, however, are restricted to the vicinity of the crack tip and do not present a complete solution of the problem at hand.

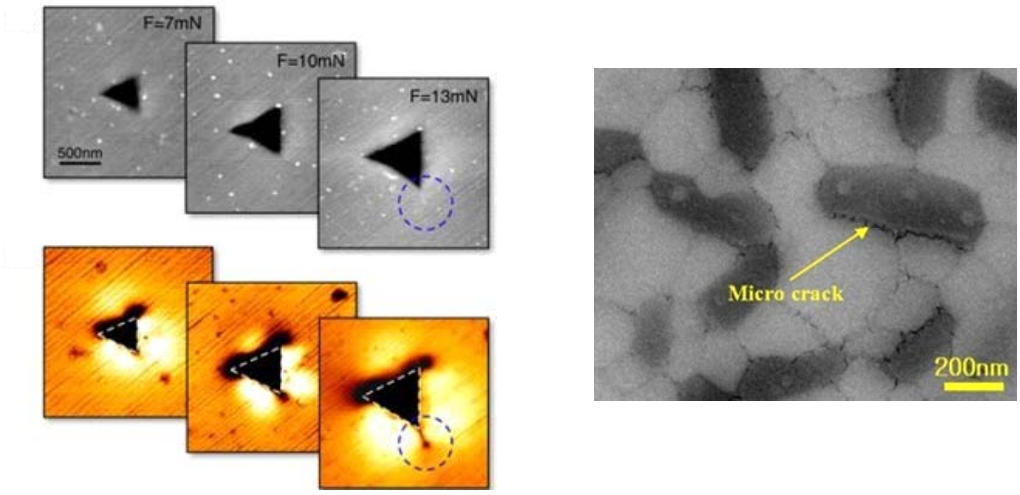

Source: Max Planck Institute for Biochemistry

Figure 7: *Examples of cracks at the nano/micro scale*

1.5 PURPOSE OF STUDY AND DISSERTATION OVERVIEW

In this dissertation, we recognize the non-negligible contribution of surface effects in the general behavior of mechanical systems at relatively small scales and subsequently formulate, develop and analyze an original theory describing the effects of first-order (curvature-independent) surface elasticity on the deformation of linearly elastic isotropic materials containing a crack with sharp edges (tips). In each case, models are developed and solved for both plane and anti-plane deformations and for cases in which cracks are present in a homogeneous material and subsequently in the interface between two dissimilar elastic materials. In the successive analyses, emphasis is placed particularly on examining: whether the refined continuum model (with surface effects incorporated) does indeed provide a more accurate description of the corresponding stress fields, and the influences of surface effects on

the singular stress fields near and at crack tips. It was also of our particular interest to see if the refined model would resolve some paradoxical results from the classical LEFM theory (e.g. infinite stresses at crack tips, material interpenetration of two bonded dissimilar media).

The surface effects (i.e. the variation of surface free energy, surface stresses and surface material properties) were incorporated using a version of the Gurtin-Murdoch surface elasticity model [47]. More precisely, since it is well-known that the thickness of 'layer' responsible for surface effects is in the range of a half to a few nanometers (see, for example, [14, 15]), we assumed that the crack (including its tips) is 'surrounded' by a correspondingly thin surface layer with elastic properties different from those of the surrounding bulk material. In terms of the Gurtin-Murdoch model, this translates into the assumption of a surface as a negligibly thin elastic membrane adhering to the bulk material without slipping. Mathematically, we modeled the crack as an interval of the $x-$axis on a typical $x-y$ plane in $\mathbb{R}^2$ onto which we projected the properties of the surface layer (much like we project the properties of a thin interphase layer onto the boundary of a fiber in the mathematical modeling of inclusion problems in composite mechanics (see, for example, [49,50])). To this end, complex variable methods [6,66,75] are extensively incorporated which, with several other mathematical techniques (e.g. the theory of Cauchy integrals [65] and collocation methods [76,77]) were used to ensure that the corresponding analysis was tractable. A commercial package (Matlab) was also used to handle the numerical part of the analysis.

The results obtained in this dissertation will advance understanding of the role of surface mechanics on the general behavior of an elastic solid incorporating a crack subjected to various types of applied loading. In particular, the complete solutions describing stress fields of the crack systems with respect to different possible

scenarios (see chapter 3-6) provide physical relevance to corresponding "real-world problems" and hence will enhance the future analysis and design of mechanical systems, especially at nono/micro scale.

The dissertation is organized as follows. Chapter 2 discusses general preliminaries such as notation and problem settings. Especially, we describe how the general governing equations from the plane and anti-plane elasticity evolve upon the introduction of a first-order theory of surface elasticity. In sequence, the general equilibrium conditions on either side of crack faces (surfaces) subjected to the most general forms of remote loading are obtained in order to tackle the proposed crack problems.

Chapter 3 examines the effects of surface mechanics on an elastic solid with a Mode-III crack arising in the anti-plane deformations. We note that the introduction of surface mechanics reduces the degree of singularity at the crack tip: from the classical strong square root singularity to the weaker logarithmic singularity and the corresponding solutions do indeed include the classical LEFM solutions when the surface effects are removed. In addition, the solution of the analogous problem, with non-uniform surface tractions is also obtained. It is shown that, as a particular case of the forgoing analysis, the classical decomposition of a Mode-III crack problem in linear elasticity continues to hold even in the presence of surface mechanics. Finally, the uniqueness theorem of the corresponding boundary value problem is developed and examined within the description of a first-order theory of surface elasticity.

Chapter 4 addresses plane strain deformations of an elastic solid incorporating a crack under the influences of the effect of surface mechanics on its surfaces. The complete semi-analytic solution (valid throughout the entire domain of interest except at the crack tips) is obtained in the case where the corresponding system

is subjected to uniform remote tension and in-plane shear. It is shown that the stress fields obtained from our solution exhibit strong dependency on the size of the crack and, in general, again reduces the order of the singularity at the crack tip. It is also worth noting that, in the absence of surface tension, in the case of Mode-I fracture, the corresponding stress distributions continue to exhibit the strong square root singularity (rather than a weaker logarithmic singularity) even in the presence of surface effects.

Chapter 5 considers, as a prerequisite for the analysis of a more general class of crack problems, a Mode-III interface crack arising in the anti-plane deformations of an elastic solid incorporating a crack and subjected to uniform remote out-plane tension. We note that the corresponding stress singularity is again reduced to the weaker logarithmic singularity but more importantly, the stress (σ_{xz}) jump across the bi-material interface upon the introduction of surface mechanics which is distinguished by the predictions from the classical LEFM theory.

Chapter 6 examines, in the presence of the effects of surface mechanics, the plane deformations of an elastic bi-material containing a crack on its interface and subjected to uniform remote loading (tension and in-plane shear) which is, perhaps, the most detailed and comprehensive description of the corresponding crack problem. We demonstrate, throughout rigorous analysis, that the incorporation of surface effects leads to a non-oscillatory solution and thus allows a non-singular stress field (except at the crack tips) of the corresponding system, in contrast to the results from LEFM theory where it is predicted that oscillatory behavior is prevalent at both stress and displacement fields [66, 70].

Chapter 7 provides a summary of results obtained and concluding remarks with some suggestions and comments in regards to the complete removal of logarithmic stress singularity at crack tips by employing the high order theory of surface

elasticity.

Finally, throughout the dissertation, we make use of a number of well-established symbols and conventions. Thus, unless otherwise stated, Greek and Latin subscripts take the values 1,3 and 1,2,3, respectively, summation over repeated subscripts is understood, (x, z) and (x, y, z) are generic points in the (x, z) $-$plane and $\mathbb{R}^3$, respectively. We also note that the notation (x, z) and (x, y, z) may also be replaced by (x_1, x_3) and (x_1, x_2, x_3) , respectively, when reference is made to $\{\underline{e}_i\}_{i=1}^3$, the standard basis for $\mathbb{R}^3$.

CHAPTER 2

GENERAL FORMULATION AND PRELIMINARIES

2.1 NOTATION AND PROBLEM SETTING

We exam the general deformations of a linearly elastic solids containing a crack with the renewed interest of the role of surface mechanics. In the following analysis, the surface mechanics is incorporated using the continuum-based surface/interface model of Gurtin and Murdoch [26, 34, 47].

Let us now consider the general deformations of a linearly elastic and homogeneous isotropic solid occupying a region in $\mathbb{R}^3$ with generators parallel to the z-axis of a rectangular Cartesian coordinate system. We assume that a cross-section of the crack (centered at $x = 0,\ y = 0$) occupies the region $[-a,\ a],\ a \in \mathbb{R}^+$ of the x-axis in rectangular Cartesian coordinate system as shown in Fig. 8. We define a displacement vector $\boldsymbol{u}$ with components denoted by u, v, and w parallel to the x, y and z-axes, respectively. S ($S = S^+ \cup S^-$) denotes the domain outside of the crack, where the "+" and "−" sides are designated by the upper ($y > 0$) and lower ($y < 0$) half-domains as depicted in Fig. 8.

Our primary objective here is to incorporate the surface mechanics into the mathematical model of deformations in an attempt to have a more accurate and comprehensive description of the general behavior of a linearly elastic solid containing a crack. The Gurtin and Murdoch surface elasticity model (see [26, 27, 34]) suggests that the role of the surface can be modeled as a pre-stretched thin elastic membrane (with properties distinct from the surrounding material) firmly attached

to the abutting bulk material without slipping. In the present case, this can be achieved by projecting the properties of the surface layer, denoted by $\lambda^s,\ \mu^s$ and σ_o, onto the boundary of the crack (i.e. upper and bottom faces of the crack $y = \pm 0, -a < x < a$, see Fig. 8). Here, λ^s and μ^s represent the surface Lame' constants where the index "s" denotes the corresponding quantity resulting from the effects of surface elasticity and σ_o is the surface tension applied on the crack faces (surfaces). It should be noted here that surface Lame constants $(\lambda^s,\ \mu^s, \sigma_o)$ have units of $[N/m]$ whereas the bulk Lame constants $(\lambda,\ \mu)$ have dimension $[N/m^2]$. In order to define the surface, we introduce the unit normal vector $\boldsymbol{n}$ to the surface with components denoted by n_1, n_2 and n_3 pointing from the "$-$" side to the "$+$" side and $\boldsymbol{k}$ denotes the mean curvature of the surface defined in such a way as to be positive if the center of curvature is within the "$-$" side. Finally, the bulk-crack system under consideration is subjected to an arbitrary remote loading on its upper and lower boundary.

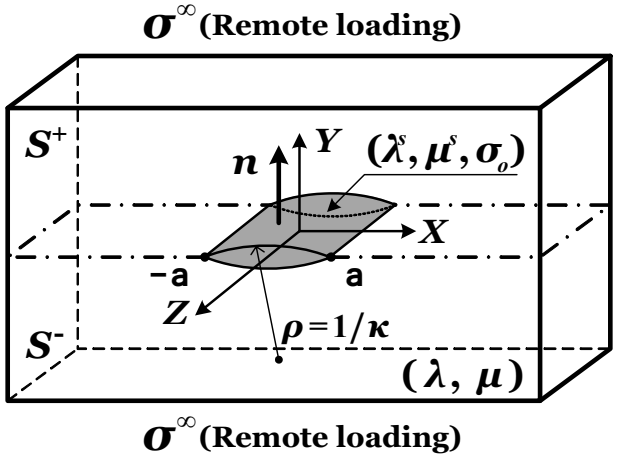

Figure 8: *Schematics of the problem*

2.2 SURFACE EQUATION

In the absence of body forces, the equilibrium equations and constitutive relations describing the deformation of a linearly elastic, homogeneous and isotropic (bulk) solid are given by:

$$\sigma_{ij,j} = 0,\ \sigma_{ij} = \lambda\delta_{ij}\varepsilon_{kk} + 2\mu\varepsilon_{ij}, \tag{2.1}$$

$$\varepsilon_{ij} = \frac{1}{2}\left(u_{i,j} + u_{j,i}\right). \tag{2.2}$$

where λ and μ are the Lame constants of the material (see Fig. 8), σ_{ij} and ε_{ij} the components of the stress and strain tensors, respectively and u_i denotes the i^{th} component of the displacement vector $\boldsymbol{u}$ in $\mathbb{R}^3$. In addition , $()_{,j}$ denotes differentiation with respect to x_j and δ_{ij} are the kronecker delta. When the separate mechanics of the (crack) surfaces are incorporated, the equilibrium condition on the crack can be described by the equations (see, [26, 34, 47], for detailed derivations):

$$\sigma^s_{\alpha\beta,\beta}\underline{e}_\alpha + [\sigma_{ij}n_j\underline{e}_i] = 0,\ \text{(tangential-direction)}, \tag{2.3}$$

$$k_{\alpha\beta}\sigma^s_{\alpha\beta} = [\sigma_{ij}n_in_j],\ \text{(normal-direction)}, \tag{2.4}$$

and

$$\sigma^s_{\alpha\beta} = \sigma_o\delta_{\alpha\beta} + 2\left(\mu^s - \sigma_o\right)\varepsilon^s_{\alpha\beta} + \left(\lambda^s + \sigma_o\right)\varepsilon^s_{\gamma\gamma}\delta_{\alpha\beta} + \sigma_o\nabla_s u. \tag{2.5}$$

Here, $[*] = (*)^{in} - (*)^{out}$ denotes the jump of the quantity "$*$" across the surface (here "*in*" and "*out*" refer, respectively, to the inside and outside of the body) and $k_{\alpha\beta}$ and n_i are the components of the principal curvature ($\boldsymbol{k}$) and the unit normal vector of the surface ($\boldsymbol{n}$), respectively. ∇_s is a surface gradient defined, for example, in rectangular Cartesian coordinate system as $\nabla_s = \frac{\partial}{\partial x}\boldsymbol{i} + \frac{\partial}{\partial z}\boldsymbol{k}$, where $\boldsymbol{i}$ and $\boldsymbol{k}$ are the unit normal vectors in the x and z direction, respectively. It is also noted here that, in the present study, the interface condition between bulk solid and adhering surface is assumed to be coherent (see the corresponding discussion

in section 1.3). Therefore, the interfacial strains in Eq. (2.5) can be replaced to those in the adjoined bulk material, i. e. $\varepsilon^s_{\alpha\beta} = \varepsilon_{\alpha\beta}$.

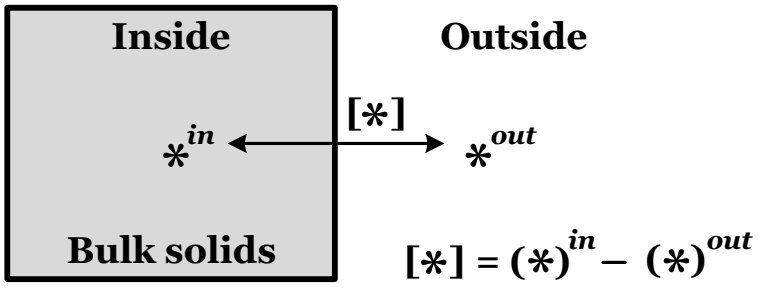

Figure 9: *The jump condition across the surface*

Remark 1 *It is well-known that the relation between the surface stresses ($\boldsymbol{\sigma}^s$) and surface energy ($\boldsymbol{\Gamma}$) can be determined by [30];*

$$\sigma^s_{\alpha\beta} = \sigma_o \delta_{\alpha\beta} + \frac{\partial \boldsymbol{\Gamma}}{\partial \varepsilon^s_{\alpha\beta}}.$$

In the Gurtin-Murdoch surface elasticity model, it is suggested that the surface energy ($\boldsymbol{\Gamma}$) has the following quadratic function of the surface strain invariants [26, 27, 47];

$$\frac{1}{2}(\lambda^s + \sigma_o)\left(\varepsilon^s_{\alpha\alpha}\right)^2 + (\mu^s - \sigma_o)\left(\varepsilon^s_{\alpha\beta}\varepsilon^s_{\alpha\beta}\right) + \sigma_o \frac{1}{2}\left|\nabla_s u\right|^2,$$

from which the expression for the surface stresses can be obtained. It should be noted here that the interface stress-strain law depends on several factors including the physical assumptions of the surface/interface elasticity and the geometrical changes of the surface with initial stress. This means that the stress-strain law may assume different forms depending on the particular mathematical/physical assumptions adopted. Currently, there is no clear physical evidence in favor of any specific surface model.

2.3 PLANE & ANTI-PLANE ELASTICITY IN THE PRESENCE OF SURFACE MECHANICS

The general displacement fields of an elastic solid can be described by a spatial vector $\boldsymbol{u}$ in $\mathbb{R}^3$ with components $u,\ v$, and w and each component is, in general, a function of three independent variables, for example, $u(x, y, z)$, $v(x, y, z)$, $w(x, y, z)$ in a rectangular Cartesian coordinate system. We note here that each component of a displacement vector $\boldsymbol{u}$ may have different forms depending on the choice of particular coordinate system (e.g. cylindrical and spherical coordinate system). The determination process of an unknown displacement vector $\boldsymbol{u}$ involves solving a highly complicated system of equations with three unknown components (i.e. u, v, w) of three independent variables and the corresponding boundary conditions which most often requires massive computational resources. In fact, there are not many options available other than employing purely numerical analysis to deal with the problem of these kinds. Instead, in the small deformation theory (linear elasticity), the general deformations of an elastic solid can be regarded as the in-plane deformation (i.e. plane deformation) and the complementary out-of-plane deformation (i.e. anti-plane deformation), respectively (see, for example, [5, 6, 65]). This further allows the corresponding analysis to be mathematically more tractable. More precisely, under the assumptions of linear elasticity, the complete three dimensional ($3D$) equations now decouple into two independent sets of equations for the plane deformation with two unknown functions (in-plane components, u, v) and anti-plane deformation with one unknown function (out-of-plane component, w), respectively. In addition, each unknown component is now a function of two independent variables instead of three independent variables. Consequently, we now have two independent reduced set of equations instead of having a complete $3D$ equation for the unknown displacement vector $\boldsymbol{u}$. This is

a huge advantage, as far as mathematical analysis is concerned, and there exist viable methods in the literature to deal with the reduced systems of equation of this kind. For example, complex variable methods can be employed in the analysis in which case, two independent variables can be treated as a one complex variable "z" where z is defined as $z = x + iy$ in complex plane (see, [6, 65, 66]).

In the following, we demonstrate that the above mentioned analogy still holds true in the present case (with surface effects incorporated) and derive equilibrium conditions on crack faces (surfaces) in the case of the plane and anti-plane deformations, respectively.

Let us now consider a half-plane infinite in extend along the $x-$axis, where $\boldsymbol{n} = (0, 1, 0)$ represents the unit normal vector to the surface (flat surface) and $\boldsymbol{u}$ again denotes the displacement vector with components (u, v, w) in a rectangular Cartesian coordinate system. Within the present setting, the Eqs. (2.3-4) can now be re-written as;

$$\sigma^s_{xx,x} + \sigma^s_{xz,z} + [\sigma_{xy}] = 0, \tag{2.6}$$

$$\sigma^s_{zx,x} + \sigma^s_{zz,z} + [\sigma_{yz}] = 0, \tag{2.7}$$

$$[\sigma_{yy}] = -\sigma_o \frac{\partial^2 v}{\partial x^2} - \sigma_o \frac{\partial^2 v}{\partial z^2}. \tag{2.8}$$

$\because$ $f_a = 0$ (for traction-free surface condition), $k_{xx} = k_{zz} = 0$ (for a flat surface). In the case of the anti-plane deformations, the displacement vector $\boldsymbol{u} = (u, v, w)$ admits the representation

$$w = w(x,\ y),\ u = v = 0,\ \frac{\partial^2 w}{\partial x^2} + \frac{\partial^2 w}{\partial y^2} = 0. \tag{2.9}$$

Applying Eq. (2.9) on Eqs. (2.1-2) , we obtain

$$\varepsilon_{xz} = \frac{1}{2}(\frac{\partial u}{\partial z} + \frac{\partial w}{\partial x}) = \frac{1}{2}\frac{\partial w}{\partial x},\quad \varepsilon_{yz} = \frac{1}{2}(\frac{\partial \nu}{\partial z} + \frac{\partial w}{\partial y}) = \frac{1}{2}\frac{\partial w}{\partial y},$$

$$\varepsilon_{xy} = \varepsilon_{xx} = \varepsilon_{yy} = \varepsilon_{zz} = 0. \tag{2.10}$$

$$\sigma_{xz} = 2\mu\varepsilon_{xz} = \mu\frac{\partial w}{\partial x}, \quad \sigma_{yz} = 2\mu\varepsilon_{yz} = \mu\frac{\partial w}{\partial y},$$
$$\sigma_{xy} = \sigma_{xx} = \sigma_{yy} = \sigma_{zz} = 0. \tag{2.11}$$

With the assumption of the coherent interface between the bulk solid and the adjoined surface ($\boldsymbol{\varepsilon}^s = \boldsymbol{\varepsilon}$), Eq. (2.5) can be re-written via Eq. (2.10) as

$$\sigma^s_{xz} = 2(\mu^s - \sigma_o)\varepsilon_{xz}. \tag{2.12}$$

Using the results in Eqs. (2.9), (2.11) and (2.12), the only non-zero components in Eqs. (2.6-8) are the out-of-plane terms

$$\sigma^s_{xz,x} + [\sigma_{yz}] = 0. \tag{2.13}$$

It should be noted that only surface strain components are included in Eq. (2.5) (i.e. strains normal to the surface are excluded). In the case of plane deformations, the displacement vector $\boldsymbol{u} = (u, v, w)$ now satisfies

$$u = u\,(x,\ y)\,,\ v = v(x,\ y),\ w = 0. \tag{2.14}$$

Similarly as in the anti-plane case, we obtain from Eq. (2.5) that

$$\sigma^s_{xx} = \sigma_o + 2\,(\mu^s - \sigma_o)\,\varepsilon_{xx} + (\lambda^s + \sigma_o)\,\varepsilon_{xx}. \tag{2.15}$$

In addition, In view of Eqs. (2.1-2) and Eq. (2.14), Eq. (2.6-8) become

$$\sigma^s_{xx,x} + [\sigma_{xy}] = 0, \tag{2.16}$$

$$[\sigma_{yy}] = -\sigma_o\frac{\partial^2\nu}{\partial x^2}. \tag{2.17}$$

Clearly, the complete $3D$ equations (2.6-8) can be decoupled into plane (Eqs. (2.16-17)) and anti-plane parts (Eq. (2.13)), even when the surface effects are incorporated. In the case of crack problems with the effects of surface elasticity the above results mean that the analysis of the general behavior of a bulk-crack

system can be accomplished by examining: Mode-I and Mode-II crack problems in plane elasticity and the Mode-III crack problem in anti-plane elasticity, separately (see Fig. 10).

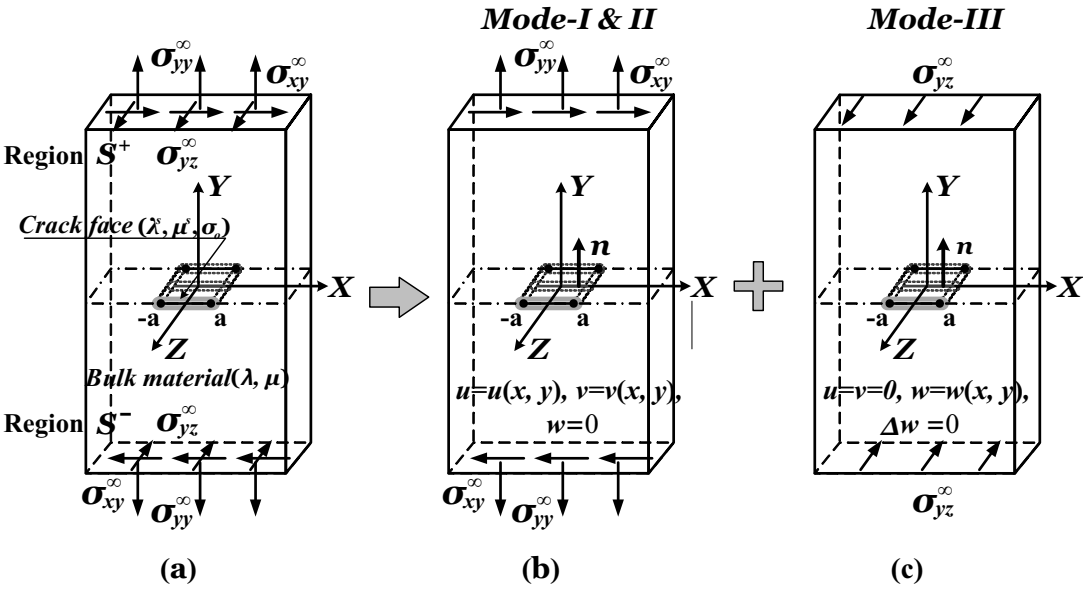

Figure 10: *Schematics of decoupling of the crack problem (C. I. Kim. IMM. (2011))*

CHAPTER 3

THE EFFECTS OF SURFACE ELASTICITY ON AN ELASTIC SOLID INCORPORATING A MODE-III CRACK

3.1 INTRODUCTION

Anti-plane shear deformations are, perhaps, one of the simplest scenarios arising in the deformation of an elastic solid. Only a single scalar displacement field in the axial direction is needed in the description of anti-plane shear motion, whereas two scalar fields are necessary in order to fully account for the in-plane deformations (see Chapter 2). This further ensures relative mathematical simplicity in the corresponding analysis (a single differential equation) compared with plane problems which, most often, require solving coupled systems of differential equations. Therefore, the anti-plane shear problem offers the advantages of exploring various possible scenarios arising in the mechanics of materials, yet still maintains a relatively simple mathematical setting. For this reason, problems involving anti-plane shear deformations of an elastic medium have drawn considerable attention in the literature within the context of linear and nonlinear elasticity (see [78], and the bibliographies therein).

In the present Chapter, we re-examine the classical Mode-III crack problem arising in the anti-plane shear deformation of a linearly elastic solid with the renewed realization of the role of surface mechanics on either side of the crack surfaces (faces). Surface effects are incorporated using the Gurtin-Murdoch surface elasticity model with the crack occupying a finite region of the real axis [79]. Using

complex variable techniques, we show that the nonstandard boundary conditions arising from the incorporation of the effects of surface elasticity on the crack face are reduced to the solution of a Cauchy singular integro-differential equation [65]. The latter is solved using an adopted collocation method [77] leading to an exact complete solution valid throughout the domain of interest. It is shown that the introduction of surface mechanics reduces the degree of singularity at the crack tip: from the classical strong square root singularity [66, 67] to the weaker logarithmic singularity. In addition, we demonstrate that the stress distributions derived from our analysis show clear signs of size dependency and do indeed tend to classical LEFM solutions [66, 67] when the surface effects approach zero. The solution of the analogous problem, when the crack faces are subjected to arbitrary surface tractions characterized by stress functions described by general polynomials of degree n, is also obtained. Finally, we show that the well-known result from classical elasticity on the decomposition of the problem concerning a solid with a mode-III crack, continues to hold when surface effects are included on the crack faces [80].

3.2 ANTI-PLANE CRACK PROBLEM WITH SURFACE EFFECTS

We consider anti-plane deformations of a linearly elastic and homogeneous isotropic solid occupying a region in $\mathbb{R}^3$with generators parallel to the z-axis of a rectangular cartesian coordinate system. We assume that the cylinder is infinite in extent and is subjected to uniform remote shear stress. Suppose that the cylinder contains a single internal crack (with traction-free faces) running the length of the cylinder. In a typical cross-section, the crack occupies the region $[-a, a]$, $a \in \mathbb{R}^+$ of the $x-$axis as shown in Fig. 11.

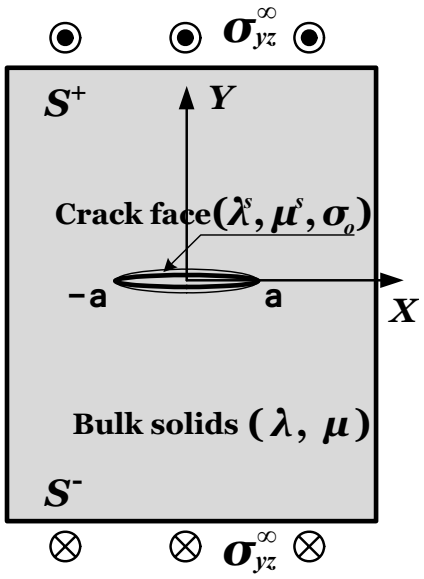

Figure 11: *Schematic of a Mode-III crack problem*

3.2.1 Equilibrium Equations and Complex-Variable Formulation

The stress and strain expressions for the bulk material can be obtained from Eqs. (2.1-2) as

$$\sigma_{ij} = \lambda\delta_{ij}\varepsilon_{kk} + 2\mu\varepsilon_{ij}, \tag{3.1a}$$

$$\varepsilon_{ij} = \frac{1}{2}\left(u_{i,j} + u_{j,i}\right). \tag{3.1b}$$

In the anti-plane shear deformations of an isotropic elastic medium (mode-III crack problem), we assume that the displacement vector $\boldsymbol{u}$ with components (u, v, w) satisfies (see also Eq. (2.9))

$$u = v = 0, \quad w = w(x, y), \ \frac{\partial^2 w}{\partial x^2} + \frac{\partial^2 w}{\partial y^2} = 0. \tag{3.2}$$

From Eq. (3.1b). the strain components are now given by

$$\varepsilon_{xz} = \frac{1}{2}(\frac{\partial u}{\partial z} + \frac{\partial w}{\partial x}) = \frac{1}{2}\frac{\partial w}{\partial x}, \quad \varepsilon_{yz} = \frac{1}{2}(\frac{\partial \nu}{\partial z} + \frac{\partial w}{\partial y}) = \frac{1}{2}\frac{\partial w}{\partial y}, \tag{3.3}$$

$$\varepsilon_{xy} = \varepsilon_{xx} = \varepsilon_{yy} = \varepsilon_{zz} = 0.$$

From Eq. (3.3), the stress components can be written as

$$\sigma_{xz} = 2\mu\varepsilon_{xz} = \mu\frac{\partial w}{\partial x}, \quad \sigma_{yz} = 2\mu\varepsilon_{yz} = \mu\frac{\partial w}{\partial y}, \tag{3.4}$$

$$\sigma_{xy} = \sigma_{xx} = \sigma_{yy} = \sigma_{zz} = 0.$$

If we denote by $\{\underline{e}_i\}_{i=1}^3$, the vectors of the standard basis for $\mathbb{R}^3$ and noting that in our case the normal to the crack face is aligned with the $y-$ direction, the equilibrium condition for the crack is given by (see Eqs. (2.6-8) and (2.13) and corresponding derivations)

$$\sigma^s_{xz,x} + [\sigma_{yz}] = 0. \tag{3.5}$$

In addition, from Eqs. (2.12) and (3.3-4), the expression for the surface stress can be obtained in terms of the bulk stress as

$$\sigma^s_{xz} = 2(\mu^s - \sigma_o)\varepsilon_{xz} = \frac{\mu^s - \sigma_o}{\mu}\sigma_{xz}, \tag{3.6}$$

where, $\varepsilon^s_{xz} = \varepsilon_{xz}$for a coherent interface. Since $w(x, y)$ is a harmonic function, we denote by $\psi(x, y)$ its conjugate harmonic function. Introducing the complex variable $z = x + iy$, we can now write

$$w = \mathrm{Re}[\Omega(z)], \quad \Omega(z) = w(x, y) + i\psi(x, y), \tag{3.7}$$

where $\Omega(z)$ is an analytic function of z in the plane $S^+ \cup S^- = S$ outside the crack (see Fig. 11.). From Eq. (3.5), we then have that

$$\frac{d\Omega}{dz}(z) = \Omega'(z) = \frac{\partial w}{\partial x} - i\frac{\partial w}{\partial y} = \frac{1}{\mu}\left(\sigma_{xz} - i\sigma_{yz}\right) \tag{3.8}$$

and

$$\sigma_{yz} = \frac{\mu i}{2}\left[\Omega'(z) - \overline{\Omega'(z)}\right], \quad \sigma_{xz} = \frac{\mu}{2}\left[\Omega'(z) + \overline{\Omega'(z)}\right]. \tag{3.9}$$

3.2.2 A Traction-free Mode-III Crack Problem with Surface Stress

Let the lower ($y < 0$) and upper ($y > 0$) half-planes be designated the "$-$" and "$+$" sides of the crack. Then, from (3.5), the boundary conditions on the crack can be written as

$$\frac{\partial \sigma_{xz}^s}{\partial x} + (\sigma_{yz})^+ - (\sigma_{yz})^- = 0. \tag{3.10}$$

In general, from Eqs. (3.3), (3.6) and (3.9-10), for the crack $[-a \leq x \leq a],\ (y = 0)$ subjected to prescribed traction P_{yz}, the surface condition on the faces can be written as

$$\begin{aligned} (\sigma_{yz})^+ &= P_{yz} - \frac{\partial \sigma_{xz}^s}{\partial x} = P_{yz} - (\mu^s - \sigma_o)\frac{\partial^2 w}{\partial x^2} \\ &= P_{yz} - \frac{\mu^s - \sigma_o}{2}[\Omega''(z) + \overline{\Omega''(z)}]^+, \text{ on the upper face,} \end{aligned} \tag{3.11a}$$

$$\begin{aligned} (\sigma_{yz})^- &= P_{yz} + \frac{\partial \sigma_{xz}^s}{\partial x} = P_{yz} + (\mu^s - \sigma_o)\frac{\partial^2 w}{\partial x^2} \\ &= P_{yz} + \frac{\mu^s - \sigma_o}{2}[\Omega''(z) + \overline{\Omega''(z)}]^-, \text{ on the lower face.} \end{aligned} \tag{3.11b}$$

As a particular case, we consider the situation when the solid is subjected to a uniform remote shear stress $\sigma_{yz} = \sigma_{yz}^{\infty}$ and a traction-free crack face ($P_{yz} = 0$). From Eqs. (3.9) and (3.11a-b), the surface condition on either side of the crack can be formulated as follows (see also Fig. 12)

$$\frac{\mu i}{2}\left[\Omega'(z) - \overline{\Omega'(z)}\right]^+ = -\frac{\mu^s - \sigma_o}{2}\left[\Omega''(z) + \overline{\Omega''(z)}\right]^+, \text{ on the upper face,} \tag{3.12a}$$

$$\frac{\mu i}{2}\left[\Omega'(z) - \overline{\Omega'(z)}\right]^- = \frac{\mu^s - \sigma_o}{2}\left[\Omega''(z) + \overline{\Omega''(z)}\right]^-, \text{ on the lower face.} \tag{3.12b}$$

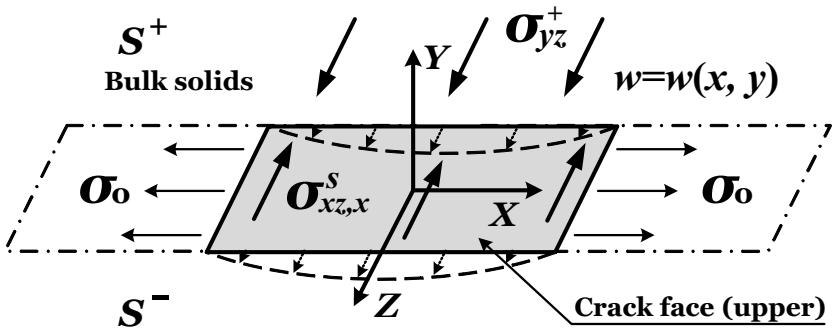

Figure 12: *Equilibrium on upper crack face under anti-plane shear motion*

In anti-plane deformations (mode-III crack) it is clear that $w^+ = -w^-$ on the crack face $y = \pm 0, -a \leq x \leq a$, which leads to a Reimann-Hilbert problem in terms of the derivatives of the unknown function $\Omega(z)$ defined by Eqs. (3.7) and (3.12a-b) as

$$\frac{\mu i}{2}\left[\Omega'(z) - \overline{\Omega'(z)}\right]^+ = \frac{\mu^s - \sigma_o}{2}\left[\Omega''(z) + \overline{\Omega''(z)}\right]^-, \text{ on the upper face,} \quad (3.13a)$$

$$\frac{\mu i}{2}\left[\Omega'(z) - \overline{\Omega'(z)}\right]^- = \frac{\mu^s - \sigma_o}{2}\left[\Omega''(z) + \overline{\Omega''(z)}\right]^-, \text{ on the lower face.} \quad (3.13b)$$

Since it is assumed that the remote stress σ_{yz}^{∞} is uniform, we have $\sigma_{yz}^+ = \sigma_{yz}^-$ on $y = \pm 0,\ x > a$[2]. Then from Eq. (3.9), we have that

$$\left[\Omega'(z) - \overline{\Omega'(z)}\right]^+ = \left[\Omega'(z) - \overline{\Omega'(z)}\right]^-.$$

Noting the equality $\overline{\Omega'(z)}^+ = \overline{\Omega'}(z)^-$ on $y = \pm 0$, the above yields

$$\Omega'(z)^+ + \overline{\Omega'}(z)^+ = \Omega'(z)^- + \overline{\Omega'}(z)^-. \quad (3.14)$$

In addition, on the crack face $y = \pm 0$, $-a \leq x \leq a$, we obtain from Eqs. (3.13a-b) that

$$\frac{\mu i}{2}\left[\Omega'(z)^+ + \overline{\Omega'}(z)^+ - \left(\Omega'(z)^- + \overline{\Omega'}(z)^-\right)\right] = 0. \quad (3.15)$$

Eqs. (3.14-15) suggest we necessarily have that

$$\Omega'(z) + \overline{\Omega'}(z) = 0,\ \Omega'(z) = -\overline{\Omega'}(z). \tag{3.16}$$

Now, adding Eqs. (3.13a) and (3.13b) yields

$$\frac{\mu i}{2}([\Omega'(z) - \overline{\Omega'}(z)]^+ + [\Omega'(z) - \overline{\Omega'}(z)]^-) = (\mu^s - \sigma_o)(\Omega''(z)^- + \overline{\Omega''}(z)^+). \tag{3.17}$$

Consequently, from Eq. (3.16), Eq. (3.17) takes the following form:

$$\mu i(\Omega'(z)^+ + \Omega'(z)^-) = (\mu^s - \sigma_o)(\Omega''(z)^- - \Omega''(z)^+) \tag{3.18}$$

Next, if we write the unknown $\Omega'(z)$ as a Cauchy integral [65], we have that

$$\Omega'(z) = \frac{1}{2i\pi}\int_{-a}^{+a}\frac{f(t)}{t-z}dt + \frac{1}{\mu i}\left[\sigma_{yz}^{\infty}\right], \tag{3.19a}$$

$$\Omega''(z) = \frac{1}{2\pi i}\int_{-a}^{+a}\frac{f(t)\,dt}{(t-z)^2} = -\left[\frac{f(t)}{t-z}\right]_{-a}^{a} + \frac{1}{2\pi i}\int_{-a}^{+a}\frac{f'(t)\,dt}{t-z}, \tag{3.19b}$$

where,

$$f(t) = \Omega'(z)^+ - \Omega'(z)^-,\quad -a \le t_o \le a.$$

Finally, from Eqs. (3.18) and (3.19a-b), we obtain the following first-order Cauchy singular integro-differential equation for the unknown $f(t), t \in [-a, a]$:

$$\frac{\mu}{\pi}\int_{-a}^{a}\frac{f(t)\,dt}{t-t_o} + 2[\sigma_{yz}^{\infty}] = -(\mu^s - \sigma_o)f'(t_o),\quad -a \le t_o \le a, \tag{3.20}$$

3.2.3 Uniqueness of Results and the Imposition of End Conditions

From Eqs. (3.2-4), (3.6) and (3.11a-b), the boundary value problem (BVP) in consideration can be summarized as

$$\begin{aligned}
\Delta w(x,\ y) &= 0,\ \text{in } S^+ \cup S^- = S \text{ (outside the crack)},\\
\frac{\partial w^{\pm}}{\partial y} &= \mp\left(\frac{\mu^s - \sigma_o}{\mu}\right)\frac{\partial^2 w^{\pm}}{\partial x^2},\ \text{on } y = \pm 0,\ -a \le x \le a,\\
\frac{\partial w}{\partial y} &= C,\quad y \to \infty.
\end{aligned} \tag{3.21}$$

The uniqueness theorem for (3.21) has been studied in [81] and proceeds as follows:

Let assume there exist two separate solutions for the corresponding BVP and we define the difference as

$$v\left(x,\ y\right) = w_1\left(x,\ y\right) - w_2\left(x,\ y\right), \tag{3.22}$$

where subscript 1 and 2 denote each different solution, respectively. Therefore, from Eqs. (3.21-22), the BVP for the difference ($v\left(x,\ y\right)$) can then be obtained as follows

$$\begin{aligned} \Delta v\left(x,\ y\right) &= 0,\ \text{in } S^+ \cup S^- = S \text{ (outside the crack)}, \\ \frac{\partial v^{\pm}}{\partial y} &= \mp\left(\frac{\mu^s - \sigma_o}{\mu}\right)\frac{\partial^2 v^{\pm}}{\partial x^2},\ \text{on } y = \pm 0, -a \le x \le a, \\ \frac{\partial v}{\partial y} &= 0,\quad y \to \infty. \end{aligned} \tag{3.23}$$

Now, we write Green's Theorem for the difference BVP in exterior domain

$$\int\int_S \Delta v dA + \int\int_S \left|\nabla v\right|^2 dA = -\int_{\partial S} v\frac{\partial v}{\partial \boldsymbol{n}} ds.$$

Since $\Delta v\left(x,\ y\right) = 0$, we obtain from the above that

$$\int\int_S \left|\nabla v\right|^2 dA = -\int_{\partial S} v\frac{\partial v}{\partial \boldsymbol{n}} ds, \tag{3.24}$$

where $\partial S = \partial S^+ \cup \partial S^-$ (∂S^+: upper crack face, ∂S^-: lower crack face see Fig. 11). In the present coordinate system, surface normal vector ($\boldsymbol{n}$) is aligned with y-axis and ∂S converges to upper and bottom crack faces on $y = \pm 0$, $-a \le x \le a$. Therefore, Eq. (3.24) can be re-written as

$$\begin{aligned} \int\int_S \left|\nabla v\right|^2 dA &= -\left\{\int_{\partial S^+} v^+\left(\frac{\partial v}{\partial \boldsymbol{n}}\right)^+ ds + \int_{\partial S^-} v^-\left(\frac{\partial v}{\partial \boldsymbol{n}}\right)^- ds\right\} \\ &= -\left\{\int_{-a}^{a} v^+\frac{\partial v}{\partial y}^+ dx + \int_{-a}^{a} v^-\frac{\partial v}{\partial y}^- (-dx)\right\}. \end{aligned}$$

Using relations in the second of Eq. (3.23), we obtain from the above that

$$\int\int_S \left|\nabla v\right|^2 dA = \left(\frac{\mu^s - \sigma_o}{\mu}\right)\left\{\int_{-a}^{a} v^+\frac{\partial^2 v^+}{\partial x^2} dx + \int_{-a}^{a} v^-\frac{\partial^2 v^-}{\partial x^2} dx\right\}.$$

Integration by part on the right side of the above, we obtain

$$\begin{aligned} & \int\int_S |\nabla v|^2 \, dA \\ = \; & \left(\frac{\mu^s - \sigma_o}{\mu}\right) \left\{ \left[v^+ \frac{\partial v^+}{\partial x} + v^- \frac{\partial v^-}{\partial x} \right]_{-a}^{a} - \int_{-a}^{a} \left[\left(\frac{\partial v^+}{\partial x}\right)^2 + \left(\frac{\partial v^-}{\partial x}\right)^2 \right] dx \right\} \end{aligned} \tag{3.25}$$

Since $w^+ = w^-$ at $x = \pm a$ (displacement continuity), Eq. (3.25) can be re-written as

$$\begin{aligned} & \int\int_S |\nabla v|^2 \, dA + \left(\frac{\mu^s - \sigma_o}{\mu}\right) \int_{-a}^{a} \left[\left(\frac{\partial v^+}{\partial x}\right)^2 + \left(\frac{\partial v^-}{\partial x}\right)^2 \right] dx \\ = \; & \left(\frac{\mu^s - \sigma_o}{\mu}\right) \left[v \left(\frac{\partial v^+}{\partial x} + \frac{\partial v^-}{\partial x} \right) \right]_{-a}^{a}. \end{aligned} \tag{3.26}$$

Next, if we impose condition such that

$$v \left(v^+_{,x} + v^-_{,x} \right) = 0, \text{ at each crack tip } (x = \pm a), \tag{3.27}$$

Eq. (3.26) now becomes

$$\int\int_S |\nabla v|^2 \, dA + \left(\frac{\mu^s - \sigma_o}{\mu}\right) \int_{-a}^{a} \left[\left(\frac{\partial v^+}{\partial x}\right)^2 + \left(\frac{\partial v^-}{\partial x}\right)^2 \right] dx = 0.$$

The above further implies that

$$v = \text{Constant, in } S, \text{ and } \frac{dv}{dx} = 0, \text{ on } y = \pm 0, \; -a \leq x \leq a.$$

However, since $v^+ = -v^-$ on $y = \pm 0, \; -a \leq x \leq a$, the constant is zero and solution is unique (i.e. $v = w_1 - w_2 = 0, \; \therefore \; w_1 = w_2$). Therefore, the conditions in Eq. (3.27) guarantee unique solution if either $v = 0$ or $v^+_{,x} + v^-_{,x}$ is zero at the tips. Consequently, if either displacements (w) or tractions ($w^+_{,x} + w^-_{,x}$) are prescribed at the tips then no further conditions can be imposed at the tips. In the present case, the physics and nature of the problem suggest $w = 0$ always at the tips ($x = \pm a$). It is, therefore the case that no further conditions can be imposed.

3.3 INVESTIGATION OF THE CAUCHY SINGULAR INTEGRO-DIFFERENTIAL EQUATION

The Cauchy singular integro-differential equation (3.20) closely resembles the well-known and well-studied classical Prandtl's singular integro-differential from aerodynamics

$$\frac{\Gamma(x)}{B(x)} - \frac{1}{2\pi}\int_{-1}^{1}\frac{\Gamma'(t)\,dt}{t-x} = f(x), \quad -1 \le x \le 1,$$
$$\Gamma(1) = \Gamma(-1) = 0,$$

where $\Gamma(x)$ is the unknown function and $B(x)$ and $f(x)$ are known functions (see, for example, [82] and the references therein). Unfortunately, the differences between Eq. (3.20) and Prandtl's equation are sufficiently significant so that the many existing results on the solution of Prandtl's equation (numerical or otherwise) do not accommodate Eq. (3.20). In [83], Frankel discusses a Galerkin approach for solving a class of singular integro-differential equations similar in form to Eq. (3.20) but appearing in the study of infrared gaseous radiation and molecular conduction as well as in elastic contact studies. Frankel's methods were among three methods used subsequently in [77] to find numerical solutions of singular integro-differential equations of the type described by Eq. (3.20). In this section, we adapt the collocation methods used in [82,83] to find numerical solutions of Eq. (3.20).

3.3.1 Solution of Singular Integro-differential Equation by a Collocation Method

Consider Eq. (3.20)

$$\frac{\mu}{\pi}\int_{-a}^{a}\frac{f(t)\,dt}{t-t_o} + 2[\sigma_{yz}^{\infty}] = -(\mu^s - \sigma_o)\frac{df(t_o)}{dt_o}, \quad -a \le t_o \le a,$$

where $f(t) = \Omega'(z)^+ - \Omega'(z)^-$, $\Omega'(z) = \dfrac{1}{2\pi i}\displaystyle\int_{-a}^{a} \frac{f(t)}{t-z}dt + \frac{1}{\mu i}[\sigma_{yz}^{\infty}]$. (3.28)

We note here that, since $w = 0$ at tips, as we discussed in the previous section, no further condition can be imposed at the tips ($t = \pm a$) in determination of $f(t)$ (see also [84]).

Now, set $\dfrac{t}{a} = x$ in Eq. (3.28) and obtain

$$\frac{\mu}{\pi}\int_{-1}^{1} \frac{f(ax)\,dx}{x - x_o} + 2[\sigma_{yz}^{\infty}] = -(\mu^s - \sigma_o)\frac{df(ax_o)}{d(ax_o)}, \quad -1 \le x_o \le 1, \tag{3.29}$$

Rewriting $x \longrightarrow t$, $x_o \longrightarrow t_o$ and further defining $f(at) = u(t)$, from Eq. (3.29), we have that

$$\frac{(\mu^s - \sigma_o)}{a}\frac{du(t_o)}{dt_o} - \frac{\mu}{\pi}\int_{-1}^{1} \frac{u(t)\,dt}{t_o - t} = -2[\sigma_{yz}^{\infty}], \quad -1 \le t_o \le 1. \tag{3.30}$$

After utilizing the inverse operator T^{-1}, as defined by the relation [77],

$$T^{-1}\psi(x) = \frac{1}{\pi\sqrt{1-x^2}}\int_{-1}^{1}\psi(x)\,dx - \frac{1}{\pi^2\sqrt{1-x^2}}\int_{-1}^{1}\frac{\sqrt{1-t^2}\psi(t)}{t-x}dt, \quad x \in (-1,1), \tag{3.31a}$$

$$T\left(T^{-1}\psi\right) = \psi,$$

and further defining

$$T(u(x)) = \int_{-1}^{1}\frac{u(x)}{x-t}dx = \psi(t), \tag{3.31b}$$

we have from Eq. (3.30) that

$$u(t_o) = \frac{1}{\pi\sqrt{1-t_o^2}}\int_{-1}^{1}u(t)\,dt - \frac{1}{\mu\pi\sqrt{1-t_o^2}}\int_{-1}^{1}\frac{\sqrt{1-t^2}}{t-t_o}\left(-2[\sigma_{yz}^{\infty}] - \frac{(\mu^s-\sigma_o)}{a}\frac{du(t)}{dt}\right)dt,$$

$$t_o \in (-1,1). \tag{3.32}$$

Multiplying by $\sqrt{1-t_o^2}$ on both sides of Eq. (3.32) yields

$$u(t_o)\sqrt{1-t_o^2} - \frac{1}{\pi}\int_{-1}^{1}u(t)\,dt - \left(\frac{\mu^s-\sigma_o}{a\mu\pi}\right)\int_{-1}^{1}\frac{\sqrt{1-t^2}}{t-t_o}\frac{du(t)}{dt}dt = \frac{2[\sigma_{yz}^{\infty}]}{\mu\pi}\int_{-1}^{1}\frac{\sqrt{1-t^2}}{t-t_o}dt. \tag{3.33}$$

Assume that the function $u(t_o)$ has an expansion of the form

$$u(t_o) = \sum_{m=0}^{N} a_m T_m(t_o), \quad t_o \in [-1,\ 1], \quad m = 0, 1, 2, ..., \tag{3.34}$$

where $T_m(t_o)$ represents the m th Chebyshev polynomial of the first kind. Further,

$$\frac{dT_m(x)}{dx} = mU_{m-1}(x). \tag{3.35}$$

Here $U_m(x)$denotes the mth Chebyshev polynomial of the second kind. Thus, from Eqs. (3.34) and (3.35), we find that

$$\frac{du(t_o)}{dt_o} = \frac{d}{dt_o}\left(\sum_{m=0}^{N} a_m T_m(t_o)\right) = \sum_{m=0}^{N} m a_m U_{m-1}(t_o),\ t_o \in [-1, 1], \quad m = 0, 1, 2, ... \tag{3.36}$$

Next, using Eqs. (3.34) and (3.36) in Eq. (3.33) yields

$$\sum_{m=0}^{N}\left[a_m T_m(t_o)\sqrt{1-t_o^2} - \frac{1}{\pi}\int_{-1}^{1} a_m T_m(t)\,dt - \left(\frac{\mu^s - \sigma_o}{a\mu\pi}\right)\int_{-1}^{1}\frac{\sqrt{1-t^2}}{t-t_o} m a_m U_{m-1}(t)\,dt\right]$$

$$= \frac{2[\sigma_{yz}^{\infty}]}{\mu\pi}\int_{-1}^{1}\frac{\sqrt{1-t^2}}{t-t_o}dt, \quad t_o \in (-1, 1) \quad m = 0,\ 1,\ 2,\ ... \tag{3.37}$$

In addition, the following properties of the Chebyshev polynomials:

$$\text{Orthogonality}: \quad \int_{-1}^{1}\frac{T_m(x)\,T_n(x)}{\sqrt{1-x^2}}dx = \left\{\begin{array}{c} 0, \quad m \neq n \\ \pi, \quad m = n = 0 \\ \frac{\pi}{2}, \quad m = n > 0 \end{array}\right\} \tag{3.38}$$

Closed-form integral relations:

$$\int_{-1}^{1}\frac{U_n(t)\sqrt{1-t^2}}{t-x}dt = -\pi T_{n+1}(x), \quad n = 0, 1, ... \tag{3.39a}$$

$$\int_{-1}^{1} T_m(x)\,dx = \frac{1+(-1)^m}{1-m^2}, \quad m = 0, 1, 2, ... \tag{3.39b}$$

Consequently, by utilizing Eqs. (3.39a-b), Eq. (3.37) reduces to

$$\sum_{m=0}^{N}\left[a_m T_m(t_o)\sqrt{1-t_o^2} - \frac{a_m}{\pi}\left(\frac{1+(-1)^m}{1-m^2}\right) + \left(\frac{\mu^s - \sigma_o}{a\mu}\right) m a_m T_m(t_o)\right]$$

$$= -\frac{2[\sigma_{yz}^{\infty}]}{\mu} T_1(t_o).$$

We now select the set of collocation points as given by $t_o = t_{oi} = -\cos(\frac{i\pi}{N})$ for $i = 1, 2, ..., N-1$ and thus derive the following system of linear equations

$$\sum_{m=0}^{N} a_m \left[T_m(t_{oi}) \sqrt{1-t_{oi}^2} - \frac{1}{\pi}\left(\frac{1+(-1)^m}{1-m^2}\right) + \left(\frac{\mu^s - \sigma_o}{a\mu}\right) m T_m(t_{oi}) \right]$$

$$= -\frac{2[\sigma_{yz}^{\infty}]}{\mu} T_1(t_{oi}), \quad i = 1, 2, ..., N-1 \tag{3.40}$$

Noting the following property of the Chebyshev polynomials of the first kind $T_n(\cos\theta) = \cos(n\theta)$, Eq. (3.40) further reduces to the following compact form

$$\sum_{m=0}^{N} a_m \left[-\cos\left(\frac{mi\pi}{N}\right) \sqrt{1-(\cos(\frac{i\pi}{N}))^2} - \frac{1+(-1)^m}{\pi(1-m^2)} - mS_e \cos(\frac{mi\pi}{N}) \right]$$

$$= 2S\cos(\frac{i\pi}{N}), \quad for \quad 1 \le i \le N-1, \tag{3.41}$$

$$\text{where,} \quad S_e = \frac{\mu^s - \sigma_o}{a\mu}, \text{ (surface effect)}, \quad S = \frac{[\sigma_{yz}^{\infty}]}{\mu}, \text{ (remote stress)}.$$

The solution of Eq. (3.28) is now reduced to the solution of the system of equations (3.41) for the constants a_m. The latter can be achieved using any of the existing commercial numerical software packages (e.g Matlab, Maple, NAG, etc.) and is the subject of the next section.

3.3.2 Results and Discussion

In this section, the numerical solution of Eq. (3.41) is performed for a range of surface parameters obtained from the work of Sharma in [16]. It is found that the numerical method performs well for problems of this type guaranteeing rapid convergence (see, for example, Fig. 13)

$$\begin{aligned} S_e &: \quad 0.1 < S_e < 0.001 \\ \mu^s &= 161.73(J/m^2), \quad \sigma_o = 1.3(J/m^2), \quad \mu = 168(Gpa). \end{aligned}$$

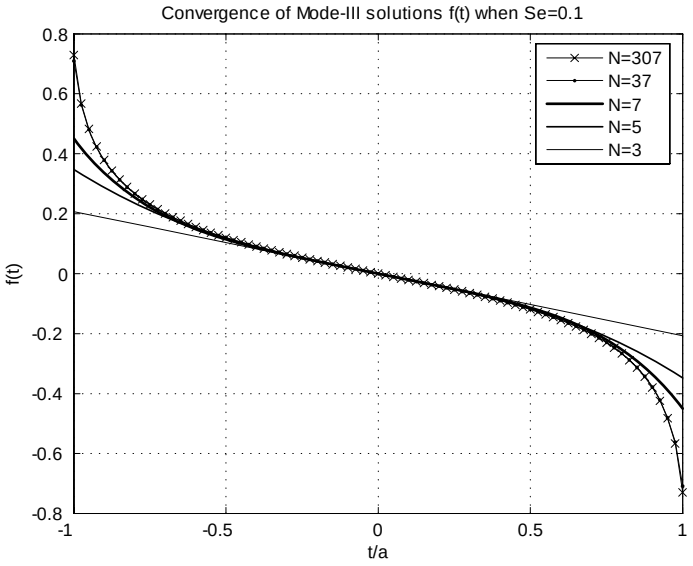

Figure 13: *Convergence of the solution $f(t)$ with respect to number of iterations (N)*

The implication of the numerical solution will be discussed in the next section. However, we note that since $f(t) \neq 0$ at the crack tips, the solution then must be singular, although reduces order of singularity.

3.3.3 Comparison with Known Classical Results

To verify the mathematical model, we first reproduce, as a special case of our analysis, the solution of the classical anti-plane crack problem in which surface effects are neglected. The latter problem has corresponding analytic solutions described by [67]:

$$\Omega'(z) = \frac{1}{\mu}[\sigma_{xz} - i\sigma_{yz}] = \frac{-i\sigma_{yz}^{\infty} z}{\mu\sqrt{z^2 - a^2}}.$$

Evaluating $\Omega'(z)$ $(-a < t < a)$, we have that

$$\Omega'(z)^{+} = \frac{-i\sigma_{yz}^{\infty} t}{\mu\sqrt{-(a^2-t^2)}} = \frac{-i\sigma_{yz}^{\infty} t}{\mu i\sqrt{(a^2-t^2)}} = \frac{-\sigma_{yz}^{\infty} t}{\mu\sqrt{a^2-t^2}}, \text{ on the upper face,} \tag{3.42a}$$

$$\Omega'(z)^{-} = \frac{i\sigma_{yz}^{\infty} t}{\mu\sqrt{-(a^2-t^2)}} = \frac{i\sigma_{yz}^{\infty} t}{\mu i\sqrt{(a^2-t^2)}} = \frac{\sigma_{yz}^{\infty} t}{\mu\sqrt{a^2-t^2}}, \text{ on the lower face.} \tag{3.42b}$$

(We note here that from Eq. (3.8), σ_{yz} is zero, yet σ_{xz} is non-zero on $y = \pm 0,\ -a \leq x \leq a$). Then the stress difference between the upper and lower face can be defined from Eqs. (3.42a-b) by

$$\Omega'(z)^{+} - \Omega'(z)^{-} = \frac{-2\sigma_{yz}^{\infty} t}{\mu\sqrt{a^2-t^2}}, \quad -a < t < a. \tag{3.43}$$

Returning to our formulation, the corresponding stress differences are defined in terms of the function $f(t)$ by (see Eq. (3.28));

$$\Omega'(z)^{+} - \Omega'(z)^{-} = f(t). \tag{3.44}$$

The values of $f(t)$ are plotted in Fig. 14, where the parameter S_e is varied by changing the dimension of the crack (i.e. $10nm < a < 1\mu m$). It is clear from Fig. 14 that as the surface effect becomes negligible, our solution reduces to that of the classical case. In particular, our solution predicts finite values of $f(t)$ at the tips, in contrast to those from the LEFM theory ($f(t)$ is infinite at the tips), which again suggest that the stresses at the tips are singular a point which we will explain in

the following section.

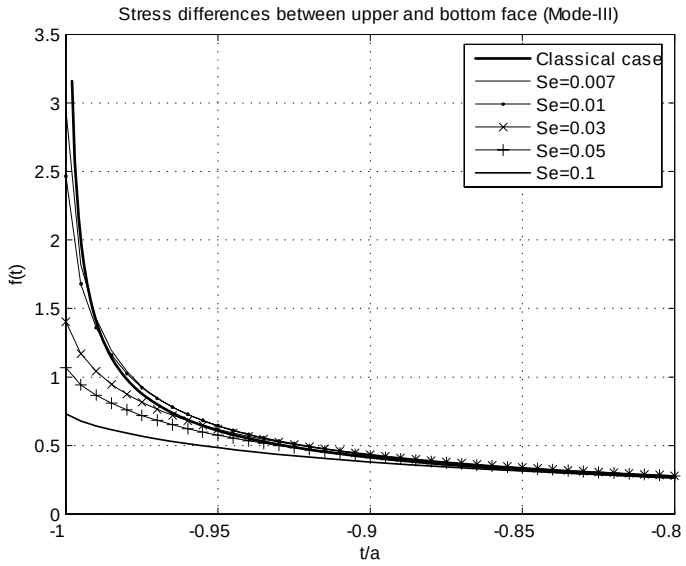

Figure 14: *Stress difference between the upper and bottom faces, when* $\sigma_{yz}^{\infty}/\mu = 0.1$

3.3.4 Stress Distributions Near the Crack Tip

Based on the numerical solution of $f(t)$ derived in the previous section, the corresponding stress distributions can be found from Eq. (3.19a):

$$\Omega'(z) = \frac{1}{2i\pi}\int_{-a}^{+a}\frac{f(t)}{t-z}dt + \frac{1}{\mu i}\left[\sigma_{yz}^{\infty}\right]. \tag{3.45}$$

The Cauchy integral in Eq. (3.45) can be expanded near the crack tip (for example at $t = a$) to obtain:

$$\int_{-a}^{+a}\frac{f(t)}{t-z}dt = f(a)\ln r + O(1), \quad r = |z-a|.$$

The above implies that stresses at the crack tips exhibit a weaker logarithmic singularity with the bounded values of $f(t)$.

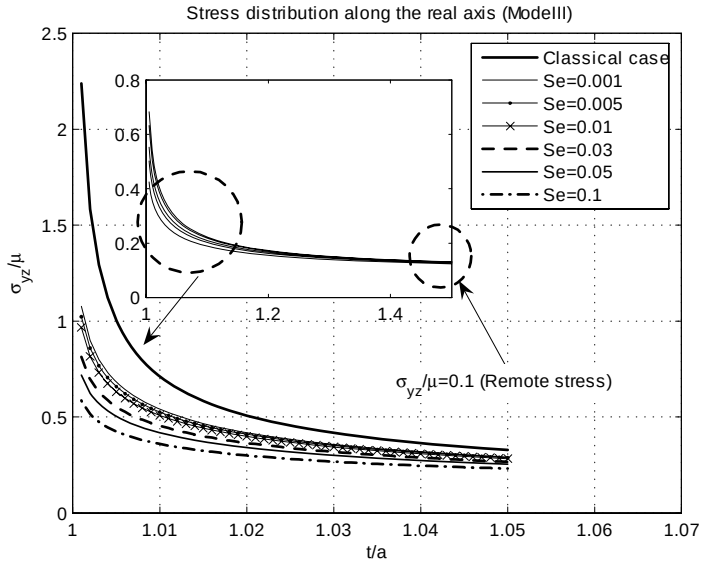

Figure 15: *Stress distribution with respect to surface parameter (S_e) when* $\sigma_{yz}^{\infty}/\mu = 0.1$

In addition, it is clear, from Fig. 15, that The corresponding stresses increase when the surface effect becomes negligible (as predicted by the corresponding classical problem where surface effects are neglected). Since the surface parameter S_e is controlled by variations in the crack length, our results also indicate that the corresponding stresses are strongly dependent on crack size. Finally, from Fig. 15 we see that stresses relatively far from the crack tips converge to the value 0.1, which is the magnitude of the applied remote stress. These results agree with the well-known results from classical elasticity (that the effect of stress concentration and surface stress/energy is localized).

3.4 TOPICS REGARDING NON-UNIFORM SURFACE TRACTION

In many engineering applications, crack surfaces can experience certain types of non-uniform loading. For example, when a crack initiates in a fiber composite material [85, 86] or in the case of a sliding crack incorporating a non-uniform frictional resistance on the crack surface. In the case of the latter, a non-uniform surface traction can be induced by varying the frictional coefficient or the normal traction along the crack face [87–89].

In this section, we extend the techniques developed in the previous section to accommodate the more general class of problems involving a mode-III crack in a linearly elastic solid in which the faces of the crack are subjected to non-uniform surface tractions.

3.4.1 A Mode-III Crack Problem with Surface Stress

Let the lower ($y < 0$) and upper ($y > 0$) half-planes again be designated the "$-$" and "$+$" sides of the crack. Then, for the crack $[-a \leq t \leq a]$, $(y = 0)$ subjected to an arbitrary surface traction P_{yz}, of polynomial form (i.e. $P_{yz}(t_o) = a_0 + a_1 t_o + a_2 t_o^2 \cdots a_n t_o^n,\ a_0,\ a_1,\ a_2 \cdots a_n \in \mathbb{R}$) and a traction-free remote boundary $\sigma_{yz}^{\infty} = 0$, the surface condition on the faces can be derived from Eqs. (3.3), (3.6) and (3.9-10) as

$$\begin{aligned}(\sigma_{yz})^{+} &= P_{yz}(t_o) - \frac{\partial \sigma_{xz}^{s}}{\partial x} = P_{yz}(t_o) - (\mu^{s} - \sigma_o)\frac{\partial^2 w}{\partial x^2} \\ &= P_{yz}(t_o) - \frac{\mu^{s} - \sigma_o}{2}[\Omega''(z) + \overline{\Omega''(z)}]^{+}, \text{ for upper face,} \quad (3.46a)\end{aligned}$$

$$\begin{aligned}(\sigma_{yz})^{-} &= P_{yz}(t_o) + \frac{\partial \sigma_{xz}^{s}}{\partial x} = P_{yz}(t_o) + (\mu^{s} - \sigma_o)\frac{\partial^2 w}{\partial x^2} \\ &= P_{yz}(t_o) + \frac{\mu^{s} - \sigma_o}{2}[\Omega''(z) + \overline{\Omega''(z)}]^{-}, \text{ for lower face.} \quad (3.46b)\end{aligned}$$

Since $w^+ = -w^-$, from Eqs. (3.7) and (3.46a-b), we obtain the following Riemann–Hilbert problem in terms of the derivatives of the unknown function $\Omega(z)$

$$\frac{\mu i}{2}\left[\Omega'(z) - \overline{\Omega'(z)}\right]^+ = P_{yz}(t_o) + \frac{\mu^s - \sigma_o}{2}\left[\Omega''(z) + \overline{\Omega''(z)}\right]^-, \text{ for upper face,} \tag{3.47a}$$

$$\frac{\mu i}{2}\left[\Omega'(z) - \overline{\Omega'(z)}\right]^- = P_{yz}(t_o) + \frac{\mu^s - \sigma_o}{2}\left[\Omega''(z) + \overline{\Omega''(z)}\right]^-, \text{ for lower face.} \tag{3.47b}$$

For the non-uniform traction case, remote loading is assumed to be zero ($\sigma_{yz}^{\infty} = 0$), we again have that (see also Eqs. (3.14-15) and corresponding discussions)

$$\Omega'(z) + \overline{\Omega'}(z) = 0, \quad \Omega'(z) = -\overline{\Omega'}(z). \tag{3.48}$$

In addition, adding Eqs. (3.47a-b) yields

$$\frac{\mu i}{2}([\Omega'(z) - \overline{\Omega'}(z)]^+ + [\Omega'(z) - \overline{\Omega'}(z)]^-) = 2P_{yz}(t_o) + (\mu^s - \sigma_o)(\Omega''(z)^- + \overline{\Omega''}(z)^+), \tag{3.49}$$

Therefore, from (3.48), Eq. (3.49) takes the following form

$$\mu i(\Omega'(z)^+ + \Omega'(z)^-) = 2P_{yz}(t_o) + (\mu^s - \sigma_o)(\Omega''(z)^- - \Omega''(z)^+). \tag{3.50}$$

Now, similar to the uniform remote loading case, we express the unknown function $\Omega'(z)$ as the following Cauchy integral

$$\Omega'(z) = \frac{1}{2i\pi}\int_{-a}^{+a}\frac{f(t)}{t-z}dt, \tag{3.51a}$$

$$\Omega''(z) = \frac{1}{2\pi i}\int_{-a}^{+a}\frac{f(t)\,dt}{(t-z)^2} = -\left[\frac{f(t)}{t-z}\right]_{-a}^{a} + \frac{1}{2\pi i}\int_{-a}^{+a}\frac{f'(t)\,dt}{t-z}, \tag{3.51b}$$

where,

$$f(t) = \Omega'(z)^+ - \Omega'(z)^-.$$

Finally, from Eqs. (3.50) and (3.51a-b), we obtain the following first-order Cauchy singular integro-differential equation for the unknown $f(t), t \in [-a, a]$:

$$\frac{\mu}{\pi}\int_{-a}^{a}\frac{f(t)\,dt}{t-t_o} = 2P_{yz}(t_o) - (\mu^s - \sigma_o)f'(t_o), \quad -a \le t_o \le a. \tag{3.52}$$

The equation (3.52) can be solved numerically by applying the techniques presented in the previous section. The corresponding stress distributions, in this case, again exhibit logarithmic singularity corresponding to finite values of $f(t)$ at each tip ($t = \pm a$). It is therefore, noted that the surface effects reduce the classical strong square root singularities normally predicted by the LEFM theory at the crack tips.

3.4.2 Examples: the cases $P_{yz}(t_o) = At_o + B$: linear loading and $P_{yz}(t_o) = At_o^2 + B$: parabolic loading

In this section, we conduct sample analyses for both linear and parabolic-type surface tractions (see, Fig. 16).

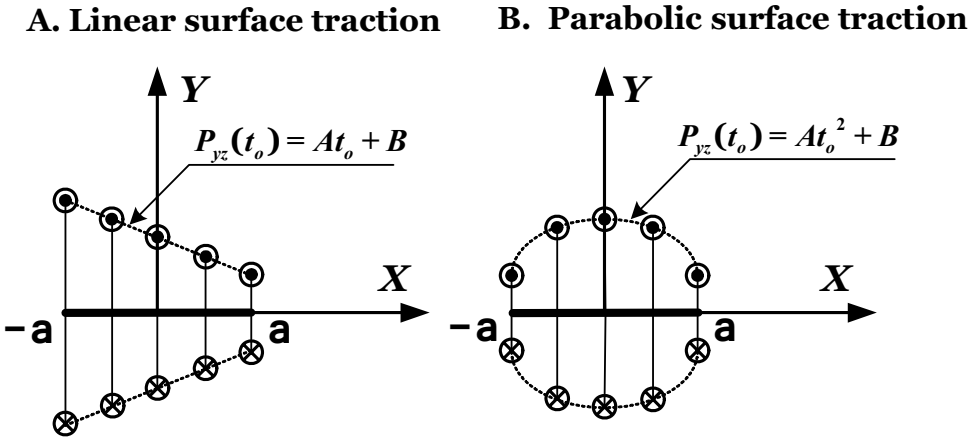

Figure 16: *Schematic of applied surface traction.* ***A*** *linear surface traction;* ***B*** *parabolic surface traction*

From Eq. (3.52), the equations for a mode-III crack problem subjected to both linear ($P_{yz}(t_o) = At_o + B$) and parabolic ($P_{yz}(t_o) = At_o^2 + B$) surface loading can

be written as

$$\frac{\mu}{\pi}\int_{-a}^{a}\frac{f\left(t\right)dt}{t-t_o}=2(At_o+B)-(\mu^s-\sigma_o)f'(t_o),\quad -a\leq t_o\leq a, \tag{3.53}$$

$$\frac{\mu}{\pi}\int_{-a}^{a}\frac{f\left(t\right)dt}{t-t_o}=2(At_o^2+B)-(\mu^s-\sigma_o)f'(t_o),\quad -a\leq t_o\leq a, \tag{3.54}$$

The Eqs. (3.53-54) can be solved using the same techniques as in the previous section. For example, in view of Eqs. (3.29-3.31), we obtain from Eq. (3.53) that

$$\begin{aligned} & u\left(t_o\right)\sqrt{1-t_o^2}-\frac{1}{\pi}\int_{-1}^{1}u\left(t\right)dt-\left(\frac{\mu^s-\sigma_o}{a\mu\pi}\right)\int_{-1}^{1}\frac{\sqrt{1-t^2}}{t-t_o}\frac{du\left(t\right)}{dt}dt \\ = & \frac{2}{\mu\pi}\left(-At_o-B\right)\int_{-1}^{1}\frac{\sqrt{1-t^2}}{t-t_o}dt. \end{aligned} \tag{3.55}$$

By using well-know Chebyshev polynomials algebraic and integral relation (Eq. (3.39a)), the right side of (3.55) becomes

$$\begin{aligned} & \frac{2}{\mu\pi}\left(\int_{-1}^{1}\frac{At_o\sqrt{1-t^2}}{t-t_o}dt-\int_{-1}^{1}\frac{B\sqrt{1-t^2}}{t-t_o}dt\right) \\ = & \frac{2}{\mu\pi}\left(\int_{-1}^{1}\frac{-AU_1\left(t\right)\sqrt{1-t^2}}{2\left(t-t_o\right)}dt-\int_{-1}^{1}\frac{BU_0\left(t\right)\sqrt{1-t^2}}{t-t_o}dt\right) \\ = & \frac{2}{\mu\pi}\left(-\frac{A\pi}{2}T_2\left(t_o\right)+B\pi T_1\left(t_o\right)\right)=\frac{AT_2\left(t_o\right)}{\mu}+\frac{2BT_1\left(t_o\right)}{\mu}. \end{aligned}$$

Therefore, we obtain from Eq. (3.55) that

$$\begin{aligned} & u\left(t_o\right)\sqrt{1-t_o^2}-\frac{1}{\pi}\int_{-1}^{1}u\left(t\right)dt-\left(\frac{\mu^s-\sigma_o}{a\mu\pi}\right)\int_{-1}^{1}\frac{\sqrt{1-t^2}}{t-t_o}\frac{du\left(t\right)}{dt}dt \\ = & \frac{AT_2\left(t_o\right)}{\mu}+\frac{2BT_1\left(t_o\right)}{\mu}. \end{aligned} \tag{3.56}$$

Assume again that the function $u\left(t_o\right)$ has an expansion of the form

$$u\left(t_o\right)=\sum_{m=0}^{N}a_mT_m\left(t_o\right),\quad t_o\in\left(-1,1\right),\quad m=0,1,2,..., \tag{3.57}$$

Using successively Eqs. (3.35-36) and (3.57), we obtain from Eq. (3.56) that

$$\begin{aligned} & \sum_{m=0}^{N}\left[a_mT_m\left(t_o\right)\sqrt{1-t_o^2}-\frac{1}{\pi}\int_{-1}^{1}a_mT_m\left(t\right)dt-\left(\frac{\mu^s-\sigma_o}{a\mu\pi}\right)\int_{-1}^{1}\frac{\sqrt{1-t^2}}{t-t_o}ma_mU_{m-1}\left(t\right)dt\right] \\ = & \frac{AT_2\left(t_o\right)}{\mu}+\frac{2BT_1\left(t_o\right)}{\mu},\quad t_o\in(-1,1)\quad m=0,\ 1,\ 2,\ ... \end{aligned} \tag{3.58}$$

In view of the properties of the Chebyshev polynomials in Eqs. (3.38-39), Eq. (3.58) becomes

$$\begin{aligned} & \sum_{m=0}^{N}\left[a_m T_m\left(t_o\right)\sqrt{1-t_o^2}-\frac{a_m}{\pi}\left(\frac{1+(-1)^m}{1-m^2}\right)+\left(\frac{\mu^s-\sigma_o}{a\mu}\right)m a_m T_m\left(t_o\right)\right] \\ = \quad & \frac{AT_2\left(t_o\right)}{\mu}+\frac{2BT_1\left(t_o\right)}{\mu}, \quad t_o\in(-1,1) \quad m=0,\ 1,\ 2,\ ... \end{aligned} \tag{3.59}$$

By selecting the set of collocation points as given by $t_o = t_{oi} = -\cos(\frac{i\pi}{N})$ for $i = 1, 2, ..., N-1$, we obtain

$$\begin{aligned} & \sum_{m=0}^{N} a_m\left[-\cos\left(\frac{mi\pi}{N}\right)\sqrt{1-(\cos(\frac{i\pi}{N}))^2}-\frac{1+(-1)^m}{\pi\left(1-m^2\right)}-mSe\cos(\frac{mi\pi}{N})\right] \\ = \quad & -Sa\cos(\frac{2i\pi}{N})-2Sb\cos(\frac{i\pi}{N}), \quad for \quad 1\le n\le N-1, \end{aligned} \tag{3.60}$$

where, $Se=\dfrac{\mu^s-\sigma_o}{a\mu}$, (surface effect), $Sa = \dfrac{A}{\mu}$, $Sb=\dfrac{B}{\mu}$ (surface traction).

In addition, by performing the same process, we derive from Eq. (3.54) that

$$\begin{aligned} & \sum_{m=0}^{N} a_m\left[-\cos\left(\frac{mi\pi}{N}\right)\sqrt{1-(\cos(\frac{i\pi}{N}))^2}-\frac{1+(-1)^m}{\pi\left(1-m^2\right)}-mSe\cos(\frac{mi\pi}{N})\right] \\ = \quad & =\frac{-Sa}{2}\cos(\frac{3i\pi}{N})-\left(\frac{Sa}{2}+2Sb\right)\cos(\frac{i\pi}{N}), \quad for \quad 1\le n\le N-1. \end{aligned} \tag{3.61}$$

Finally, Eq. (3.53-54) is now reduced to the system of equations in (3.60-61) for the constants a_m and can be solved numerically as in the previous section

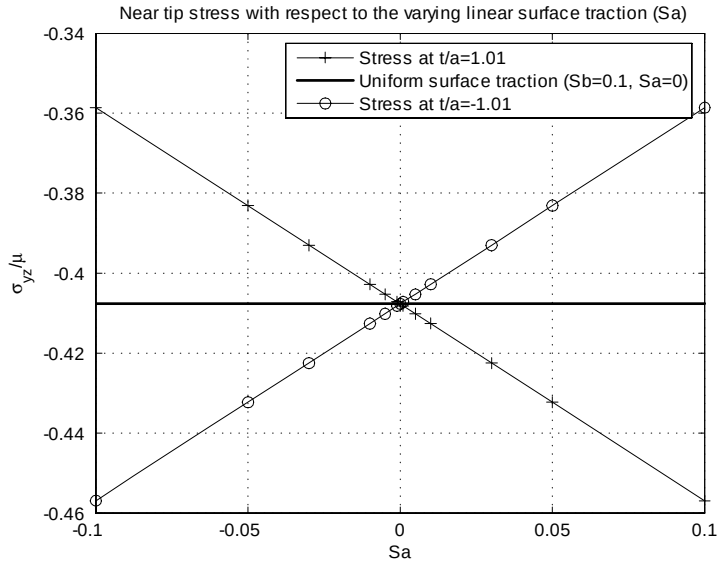

Figure 17: *Near tip stress for linear surface traction case, where* $B/\mu = S_b = 0.1,\ -0.1 \leq A/\mu = S_a \leq 0.1$

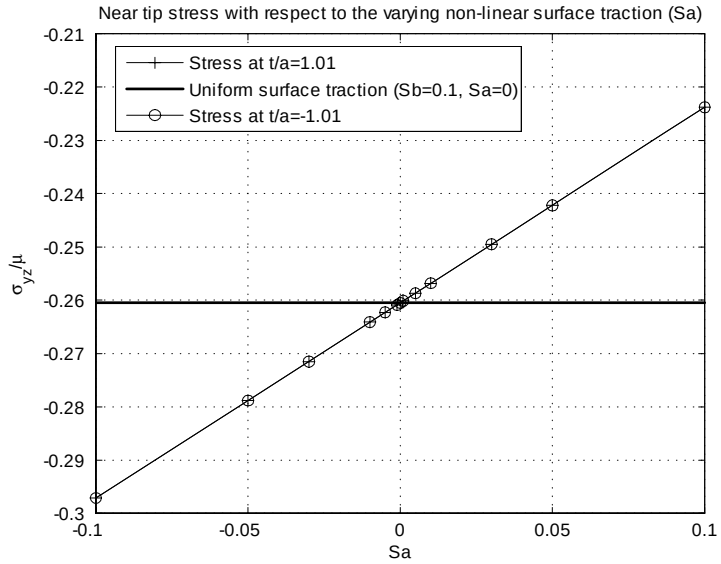

Figure 18: *Near tip stress for non-linear surface traction case, where* $B/\mu = S_b = 0.1,\ -0.1 \leq A/\mu = S_a \leq 0.1$

Figs. 17-18 demonstrate the relation between stress at $t/a = \pm 1.01$ and the variation of the surface traction parameter ($S_a = A/\mu$). It is clear that for both the linear and parabolic cases, the state of stress reduces to the corresponding case of uniform surface traction when the surface traction parameter is set equal to zero ($S_a = 0$). Further, in case of linear surface traction, an applied load is not symmetric about the $y-$axis (see Fig. 16A) resulting in different stresses, for example, at $t/a = \pm 1.01$ (see Fig. 17), yet exchanging their values as the slop S_a varies from -0.1 to 0.1. For the parabolic surface traction case, the stress, for example, at $t/a = \pm 1.01$ are identical with the variation of surface traction parameter S_a (see Fig. 18), since an applied load is symmetric about the $y-$axis (see Fig. 16B).

3.4.3 Decomposition Theory in Surface Elasticity

In this section, we discuss an interesting result in the theory of elasticity, which is derived from the particular case of the above mentioned problem (a mode-III crack subjected to uniform surface traction). In the corresponding problem from classical elasticity (without surface effects), a traction-free mode-III crack problem subjected to a uniform remote stress ($\sigma^{\infty}_{yz} = \sigma_{yz}$) (here referred to as type 1 problem in Fig. 19) can be uniquely decomposed into a sum of two problems: a plane (without crack) undergoing uniform remote stress ($\sigma^{\infty}_{yz} = \sigma_{yz}$) and a mode-III crack with a uniform surface traction ($P_{yz} = -\sigma_{yz}$) and stress-free remote boundary ($\sigma^{\infty}_{yz} = 0$) (here referred to as type 2 and 3 problems in Fig. 19, respectively). The analogy is important in a sense that it allows us to treat more complex boundary value problems by treating type 3 problems instead of directly solving problems of type 1. Here, we demonstrate that the above mentioned decomposition holds true even with the introduction of surface elasticity on the crack face.

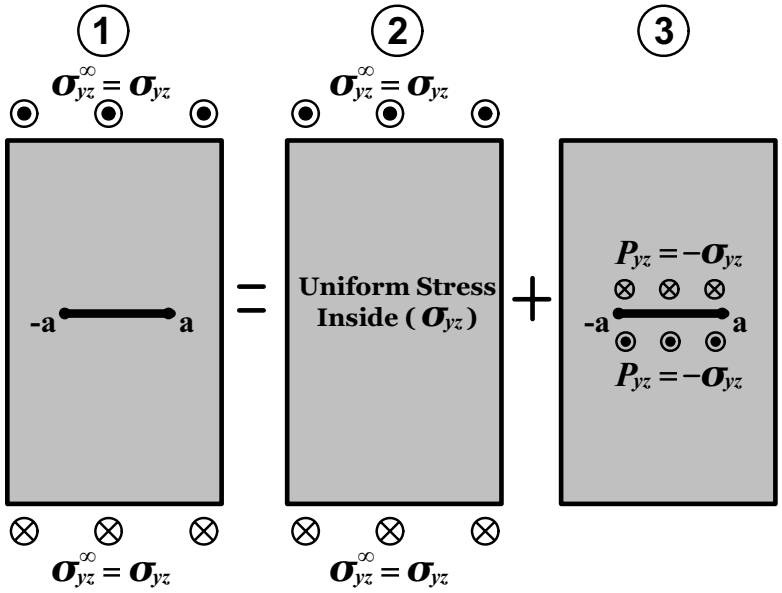

Figure 19: *Schematic of the decomposition in mode-III crack problem*

3.4.4 An Analysis of Type 2 Problem in Surface Elasticity

First, we re-examine a type 2 problem in the presence of surface elasticity. The objective here is to investigate the surface effects on the stress distribution (uniform) through the entire plane (see Fig. 19). The suggested solution of the problem requires that $\Omega(z)$ needs to be linear in "z" (where, $z \in \mathbb{C}$) to ensure uniform stress distribution at the remote boundary ($\sigma^{\infty}_{yz} = \sigma_{yz}$). That is;

$$\Omega(z) = Az + B, \quad \forall\ A,\ B \in \mathbb{C},$$

$$\Omega'(z) = \frac{d\Omega(z)}{dz} = \frac{1}{\mu}[\sigma_{xz} - i\sigma_{yz}] = A = \text{constant (uniform stress distribution).} \tag{3.62}$$

Eq. (3.62) further implies that the second derivative of $\Omega(z)$ remains zero

$$\Omega''(z) = \frac{d^2\Omega(z)}{dz^2} = \frac{d\Omega'(z)}{dz} = \frac{dA}{dz} = 0.$$

Finally, from the surface Eqs. (3.46a-b), we derive that

$$(\sigma_{yz})^{+} = -\frac{\partial \sigma^{s}_{xz}}{\partial x} = (\mu^{s} - \sigma_{o})\frac{\partial^{2} w}{\partial x^{2}} = \frac{\mu^{s} - \sigma_{o}}{2}[\Omega''(z) + \overline{\Omega''(z)}]^{+} = 0, \tag{3.63a}$$

$$(\sigma_{yz})^{-} = \frac{\partial \sigma^{s}_{xz}}{\partial x} = (\mu^{s} - \sigma_{o})\frac{\partial^{2} w}{\partial x^{2}} = \frac{\mu^{s} - \sigma_{o}}{2}[\Omega''(z) + \overline{\Omega''(z)}]^{-} = 0, \because \Omega''(z) = 0. \tag{3.63b}$$

Remark 2 *Since, through the entire plane ($S^{+} \cup S^{-} = S$), $(\sigma_{yz})^{+} = (\sigma_{yz})^{-} = 0$, it is clear from (3.5) and (3.63a-b) that the jump in stress is:*

$$[\sigma_{yz}] = (\sigma_{yz})^{+} - (\sigma_{yz})^{-} = 0 \iff \left|\frac{\partial \sigma^{s}_{xz}}{\partial x}\right| = 0.$$

Consequently, surface energy effects make no contribution to the stress distribution of the plane (without crack), which further implies that the stress is continuous and thus remains uniform through the entire plane.

3.4.5 An Analysis of Type 1 and 3 Problems in Surface Elasticity

Next, we reconsider the solutions of problems type 1 and 3 with the introduction of surface elasticity. In classical elasticity, the solutions of type 1 and 3 problems differ by only a constant which corresponds to the magnitude of the applied remote stress (see, for example, Fig. 19). Our purpose is to verify that the previously mentioned analogy still holds true for the case when the surface effects are taken into account.

The formulation of the type 3 problem can be obtained through Eq. (3.52) for uniform surface traction case ($P_{yz}(t_o) = P_{yz}$)

$$\frac{\mu}{\pi}\int_{-a}^{a}\frac{f(t)\,dt}{t - t_o} = 2P_{yz} - (\mu^{s} - \sigma_{o})f'(t_o), \quad -a \le t_o \le a, \tag{3.64}$$

which can be solved as in the previous section. The solution can also be obtained directly from either Eq. (3.60) or (3.61) by simply setting $Sa = 0$ and $Sb = P_{yz}$. Fig. 20 illustrates the corresponding stress distributions with respect to surface effect parameters. Stress distributions in this case again demonstrate a weaker logarithmic singularity, since, from Eq. (3.51), we obtain near the crack tip as

$$\begin{aligned} \Omega'(z) &= \frac{1}{2i\pi}\int_{-a}^{+a}\frac{f(t)}{t-z}dt, \quad \text{and} \\ \int_{-a}^{+a}\frac{f(t)}{t-z}dt &= f(\pm a)\ln r + O(1), \quad r = |z-a|. \end{aligned}$$

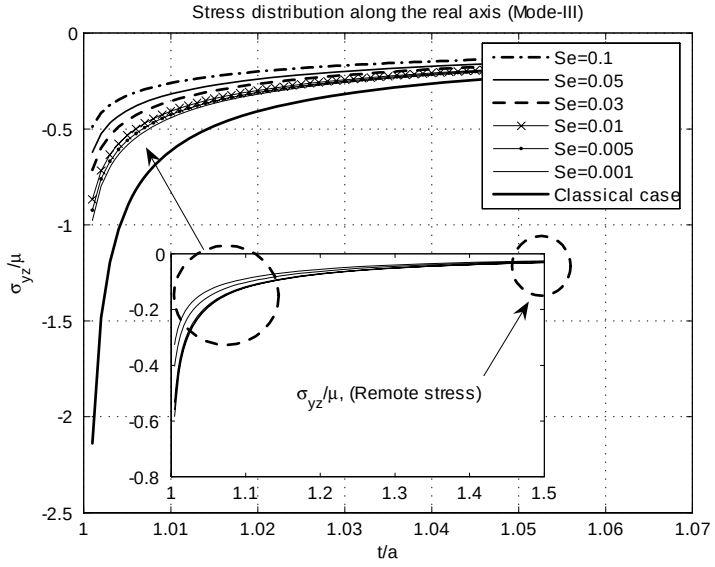

Figure 20: *Stress distribution with respect to surface parameter (S_e)*,when $P_{yz}/\mu = 0.1$

It is clear from Fig. 20 that as the surface effect becomes negligible, our solution reduces to that of the classical case. Further, from Fig. 20, we see that stresses relatively far from the crack tips converge to zero,which agrees with the imposed condition that stress at the remote boundary is zero ($\sigma_{yz}^{\infty} = 0$). In the

analysis of decomposition theory, we consider only the following case;

$$S = \frac{P_{yz}}{\mu} = -0.2, \quad Se = 0.01, \text{ (for Type 3 problem).}$$

The solution of the type 1 problem is available in the previous section (uniform remote loading problem), in which case we consider the counter part of type 3 problem as

$$\frac{\sigma_{yz}^{\infty}}{\mu} = 0.2, \quad Se = 0.01.$$

In addition, the known classical cases (without surface energy) are also evaluated using the corresponding analytic solutions described by [65–67] for comparison purposes;

$$\Omega'(z) = \frac{1}{\mu}[\sigma_{xz} - i\sigma_{yz}] = \frac{-i\sigma_{yz}^{\infty} z}{\mu\sqrt{z^2 - a^2}}, \text{(type 1 problem where } \sigma_{yz}^{\infty} \neq 0,\ P_{yz} = 0),$$

$$\Omega'(z) = \frac{1}{\mu}[\sigma_{xz} - i\sigma_{yz}] = \frac{iP_{yz}}{\mu}\left(\frac{z}{\sqrt{z^2 - a^2}} - 1\right), (type3problem where \sigma_{yz}^{\infty} = 0, P_{yz} \neq 0).$$

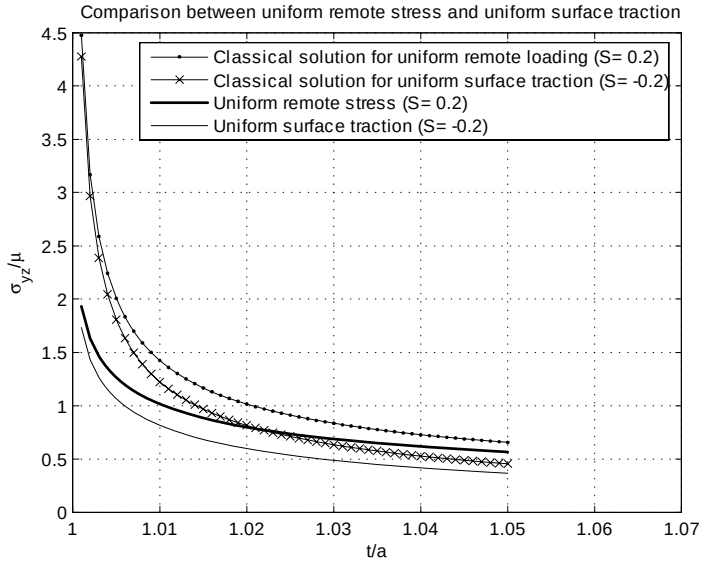

Figure 21: *Stress distribution for type 1 and type 3 problems along the real axis*

It is clear from Fig. 21 that the solutions of Type 1 and 3 differ by only a constant (the vertical distance in each case), which is identical to the magnitude of the applied remote loading ($\frac{\sigma_{yz}^{\infty}}{\mu} = 0.2$) for both our case (with surface effect) and the classical case (without surface effect).

Remark 3 *As a direct consequence of the above results (see Fig. 21) and Remark 2, we have that, for the case when the surface elasticity is included, the solution of type 1 problem is equivalent to the superposition of solutions of type 2 and 3 problem. In other words, the decomposition theory holds true with the introduction of surface elasticity.*

3.5 SUMMARY

In this Chapter, we have examined the effects of surface elasticity in a classical mode-III crack problem arising in the anti-plane shear deformations of a linearly elastic solid. It is shown that stress singularity at the crack tip reduces from the strong square root singularity to a weaker logarithmic singularity with the introduction of the effects of surface elasticity. In addition, the corresponding stress fields derived from our analysis exhibit clear signs of size dependency and do indeed accommodate those in the classical LEFM solutions when the surface effects are neglected. The uniqueness theorem of the corresponding boundary value problem is also examined leading to the conclusion that a solution is unique without imposing any further extra end conditions other than the natural end conditions (the normal displacement (w) is zero at both crack tips).

In the case of a mode-III crack subjected to non-uniform surface tractions, we have obtained a complete numerical solution, when the crack faces are subjected to arbitrary surface tractions characterized by stress functions described by general polynomials of degree n. In particular, we have proved that, from the particular

case of our general solution (when the crack faces are subjected to uniform traction), the decomposition theory in classical elasticity still holds true when surface elasticity is taken into account on the crack faces. The above results are important in that, when used in conjunction with the general methodology presented in this chapter, they essentially lead to the solutions of a class of problems in which the surface traction is characterized by a much wider and more practically realistic class of functions.

CHAPTER 4

PLANE-STRAIN CRACK PROBLEMS (MODE-I & MODE-II) IN THE PRESENCE OF SURFACE ELASTICITY

4.1 INTRODUCTION

The analysis of the plane-strain deformations of an elastic solid incorporating a crack (mode-I/mode-II) is of fundamental importance in the understanding of failure modes and in the general stress analysis of engineering materials. As discussed in earlier sections, the role of surface elasticity can be quite significant on the mechanics and mechanisms of fracture, especially when the high surface area to volume ratio is present at the nano/micro scale.

With that said, in this chapter, we consider the plane-strain deformation of a linearly elastic solid incorporating a crack in the presence of surface elasticity. Using the same surface elasticity theory as adopted in the Mode-III crack case, we model the crack as an interval of the x-axis onto which we project the properties of the surface layer [90] (much like we project the properties of a thin interphase layer onto the boundary of a fiber in the modeling of fiber-reinforced composites). The analysis of our mathematical model involves the use of complex variable methods to reduce the corresponding (highly non-standard) boundary value problem to a series of two coupled Cauchy singular integro-differential equations [65]. The latter is solved numerically using an adapted collocation technique [76] leading to a complete semi-analytic solution valid within the entire domain of interest (except at the tips).

It is shown that the incorporation of surface effects, in most cases, leads to the reduction of the classical strong square root singularity to a weaker singularity. In addition, the corresponding stresses derived from our analysis show that the presence of surface effects results in the elastic response and stress fields being size-dependent and do indeed converge to the well known classical solutions [65, 66], in the limit as surface effects are neglected. We note also that the solution of the corresponding mixed mode crack problem (in which mode-I and mode-II cracks are considered simultaneously) derived in this chapter is sufficiently general in that, it incorporates the solutions corresponding to both mode-I and mode-II separately, when the corresponding far-field stress conditions are applied (remote tension and in-plane shear for mode-I and mode-II cases, respectively). Finally, the imposition of end conditions at the crack tips is discussed in order to uniquely determine a solution of the coupled BVP. This includes the clarification of the role end of conditions within the maximum number allowed [84].

4.2 PLANE-STRAIN CRACK PROBLEM WITH SURFACE EFFECTS

We consider plane-strain deformations of a linearly elastic and homogeneous isotropic solid occupying a region in $\mathbb{R}^3$ with generators parallel to the $z-$axis of a rectangular cartesian coordinate system. We assume that a cross-section of the crack occupies the region $[-a,\ a]$, $a \in \mathbb{R}^+$ of the $x-$axis as shown in Fig. 22.

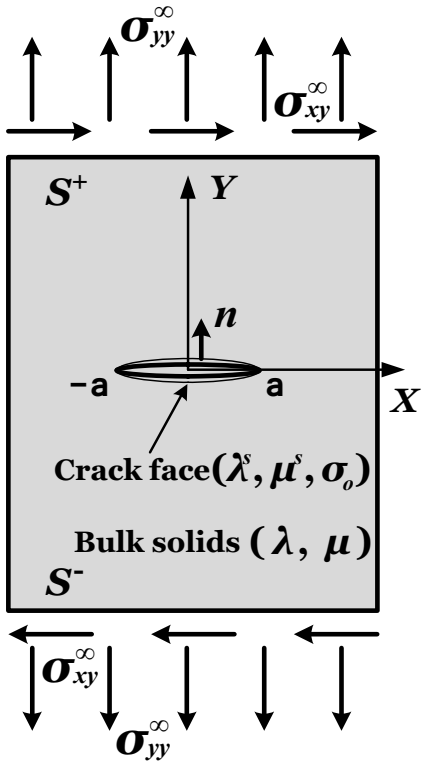

Figure 22: *Schematic of a plane-strain crack problem*

4.2.1 Complex-Variable Formulation

The stress and strain expressions for the bulk material can be obtained from Eqs. (2.1-2) as

$$\sigma_{ij} = \lambda\delta_{ij}\varepsilon_{kk} + 2\mu\varepsilon_{ij}, \tag{4.1a}$$

$$\varepsilon_{ij} = \frac{1}{2}\left(u_{i,j} + u_{j,i}\right). \tag{4.1b}$$

In plane-strain deformations of an isotropic elastic medium, we assume that the displacement vector $\boldsymbol{u}$ with components now denoted by (u, v, ω) admits the rep-

resentation (see also Eq. (2.14))

$$u = u\,(x,\ y)\,,\ v = v\,(x,\ y)\,,\quad \omega = 0. \tag{4.2}$$

In the absence of body forces, the corresponding governing equations of two-dimensional elasticity are described by by (see [65])

$$2\mu\,(u + iv) = \kappa\Omega(z) - z\overline{\Omega'(z)} - \overline{w\,(z)}, \tag{4.3a}$$

$$\sigma_{yy} - i\sigma_{xy} = \Omega'(z) + \overline{\Omega'(z)} + z\overline{\Omega''(z)} + \overline{w'\,(z)}. \tag{4.3b}$$

Here $\Omega(z)$ and $w\,(z)$ are analytic functions of the complex variable $z = x + iy$ in the cut plane $S^+ \cup S^- = S$ outside the crack (see Fig. 22.) and κ is defined as;

$$\kappa = \frac{\lambda + 3\mu}{\lambda + \mu} = 3 - 4\upsilon \text{ (for plane-strain)},$$

where υ is Poisson's ratio taking values in the range $0 < \upsilon < \frac{1}{2}$. Thus, κ satisfies the following inequality

$$1 < \kappa < 3. \tag{4.4}$$

Since the displacements and stresses are continuous across $y = 0$, $x > |a|$ (outside the crack) , from Eq. (4.3b), following [66], we can now define an analytic function $\theta\,(z)$ in the whole plane cut along $L = -a < x < a$ by

$$\Omega(z) - z\overline{\Omega'(\overline{z})} - \overline{w\,(\overline{z})} = \ \theta\,(z)\,. \tag{4.5}$$

From Eq. (4.5), Eqs. (4.3a-b) can now be re-written as;

$$2\mu\,(u + iv) = \kappa\Omega(z) - \Omega(\overline{z}) - (\overline{z} - z)\,\overline{\Omega'(z)} + \theta\,(\overline{z})\,, \tag{4.6a}$$

$$\sigma_{yy} - i\sigma_{xy} = \Omega'(z) + \Omega'(\overline{z}) + (z - \overline{z})\,\overline{\Omega''(z)} - \theta'\,(\overline{z})\,. \tag{4.6b}$$

4.2.2 Equilibrium Equations on the Crack Surface

In the present case, the normal to the crack face is aligned with the $y-$direction (see Fig. 22) the equilibrium condition for the crack is given by (see. Eqs. (2.16-17) and the corresponding derivation)

$$\sigma^s_{xx,x} + [\sigma_{xy}] = 0, \tag{4.7a}$$

$$[\sigma_{yy}] = -\sigma_o \frac{\partial^2 \nu}{\partial x^2}. \tag{4.7b}$$

It should also be noted that we retain only the normal component v of the surface Laplacian of the displacement vector $\boldsymbol{u}$ from Eq. (2.5) (see [47] for details). From Eqs. (4.7a) and (4.7b), we have

$$[\sigma_{yy} - i\sigma_{xy}] = i\sigma^s_{xx,x} - \sigma_o \frac{\partial^2 \nu}{\partial x^2}. \tag{4.8}$$

In addition, from Eqs. (2.15) and (4.1a-b) and (4.2), the expression for the surface stress can be obtained explicitly in terms of displacements:

$$\sigma^s_{xx} = \sigma_o + (2\mu^s - \sigma_o + \lambda^s) \frac{\partial u}{\partial x},$$

where, $\varepsilon^s_{xx} = \varepsilon_{xx}$ for a coherent interface. By taking the derivative with respect to x, the above expression becomes

$$\sigma^s_{xx,x} = \frac{\partial \left(\sigma_o + (2\mu^s - \sigma_o + \lambda^s) \frac{\partial u}{\partial x} \right)}{\partial x} = (2\mu^s - \sigma_o + \lambda^s) \frac{\partial^2 u}{\partial x^2}. \tag{4.9}$$

Finally, by substituting Eq. (4.9) back into Eq. (4.8), we derive the equilibrium condition on the surface as

$$[\sigma_{yy} - i\sigma_{xy}] = iJ_o \frac{\partial^2 u}{\partial x^2} - \sigma_o \frac{\partial^2 \nu}{\partial x^2}, \quad \text{where} \quad J_o \equiv 2\mu^s - \sigma_o + \lambda^s. \tag{4.10}$$

4.2.3 Plane-strain Crack Problem with Surface Stress

Let the lower ($y < 0$) and upper ($y > 0$) half-planes be designated the "$-$" and "$+$" sides of the crack, respectively. If we assume that the faces of the crack are traction-free, then, from Eq. (4.10), the boundary conditions on the upper and lower crack faces are given by;

$$(\sigma_{yy} - i\sigma_{xy})^{+} - (\sigma_{yy} - i\sigma_{xy})^{-} = iJ_o\frac{\partial^2 u}{\partial x^2} - \sigma_o\frac{\partial^2 \nu}{\partial x^2}, \text{on the upper face,} \tag{4.11a}$$

$$(\sigma_{yy} - i\sigma_{xy})^{+} - (\sigma_{yy} - i\sigma_{xy})^{-} = iJ_o\frac{\partial^2 u}{\partial x^2} - \sigma_o\frac{\partial^2 \nu}{\partial x^2}, \text{on the lower face.} \tag{4.11b}$$

In the case of the present crack problem, the terms $(\sigma_{yy} - i\sigma_{xy})^{-}$ in Eq. (4.11a) and $(\sigma_{yy} - i\sigma_{xy})^{+}$ in Eq. (4.11b) are zero, since no material is defined between the upper and lower crack face (material discontinuity along the cut $y = 0, -a < x < a$).

In the more general case when the crack face is subjected to a prescribed traction $P_{yy} - iP_{xy}$, from Eq. (4.11a-b), the boundary conditions on the crack faces ($-a < x < a,\ \ y = \pm 0$) can be written as;

$$(\sigma_{yy} - i\sigma_{xy})^{+} = P_{yy} - iP_{xy} + iJ_o\frac{\partial^2 u}{\partial x^2} - \sigma_o\frac{\partial^2 \nu}{\partial x^2},\ \text{on the upper face,} \tag{4.12a}$$

$$(\sigma_{yy} - i\sigma_{xy})^{-} = P_{yy} - iP_{xy} - iJ_o\frac{\partial^2 u}{\partial x^2} + \sigma_o\frac{\partial^2 \nu}{\partial x^2}, \text{ on the lower face.} \tag{4.12b}$$

We consider here the situation when the solid is subjected to uniform remote normal and shear stress ($\sigma_{yy} = \sigma_{yy}^{\infty},\ \sigma_{xy} = \sigma_{xy}^{\infty}$) and a traction-free crack face ($P_{yy} = P_{xy} = 0$) ((see also Fig. 23)).

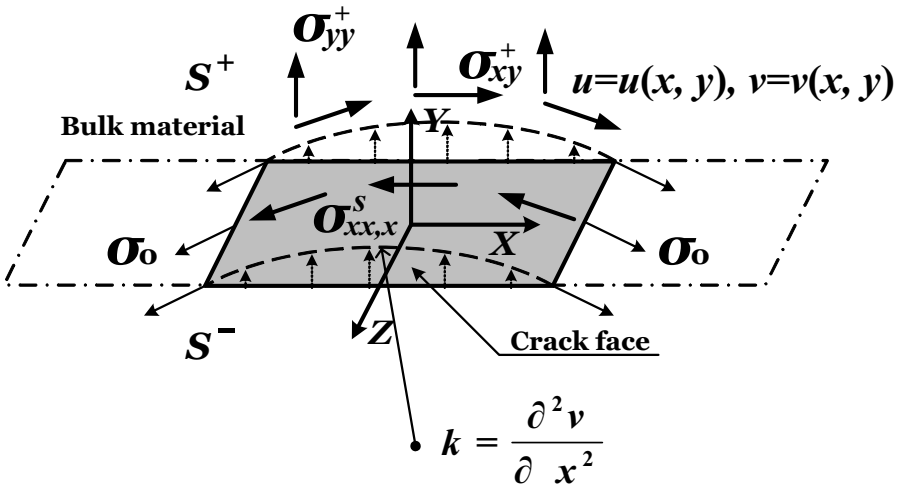

Figure 23: *Equilibrium on upper crack face under the plane-strain deformation*

From Eqs. (4.6b) and 4.12(a-b), the surface conditions on either side of the crack face can then be formulated as follows;

$$(\sigma_{yy} - i\sigma_{xy})^{+} = \Omega'(z)^{+} + \Omega'(z)^{-} - \theta'(z)^{-} = iJ_o\frac{\partial^2 u}{\partial x^2} - \sigma_o\frac{\partial^2 \nu}{\partial x^2}, \text{ on the upper face,} \tag{4.13a}$$

$$(\sigma_{yy} - i\sigma_{xy})^{-} = \Omega'(z)^{-} + \Omega'(z)^{+} - \theta'(z)^{+} = -iJ_o\frac{\partial^2 u}{\partial x^2} + \sigma_o\frac{\partial^2 \nu}{\partial x^2}, \text{ on the lower face.} \tag{4.13b}$$

Adding and subtracting Eqs. (4.13a) and (4.13b) yields

$$\left[\theta'(z)^{+} - \theta'(z)^{-}\right] = iJ_o\left(\frac{\partial^2 u^{+}}{\partial x^2} + \frac{\partial^2 u^{-}}{\partial x^2}\right) - \sigma_o\left(\frac{\partial^2 \nu^{+}}{\partial x^2} + \frac{\partial^2 \nu^{-}}{\partial x^2}\right), \tag{4.14a}$$

$$\left[2\Omega'(z)^{+} - \theta'(z)^{+}\right] + \left[2\Omega'(z)^{-} - \theta'(z)^{-}\right] = iJ_o\left(\frac{\partial^2 u^{+}}{\partial x^2} - \frac{\partial^2 u^{-}}{\partial x^2}\right) - \sigma_o\left(\frac{\partial^2 \nu^{+}}{\partial x^2} - \frac{\partial^2 \nu^{-}}{\partial x^2}\right). \tag{4.14b}$$

Now, from Eq. (4.6a), we have that

$$\left(\frac{\partial^2 u}{\partial x^2} + i\frac{\partial^2 \nu}{\partial x^2}\right) = \frac{1}{2\mu}\left[\kappa\Omega''(z) - \Omega''(\overline{z}) - (\overline{z} - z)\,\overline{\Omega'''(z)} + \theta''(\overline{z})\right].$$

Therefore, by applying the relations $\Omega''(\overline{z})^{+} = \Omega''(z)^{-}$, $\overline{z} = z$ on $y = \pm 0$, we have

$$\begin{aligned}
&\left[\left(\frac{\partial^2 u^{+}}{\partial x^2} + \frac{\partial^2 u^{-}}{\partial x^2}\right) + i\left(\frac{\partial^2 \nu^{+}}{\partial x^2} + \frac{\partial^2 \nu^{-}}{\partial x^2}\right)\right] \\
&= \frac{1}{2\mu}\left[(\kappa - 1)\left\{\Omega''(z)^{+} + \Omega''(z)^{-}\right\} + \left\{\theta''(z)^{+} + \theta''(z)^{-}\right\}\right], \quad (4.15a)
\end{aligned}$$

$$\begin{aligned}
&\left[\left(\frac{\partial^2 u^{+}}{\partial x^2} - \frac{\partial^2 u^{-}}{\partial x^2}\right) + i\left(\frac{\partial^2 \nu^{+}}{\partial x^2} - \frac{\partial^2 \nu^{-}}{\partial x^2}\right)\right] \\
&= \frac{1}{2\mu}\left[(\kappa + 1)\left\{\Omega''(z)^{+} - \Omega''(z)^{-}\right\} - \left\{\theta''(z)^{+} - \theta''(z)^{-}\right\}\right]. \quad (4.15b)
\end{aligned}$$

Consequently, from Eqs. (4.15a-b), Eqs. (4.14a-b) take the following forms

$$\begin{aligned}
&\left[\theta'(z)^{+} - \theta'(z)^{-}\right] = \frac{iJ_o}{2\mu}\,\mathrm{Re}[(\kappa - 1)\left\{\Omega''(z)^{+} + \Omega''(z)^{-}\right\} + \left\{\theta''(z)^{+} + \theta''(z)^{-}\right\}] \\
&- \frac{\sigma_o}{2\mu}\,\mathrm{Im}[(\kappa - 1)\left\{\Omega''(z)^{+} + \Omega''(z)^{-}\right\} + \left\{\theta''(z)^{+} + \theta''(z)^{-}\right\}], \quad (4.16)
\end{aligned}$$

$$\begin{aligned}
&\left[2\Omega'(z)^{+} - \theta'(z)^{+}\right] + \left[2\Omega'(z)^{-} - \theta'(z)^{-}\right] \\
&= \frac{iJ_o}{2\mu}\,\mathrm{Re}[(\kappa + 1)\left\{\Omega''(z)^{+} - \Omega''(z)^{-}\right\} - \left\{\theta''(z)^{+} - \theta''(z)^{-}\right\}] \\
&- \frac{\sigma_o}{2\mu}\,\mathrm{Im}[(\kappa + 1)\left\{\Omega''(z)^{+} - \Omega''(z)^{-}\right\} - \left\{\theta''(z)^{+} - \theta''(z)^{-}\right\}]. \quad (4.17)
\end{aligned}$$

Next, if we express the unknowns $\Omega'(z)$ and $\theta'(z)$ as Cauchy integrals [65], given the behaviour of $\theta'(z)$ [66] we have that

$$\Omega'(z) = \frac{1}{2\pi i}\int_{-a}^{+a} \frac{f(t) + ig(t)}{t - z}dt + \frac{1}{2}(\sigma_{yy}^{\infty} - i\sigma_{xy}^{\infty}), \quad (4.18)$$

$$\begin{aligned}
\Omega''(z) &= \frac{1}{2\pi i}\int_{-a}^{+a} \frac{f(t) + ig(t)}{(t - z)^2}dt \\
&= -\left[\frac{f(t) + ig(t)}{t - z}\right]_{-a}^{+a} + \frac{1}{2\pi i}\int_{-a}^{+a} \frac{f'(t) + ig'(t)}{t - z}d,
\end{aligned}$$

where,

$$\begin{aligned}
f(t_o) + ig(t_o) &= \Omega'(z)^{+} - \Omega'(z)^{-}, \ -a \le t_o \le a, \\
\theta'(z) &= \frac{1}{2\pi i}\int_{-a}^{+a} \frac{\alpha(t) + i\beta(t)}{t - z}dt, \quad (4.19)
\end{aligned}$$

$$\theta''(z) = \frac{1}{2\pi i}\int_{-a}^{+a}\frac{\alpha(t)+i\beta(t)}{(t-z)^2}dt$$
$$= -\left[\frac{\alpha(t)+i\beta(t)}{t-z}\right]_{-a}^{+a} + \frac{1}{2\pi i}\int_{-a}^{+a}\frac{\alpha'(t)+i\beta'(t)}{t-z}dt$$

Here,

$$\alpha(t_o)+i\beta(t_o) = \theta'(z)^+ - \theta'(z)^-,\ -a \le t_o \le a.$$

In addition, the boundary values of Ω' and $\theta'(z)$ on the crack faces ($y = \pm 0,\ -a < x < a$) can be found as (see [65]):

$$\Omega'(z)^+ = \frac{1}{2}(f(t_o)+ig(t_o)) + \frac{1}{2\pi i}\int_{-a}^{+a}\frac{f(t)+ig(t)}{t-z}dt + \frac{1}{2}(\sigma_{yy}^{\infty} - i\sigma_{xy}^{\infty}), \quad (4.20a)$$

$$\Omega'(z)^- = -\frac{1}{2}(f(t_o)+ig(t_o)) + \frac{1}{2\pi i}\int_{-a}^{+a}\frac{f(t)+ig(t)}{t-z}dt + \frac{1}{2}(\sigma_{yy}^{\infty} - i\sigma_{xy}^{\infty}), \quad (4.20b)$$

$$\theta'(z)^+ = \frac{1}{2}(\alpha(t_o)+i\beta(t_o)) + \frac{1}{2\pi i}\int_{-a}^{+a}\frac{\alpha(t)+i\beta(t)}{t-z}dt, \quad (4.21a)$$

$$\theta'(z)^- = -\frac{1}{2}(\alpha(t_o)+i\beta(t_o)) + \frac{1}{2\pi i}\int_{-a}^{+a}\frac{\alpha(t)+i\beta(t)}{t-z}dt. \quad (4.21b)$$

Thus, in view of Eqs (4.18-4.21), Eqs. (4.16) and (4.17) can be re-written as

$$\alpha(t_o)+i\beta(t_o) = \frac{iJ_o}{2\mu}\,\mathrm{Re}\left[\frac{(\kappa-1)}{\pi i}\int_{-a}^{+a}\frac{f(t)+ig(t)}{(t-t_o)^2}dt + \frac{1}{\pi i}\int_{-a}^{+a}\frac{\alpha(t)+i\beta(t)}{(t-t_o)^2}dt\right]$$
$$- \frac{\sigma_o}{2\mu}\,\mathrm{Im}\left[\frac{(\kappa-1)}{\pi i}\int_{-a}^{+a}\frac{f(t)+ig(t)}{(t-t_o)^2}dt + \frac{1}{\pi i}\int_{-a}^{+a}\frac{\alpha(t)+i\beta(t)}{(t-t_o)^2}dt\right], \quad (4.22)$$

$$\frac{2}{\pi i}\int_{-a}^{+a}\frac{f(t)+ig(t)}{t-t_o}dt + 2(\sigma_{yy}^{\infty} - i\sigma_{xy}^{\infty}) - \frac{1}{\pi i}\int_{-a}^{+a}\frac{\alpha(t)+i\beta(t)}{t-t_o}dt$$
$$= \frac{iJ_o}{2\mu}\,\mathrm{Re}\left[(\kappa+1)(f'(t_o)+ig'(t_o)) - (\alpha'(t_o)+i\beta'(t_o))\right]$$
$$- \frac{\sigma_o}{2\mu}\,\mathrm{Im}[(\kappa+1)(f'(t_o)+ig'(t_o)) - (\alpha'(t_o)+i\beta'(t_o))]. \quad (4.23)$$

Finally, by separating the real and imaginary parts of Eqs. (4.22-23), we obtain the following coupled first-order Cauchy singular integro-differential equations for

the unknowns $f(t)$, $g(t)$, $\alpha(t)$ and $\beta(t)$:

$$\alpha(t_o) = \frac{\sigma_o}{2\mu}\left[\frac{(\kappa-1)}{\pi}\int_{-a}^{+a}\frac{f(t)}{(t-t_o)^2}dt + \frac{1}{\pi}\int_{-a}^{+a}\frac{\alpha(t)}{(t-t_o)^2}dt\right], \tag{4.24a}$$

$$\frac{2}{\pi}\int_{-a}^{+a}\frac{f(t)}{t-t_o}dt + 2\sigma_{xy}^{\infty} - \frac{1}{\pi}\int_{-a}^{+a}\frac{\alpha(t)}{t-t_o}dt = -\frac{J_o}{2\mu}\left[(\kappa+1)f'(t_o) - \alpha'(t_o)\right], \tag{4.24b}$$

$$\beta(t_o) = \frac{J_o}{2\mu}\left[\frac{(\kappa-1)}{\pi}\int_{-a}^{+a}\frac{g(t)}{(t-t_o)^2}dt + \frac{1}{\pi}\int_{-a}^{+a}\frac{\beta(t)}{(t-t_o)^2}dt\right], \tag{4.25a}$$

$$\frac{2}{\pi}\int_{-a}^{+a}\frac{g(t)}{t-t_o}dt + 2\sigma_{yy}^{\infty} - \frac{1}{\pi}\int_{-a}^{+a}\frac{\beta(t)}{t-t_o}dt = -\frac{\sigma_o}{2\mu}[(\kappa+1)g'(t_o) - \beta'(t_o)]. \tag{4.25b}$$

4.2.4 Analysis of End Conditions

Using a process similar to that used in the chapter 3, the natural end conditions which guarantee unique solutions of the BVPs for the plane crack problems are given by (see [84])

$$\left(u_{,x}^{+} + u_{,x}^{-}\right)u = 0,\ \sigma_o\left(v_{,x}^{+} + v_{,x}^{-}\right)v = 0,\ \text{at each tip } (z = \pm a). \tag{4.26}$$

Eq. (4.26) suggests that two conditions can be imposed at each crack tip, for example, either displacements $(u,\ v)$ or tractions $(u_{,x}^{+} + u_{,x}^{-},\ v_{,x}^{+} + v_{,x}^{-})$ can be prescribed at the tips or the combination of these two. In the Mode-I case, similar to the Mode-III fracture, the natural displacement fields at the crack tips admit $v(\pm a) = 0$ at each tip. Therefore, *only one* end condition is admissible at each tip for the Mode-I case. A similar situations holds true for Mode-II fracture. In this case $u(\pm a) = 0$ at the tips (the number of end conditions is again reduced to one). Consequently, the number of allowable end conditions is reduced to one, at each end, in each case. The one interesting exception is the case of Mode-II fracture in which $\sigma_o = 0$. In this case, not one single end condition can be imposed since, $u(\pm a) = 0$ so that both expressions in Eq. (4.26) are automatically satisfied. We further note that, in the successive analysis, the admissible end conditions in each

case are chosen in such a way that the terms involving the derivatives of Cauchy integrals in Eqs. (4.24a-b) and (4.25a-b) can be reduced to Cauchy-singular rather than hyper-singular form. More precisely, by imposing $(k-1)g(\pm a)+\beta(\pm a)=0$, $(k-1)f(\pm a)+\alpha(\pm a)=0$ at each crack tip, we obtain from Eqs. (4.18) and (4.25a) that

$$\alpha(t_o)=\frac{\sigma_o}{2\mu}\left[\frac{(\kappa-1)}{\pi}\int_{-a}^{+a}\frac{f(t)}{(t-t_o)^2}dt+\frac{1}{\pi}\int_{-a}^{+a}\frac{\alpha(t)}{(t-t_o)^2}dt\right]$$

$$= -\frac{\sigma_o}{2\mu}\left[\frac{(k-1)f(t)+\alpha(t)}{t-z}\right]_{-a}^{+a}+\frac{\sigma_o}{2\mu}\left[\frac{(\kappa-1)}{\pi}\int_{-a}^{+a}\frac{f'(t)}{t-t_o}dt+\frac{1}{\pi}\int_{-a}^{+a}\frac{\alpha'(t)}{t-t_o}dt\right]$$

$$= \frac{\sigma_o}{2\mu}\left[\frac{(\kappa-1)}{\pi}\int_{-a}^{+a}\frac{f'(t)}{t-t_o}dt+\frac{1}{\pi}\int_{-a}^{+a}\frac{\alpha'(t)}{t-t_o}dt\right],\ \because (k-1)f(\pm a)+\alpha(\pm a)=0.$$

Similarly, from Eqs. (4.19) and (4.25a), we obtain

$$\beta(t_o)=\frac{J_o}{2\mu}\left[\frac{(\kappa-1)}{\pi}\int_{-a}^{+a}\frac{g'(t)}{t-t_o}dt+\frac{1}{\pi}\int_{-a}^{+a}\frac{\beta'(t)}{t-t_o}dt\right].$$

Finally, by imposing the above mentioned natural end conditions, the corresponding hyper singular equations in (4.24a-b) and (4.25a-b) are now reduced to the following Cauchy-singular integro-differential equations:

$$\alpha(t_o)=\frac{\sigma_o}{2\mu}\left[\frac{(\kappa-1)}{\pi}\int_{-a}^{+a}\frac{f'(t)}{t-t_o}dt+\frac{1}{\pi}\int_{-a}^{+a}\frac{\alpha'(t)}{t-t_o}dt\right], \tag{4.27a}$$

$$\frac{2}{\pi}\int_{-a}^{+a}\frac{f(t)}{t-t_o}dt+2\sigma_{xy}^{\infty}-\frac{1}{\pi}\int_{-a}^{+a}\frac{\alpha(t)}{t-t_o}dt=-\frac{J_o}{2\mu}\left[(\kappa+1)\,f'(t_o)-\alpha'(t_o)\right], \tag{4.27b}$$

$$\beta(t_o)=\frac{J_o}{2\mu}\left[\frac{(\kappa-1)}{\pi}\int_{-a}^{+a}\frac{g'(t)}{t-t_o}dt+\frac{1}{\pi}\int_{-a}^{+a}\frac{\beta'(t)}{t-t_o}dt\right], \tag{4.28a}$$

$$\frac{2}{\pi}\int_{-a}^{+a}\frac{g(t)}{t-t_o}dt+2\sigma_{yy}^{\infty}-\frac{1}{\pi}\int_{-a}^{+a}\frac{\beta(t)}{t-t_o}dt=-\frac{\sigma_o}{2\mu}[(\kappa+1)\,g'(t_o)-\beta'(t_o)]. \tag{4.28b}$$

It is of interest to see if other end conditions can be used (other than those mentioned above). We will return to this point later in the thesis.

4.3 ANALYSIS OF THE SINGULAR INTEGRO - DIFFERENTIAL EQUATIONS

The series of coupled Cauchy singular integro-differential equations in Eqs. (4.27-28) are similar in form to equations of the type:

$$2\frac{\phi(x)}{dx} - \lambda \int_{-1}^{1} \frac{\phi(t)}{x-t} dt = f(x), \quad -1 \leq x \leq 1, \ \lambda > 0, \quad \phi(1) = \phi(-1) = 0,$$

$$-\frac{1}{\pi} \int_{-1}^{1} \frac{v(y)}{(x-y)^2} dy = g(x), \quad -1 \leq x \leq 1,$$

where ϕ and v are the unknown functions and f and g are considered as 'known' functions. The first of these equations often arises in the study of molecular conduction, gaseous radiation and heat conduction problems while the second type appears in the analysis of a crack mounted in an infinite strip. In [77, 83], the authors provide a full analysis of the first equation and derive complete numerical solutions with the aid of a collocation method. The second equation has been well-studied in [66, 76, 83, 91] using Chebychev polynomials of the second kind. Unfortunately, the methods used in the aforementioned studies are not directly applicable to the current problem since Eqs. (4.27-28) combine characteristics of both equations.

In this section, inspired by the techniques presented in [76,77], we propose quite novel approaches and provide complete numerical solutions of Eqs. (4.27-28). We also note here that the present problem displays strong dependency on the choice of methods so that other existing methods such as Fourier series methods and direct Chebychev methods have failed to deliver successful results.

4.3.1 Solution of Singular Integro-differential Equations by a Collocation Method

Eqs. (4.28a-b) can be re-written as;

$$\int_{-a}^{+a} \frac{g'(t) + \frac{1}{(\kappa-1)}\beta'(t)}{t - t_o} dt = \frac{2\mu\pi}{J_o\,(\kappa - 1)}\beta(t_o), \tag{4.29a}$$

$$\int_{-a}^{+a} \frac{g(t) - \frac{1}{2}\beta(t)}{t - t_o} dt = -\sigma_{yy}^{\infty}\pi - \frac{\pi\sigma_o}{4\mu}\left[(\kappa + 1)\, g'(t_o) - \beta'(t_o)\right]. \tag{4.29b}$$

Set $\dfrac{t}{a} = x$ in Eqs. (4.29a-b) and obtain

$$\int_{-1}^{+1} \frac{\frac{dg(ax)}{d(ax)} + \frac{1}{(\kappa-1)}\frac{d\beta(ax)}{d(ax)}}{a(x - x_o)}\,(a)\, dx = \frac{2\mu\pi}{J_o\,(\kappa - 1)}\beta(ax_o), \tag{4.30a}$$

$$\int_{-1}^{+1} \frac{g(ax) - \frac{1}{2}\beta(ax)}{a\,(x - x_o)}\,(a)\, dx = -\sigma_{yy}^{\infty}\pi - \frac{\pi\sigma_o}{4\mu}\left[(\kappa + 1)\,\frac{dg(ax_o)}{d(ax_o)} - \frac{d\beta(ax_o)}{d(ax_o)}\right]. \tag{4.30b}$$

Rewriting $x \to t,\ x_o \to t_o$ and further defining $g(at) = v(t),\ \beta(at) = \xi(t)$, from Eqs. (4.30a-b), we have that

$$\int_{-1}^{+1} \frac{v'(t) + \frac{1}{(\kappa-1)}\xi'(t)}{t - t_o} dt = \frac{2\mu a\pi}{J_o\,(\kappa - 1)}\xi(t_o), \tag{4.31a}$$

$$\int_{-1}^{+1} \frac{v(t) - \frac{1}{2}\xi(t)}{t - t_o} dt = -\sigma_{yy}^{\infty}\pi - \frac{\pi\sigma_o}{4\mu a}\left[(\kappa + 1)\, v'(t_o) - \xi'(t_o)\right], \tag{4.31b}$$

$$where,\ -1 \le t_o \le 1,\ v(1) = v(-1) = \xi(1) = \xi(-1) = 0.$$

We utilize the first inverse operator T^{-1}defined in the following manner (see [92, 93]) ;

$$T^{-1}\psi\,(t) = \frac{\sqrt{1 - t_o^2}}{\pi}\int_{-1}^{1} \psi\,(t)\, dt - \frac{\sqrt{1 - t_o^2}}{\pi^2}\int_{-1}^{1} \frac{\psi\,(t)}{(t - t_o)\sqrt{1 - t^2}} dt, \quad t_o \in (-1, 1), \tag{4.32a}$$

$$T\left(T^{-1}\psi\right) = \psi,$$

and further define

$$T\left(v'(t_o) + \frac{1}{(\kappa - 1)}\xi'(t_o)\right) = \int_{-1}^{1} \frac{v'(t_o) + \frac{1}{(\kappa-1)}\xi'(t_o)}{t_o - t} dt_o = \psi\,(t). \tag{4.32b}$$

It follows then from Eq. (4.31a) that

$$v'(t_o)+\frac{1}{(\kappa-1)}\xi'(t_o)$$
$$=\frac{\sqrt{1-t_o^2}}{\pi}\int_{-1}^{1}\left(v'(t)+\frac{1}{(\kappa-1)}\xi'(t)\right)dt-\frac{2\mu a\sqrt{1-t_o^2}}{\pi J_o\left(\kappa-1\right)}\int_{-1}^{1}\frac{\xi(t)}{(t-t_o)\sqrt{1-t^2}}dt,\quad t_o\in(-1,1). \tag{4.33}$$

Similarly, by applying the second inverse operator T^{-1} as defined by the relation in [77], we have that

$$T^{-1}\psi\left(t\right)=\frac{1}{\pi\sqrt{1-t_o^2}}\int_{-1}^{1}\psi\left(t\right)dt-\frac{1}{\pi^2\sqrt{1-t_o^2}}\int_{-1}^{1}\frac{\sqrt{1-t^2}\psi\left(t\right)}{t-t_o}dt,\quad t_o\in(-1,1), \tag{4.34a}$$

$$T\left(T^{-1}\psi\right)=\psi,$$
$$T\left(v(t_o)-\frac{1}{2}\xi(t_o)\right)=\int_{-1}^{1}\frac{v(t_o)-\frac{1}{2}\xi(t_o)}{t_o-t}dt_o=\psi\left(t\right). \tag{4.34b}$$

From Eq. (4.31b) we have that

$$v(t_o)-\frac{1}{2}\xi(t_o)$$
$$=\frac{1}{\pi\sqrt{1-t_o^2}}\int_{-1}^{1}\left(v(t)-\frac{1}{2}\xi(t)\right)dt$$
$$-\frac{1}{\pi^2\sqrt{1-t_o^2}}\int_{-1}^{1}\frac{\sqrt{1-t^2}}{t-t_o}\left(-\sigma_{yy}^{\infty}\pi-\frac{\sigma_o\pi}{4\mu a}\left(\left(\kappa+1\right)v'(t)-\xi'(t)\right)\right)dt. \tag{4.35}$$

Multiplying by $\sqrt{1-t_o^2}$ on both sides of Eq. (4.35) yields

$$\sqrt{1-t_o^2}\left(v(t_o)-\frac{1}{2}\xi(t_o)\right)-\frac{1}{\pi}\int_{-1}^{1}\left(v(t)-\frac{1}{2}\xi(t)\right)dt$$
$$=\frac{\sigma_o}{4\mu a\pi}\int_{-1}^{1}\frac{\sqrt{1-t^2}}{t-t_o}\left(\left(\kappa+1\right)v'(t)-\xi'(t)\right)dt+\frac{1}{\pi}\int_{-1}^{1}\frac{\sqrt{1-t^2}}{t-t_o}\sigma_{yy}^{\infty}dt,\ t_o\in(-1,1). \tag{4.36}$$

now we assume approximations for the v and ξ can be written in the form

$$v(t_o)\approx v_N(t_o)=\sum_{m=0}^{N}a_mT_m\left(t_o\right),\quad \xi(t_o)\approx\ \xi_N(t_o)=\sum_{m=0}^{N}b_mT_m\left(t_o\right),\ m=0,1,2,..., \tag{4.37}$$

where $T_m(t_o)$ represents the m th Chebychev polynomial of the first kind. In addition, the Chevychev polynomials have the following properties:

$$\frac{dT_m(x)}{dx} = mU_{m-1}(x). \tag{4.38}$$

Here, $U_m(x)$ denotes the m th Chevychev polynomial of the second kind. Therefore, from (4.37) and (4.38), we find that

$$\frac{dv_N(t_o)}{dt_o} = \frac{d}{dt_o}\left(\sum_{m=0}^{N} a_m T_m(t_o)\right) = \sum_{m=0}^{N} m a_m U_{m-1}(t_o),$$

$$\frac{d\xi_N(t_o)}{dt_o} = \frac{d}{dt_o}\left(\sum_{m=0}^{N} b_m T_m(t_o)\right) = \sum_{m=0}^{N} m b_m U_{m-1}(t_o),\ t_o \in [-1,1],\ m = 0,1,2,... \tag{4.39}$$

Next, in view of Eqs. (4.37) and (4.39), Eq. (4.33) becomes

$$\sum_{m=0}^{N} mU_{m-1}(t_o)\left(a_m + \frac{b_m}{(\kappa-1)}\right)$$
$$= \frac{\sqrt{1-t_o^2}}{\pi}\int_{-1}^{1}\sum_{m=0}^{N} mU_{m-1}(t)\left(a_m + \frac{b_m}{(\kappa-1)}\right)dt - \frac{2\mu a\sqrt{1-t_o^2}}{\pi J_o(\kappa-1)}\int_{-1}^{1}\frac{\sum_{m=0}^{N} b_m T_m(t)}{(t-t_o)\sqrt{1-t^2}}dt. \tag{4.40}$$

By utilizing the following properties of the Chebychev polynomials:

$$\int_{-1}^{1} U_{m-1}(t)dt = \frac{1-(-1)^m}{m}, \quad \int_{-1}^{1}\frac{T_m(t)}{(t-t_o)\sqrt{1-t^2}}dt = \pi U_{m-1}(t_o),$$

Eq. (4.40) reduces to

$$\sum_{m=0}^{N} a_m\left[mU_{m-1}(t_o) - \frac{\sqrt{1-t_o^2}\,(1-(-1)^m)}{\pi}\right]$$
$$= \sum_{m=0}^{N} b_m\left[-\frac{mb_m U_{m-1}(t_o)}{(\kappa-1)} + \frac{\sqrt{1-t_o^2}\,(1-(-1)^m)}{\pi(\kappa-1)} - \frac{2\mu a\sqrt{1-t_o^2}}{J_o(\kappa-1)}U_{m-1}(t_o)\right].$$

Consequently, we derive the relation between a_m and b_m as;

$$b_m = a_m\left(\frac{J_o(\kappa-1)\left[\pi m U_{m-1}(t_o) - \sqrt{1-t_o^2}\,(1-(-1)^m)\right]}{J_o\sqrt{1-t_o^2}\,(1-(-1)^m) - \pi U_{m-1}(t_o)\left(mJ_o + 2\mu a\sqrt{1-t_o^2}\right)}\right) \equiv \boldsymbol{K}_1 a_m. \tag{4.41}$$

Similarly, from Eqs. (4.37) and (4.39), Eq. (4.36) becomes

$$\sum_{m=0}^{N}\left[T_m\left(t_o\right)\sqrt{1-t_o^2}\left(a_m-\frac{b_m}{2}\right)-\frac{1}{\pi}\int_{-1}^{1}T_m\left(t\right)\left(a_m-\frac{b_m}{2}\right)dt\right] \tag{4.42}$$

$$=\sum_{m=0}^{N}\left[\frac{\sigma_o}{4\mu a\pi}\int_{-1}^{1}\frac{\sqrt{1-t^2}mU_{m-1}\left(t\right)}{t-t_o}\left(\left(\kappa+1\right)a_m-b_m\right)dt\right]+\frac{1}{\pi}\int_{-1}^{1}\frac{\sqrt{1-t^2}}{t-t_o}\sigma_{yy}^{\infty}dt,\quad t_o\in(-1,1).$$

Again, the Chebychev polynomials have the following properties:

$$\int_{-1}^{1}T_m\left(t\right)dt=\frac{1+(-1)^m}{1-m^2},\ \int_{-1}^{1}\frac{\sqrt{1-t^2}U_{m-1}\left(t\right)}{t-t_o}dt=-\pi T_m\left(t_o\right),\ \int_{-1}^{1}\frac{\sqrt{1-t^2}}{t-t_o}dt=-\pi t_o.$$

Therefore, Eq. (4.42) reduces to

$$\sum_{m=0}^{N}\left[\left(a_m-\frac{b_m}{2}\right)\left(T_m\left(t_o\right)\sqrt{1-t_o^2}-\frac{1+(-1)^m}{\pi\left(1-m^2\right)}\right)+\frac{\sigma_o m}{4\mu a}T_m\left(t_o\right)\left[\left(\kappa+1\right)a_m-b_m\right]\right]=-\sigma_{yy}^{\infty}t_o, \tag{4.43}$$

where, $t_o\in(-1,1)$. We now select the set of collocation points as given by $t_o=t_{oi}=-\cos(\frac{i\pi}{N})$ for $i=1,2,...,N-1$. Further, by evaluating $T_m(t_{oi})$ and $U_{m-1}(t_{oi})$ with respect to each collocation points, we find that

$$T_m\left(-\cos\left(\frac{i\pi}{N}\right)\right)=-\cos\left(\frac{im\pi}{N}\right),\quad U_{m-1}\left(-\cos\left(\frac{i\pi}{N}\right)\right)=\frac{\sin\left(\frac{mi\pi}{N}\right)}{\sin\left(\frac{i\pi}{N}\right)}. \tag{4.44}$$

Noting the following properties of the Cheychev polynomials of the first kind $T_n\left(\cos\theta\right)=\cos n\theta$ and the second kind $U_n\left(\cos\theta\right)=\sin((n+1)\theta)/\sin\theta$, Eq. (4.43) further reduces to the following system of linear equations

$$\sum_{m=0}^{N}\left[\left(a_m-\frac{b_m}{2}\right)\left(-\cos\left(\frac{im\pi}{N}\right)\sqrt{1-(\cos(\frac{i\pi}{N}))^2}-\frac{1+(-1)^m}{\pi\left(1-m^2\right)}\right)\right]$$

$$+\sum_{m=0}^{N}\left[-\frac{\sigma_o m}{4\mu a}\left[\left(\kappa+1\right)a_m-b_m\right]\cos\left(\frac{im\pi}{N}\right)\right]=\sigma_{yy}^{\infty}\cos\left(\frac{i\pi}{N}\right), \tag{4.45}$$

where, from Eq (4.41):

$$b_m=\mathbf{K}_1a_m,\ \ \mathbf{K}_1=\left(\frac{J_o\left(\kappa-1\right)\left[\pi m\frac{\sin\left(\frac{mi\pi}{N}\right)}{\sin\left(\frac{i\pi}{N}\right)}-\sqrt{1-(\cos(\frac{i\pi}{N}))^2}\left(1-(-1)^m\right)\right]}{J_o\sqrt{1-(\cos(\frac{i\pi}{N}))^2}\left(1-(-1)^m\right)-\pi\frac{\sin\left(\frac{mi\pi}{N}\right)}{\sin\left(\frac{i\pi}{N}\right)}\left(mJ_o+2\mu a\sqrt{1-(\cos(\frac{i\pi}{N}))^2}\right)}\right),$$

for $1 \leq i \leq N-1$.

The same technique can be applied to determine the unknown functions $f(t)$ and $\alpha(t)$. After scaling the funtions $f(t)$ and $\alpha(t)$, we derive from Eqs. (4.27a-b) that

$$\int_{-1}^{+1} \frac{u'(t) + \frac{\eta'(t)}{(\kappa-1)}}{t - t_o} dt = \frac{2\mu\pi}{\sigma_o(\kappa-1)} \eta(t_o), \tag{4.46a}$$

$$\int_{-a}^{+a} \frac{u(t) - \frac{1}{2}\eta(t)}{t - t_o} dt = -\sigma_{xy}^{\infty}\pi - \frac{J_o\pi}{4\mu}\left[(\kappa+1)u'(t_o) - \eta'(t_o)\right], \text{ where}, -1 \leq t_o \leq 1. \tag{4.46b}$$

Next, express unknown functions $u(t_o)$ and $\eta(t_o)$ in the form:

$$u(t_o) \approx u_N(t_o) = \sum_{m=0}^{N} c_m T_m(t_o), \quad \eta(t_o) \approx \eta_N(t_o) = \sum_{m=0}^{N} d_m T_m(t_o), \quad m = 0, 1, 2, ..., \tag{4.47}$$

and following the techniques through Eqs. (4.29-4.45), we obtain the following system of linear equations for the unknown constants c_m and d_m as;

$$\sum_{m=0}^{N}\left[\left(c_m - \frac{d_m}{2}\right)\left(-\cos\left(\frac{im\pi}{N}\right)\sqrt{1-(\cos(\frac{i\pi}{N}))^2} - \frac{1+(-1)^m}{\pi(1-m^2)}\right)\right]$$

$$+\sum_{m=0}^{N}\left[-\frac{J_o m}{4\mu a}\left[(\kappa+1)c_m - d_m\right]\cos\left(\frac{im\pi}{N}\right)\right] = \sigma_{xy}^{\infty}\cos\left(\frac{i\pi}{N}\right), \tag{4.48}$$

where

$$d_m = \mathbf{K}_2 c_m, \ \mathbf{K}_2 = \left(\frac{\sigma_o(\kappa-1)\left[\pi m\frac{\sin\left(\frac{mi\pi}{N}\right)}{\sin\left(\frac{i\pi}{N}\right)} - \sqrt{1-(\cos(\frac{i\pi}{N}))^2}\,(1-(-1)^m)\right]}{\sigma_o\sqrt{1-(\cos(\frac{i\pi}{N}))^2}\,(1-(-1)^m) - \pi\frac{\sin\left(\frac{mi\pi}{N}\right)}{\sin\left(\frac{i\pi}{N}\right)}\left(m\sigma_o + 2\mu a\sqrt{1-(\cos(\frac{i\pi}{N}))^2}\right)}\right),$$

for $1 \leq i \leq N-1$. Consequently, the solution of coupled Eqs. (4.27-4.28) is now reduced to the solution of the two systems of equations Eqs. (4.45) and Eqs. (4.48), respectively for the unknown constants a_m, b_m, c_m and d_m. The latter can be obtained by using any of the existing numerical software packages (e.g. Matlab, Maple, NAG, etc.).

4.3.2 Examples: Mode-I ($\sigma_{yy}^{\infty} \neq 0, \quad \sigma_{xy}^{\infty} = 0$) problem

In view of the remote loading condition, the unknown complex functions $\Omega'(z)$ and $\theta'(z)$ can be expressed as;

$$\Omega'(z) = \frac{1}{2\pi i} \int_{-a}^{+a} \frac{f(t) + ig(t)}{t - z} dt + \frac{1}{2}\sigma_{yy}^{\infty}, \tag{4.49}$$

$$\theta'(z) = \frac{1}{2\pi i} \int_{-a}^{+a} \frac{\alpha(t) + i\beta(t)}{t - z} dt. \tag{4.50}$$

Then, Eq. (4.48) reduces to

$$\sum_{m=0}^{N} \left[\left(c_m - \frac{\mathbf{K}_2 c_m}{2} \right) \left(-\cos\left(\frac{im\pi}{N}\right) \sqrt{1 - (\cos(\frac{i\pi}{N}))^2} - \frac{1 + (-1)^m}{\pi(1 - m^2)} \right) \right]$$

$$+ \sum_{m=0}^{N} \left[-\frac{J_o m}{4\mu a} \left[(\kappa + 1) c_m - \mathbf{K}_2 c_m \right] \cos\left(\frac{im\pi}{N}\right) \right] = 0.$$

We found from the above equation that

$$f(t) = \alpha(t) = 0. \tag{4.51}$$

Also, Eq. (4.45) yields

$$\sum_{m=0}^{N} \left[\left(a_m - \frac{\mathbf{K}_1 a_m}{2} \right) \left(-\cos\left(\frac{im\pi}{N}\right) \sqrt{1 - (\cos(\frac{i\pi}{N}))^2} - \frac{1 + (-1)^m}{\pi(1 - m^2)} \right) \right]$$

$$+ \sum_{m=0}^{N} \left[-\frac{\sigma_o m}{4\mu a} \left[(\kappa + 1) a_m - \mathbf{K}_1 a_m \right] \cos\left(\frac{im\pi}{N}\right) \right] = \sigma_{yy}^{\infty} \cos\left(\frac{i\pi}{N}\right). \tag{4.52}$$

Eqs. (4.52) give a non-zero solution of $g(t)$ and $\beta(t)$ (see Fig. 24). Therefore, the unknown complex potential can be determined through Eqs. (4.49-50) as

$$\Omega'(z) = \frac{1}{2\pi} \int_{-a}^{+a} \frac{g(t)}{t - z} dt + \frac{1}{2}\sigma_{yy}^{\infty}, \tag{4.53}$$

$$\theta'(z) = \frac{1}{2\pi} \int_{-a}^{+a} \frac{\beta(t)}{t - z} dt. \tag{4.54}$$

4.3.3 Examples: Mode-II ($\sigma_{yy}^{\infty} = 0, \quad \sigma_{xy}^{\infty} \neq 0$) problem

Similarly, the unknown complex functions $\Omega'(z)$ and $\theta'(z)$ can be expressed for the Mode-II case as;

$$\Omega'(z) = \frac{1}{2\pi i} \int_{-a}^{+a} \frac{f(t) + ig(t)}{t - z} dt + \frac{1}{2}\sigma_{xy}^{\infty}, \tag{4.55}$$

$$\theta'(z) = \frac{1}{2\pi i} \int_{-a}^{+a} \frac{\alpha(t) + i\beta(t)}{t - z} dt. \tag{4.56}$$

Since $\sigma_{yy}^{\infty} = 0$ for Mode-II case, Eq. (4.45) yields

$$g(t) = \beta(t) = 0. \tag{4.57}$$

In addition, Eqs. (4.48) give non-zero solutions for $f(t)$ and $\alpha(t)$ (see Fig. 25) by solving the following reduced system of linear equations

$$\sum_{m=0}^{N} \left[\left(c_m - \frac{c_m \mathbf{K}_2}{2} \right) \left(-\cos\left(\frac{im\pi}{N} \right) \sqrt{1 - (\cos(\frac{i\pi}{N}))^2} - \frac{1 + (-1)^m}{\pi (1 - m^2)} \right) \right]$$

$$+ \sum_{m=0}^{N} \left[-\frac{J_o m}{4\mu a} \left[(\kappa + 1) c_m - c_m \mathbf{K}_2 \right] \cos\left(\frac{im\pi}{N} \right) \right] = \sigma_{xy}^{\infty} \cos\left(\frac{i\pi}{N} \right).$$

Finally, from Eqs. (4.55-56) the unknown complex potentials can be determined as;

$$\Omega'(z) = \frac{1}{2\pi i} \int_{-a}^{+a} \frac{f(t)}{t - z} dt + \frac{1}{2}\sigma_{xy}^{\infty}, \tag{4.58}$$

$$\theta'(z) = \frac{1}{2\pi i} \int_{-a}^{+a} \frac{\alpha(t)}{t - z} dt. \tag{4.59}$$

4.4 RESULTS AND DISCUSSION

In this section, the numerical solution of Eqs. (4.45) and (4.48) is derived for the two cases when a crack is subjected to a uniform remote tension (Mode -I crack problem) and a uniform remote in-plane shear (Mode-II crack problem), respectively. Throughout the analysis, we adopt the following range of surface

parameters. The listed values are estimated properties of "GaN" obtained from the work of Sharma & Ganti [16]. GaN is composed of a mixture of nitrified aluminum (AI), gallium (Ga) and indium (In) and used in the manufacture of a semiconductor.

$$
\begin{aligned}
Se_1 &= \frac{\sigma_o}{2a\mu} : \ 0.0005 < Se_1 < 0.05, \\
Se_2 &= \frac{J_o}{2a\mu} : \ 0.0005 < Se_2 < 0.1, \\
\mu^s &= 161.73(J/m^2), \quad \sigma_o = 1.3(J/m^2), \ J_o = 400(J/m^2), \ \mu = 168(Gpa).
\end{aligned}
\tag{4.60}
$$

It is found that the numerical method overall, performs well ensuring rapid convergence (see, for example, Figs. 24-25).

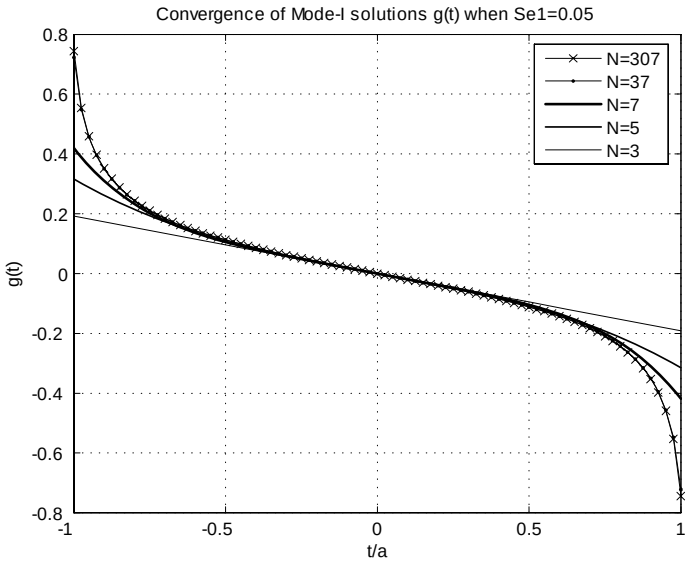

Figure 24: *Convergence of the solution g(t) with respect to number of iterations (N)*

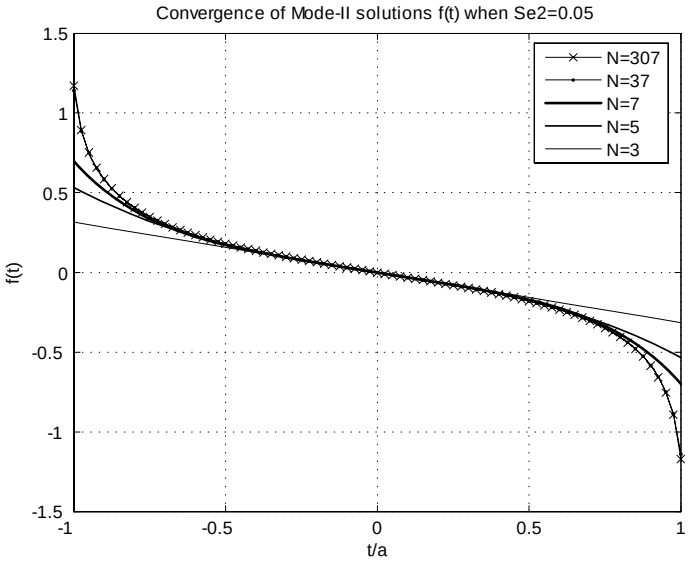

Figure 25: *Convergence of the solution f(t) with respect to number of iterations (N)*

The results in Figs. 24-25 clearly indicate that the solutions have non-zero finite values at the crack tips (e.g. $g(t) \neq 0$). This implies that, similar to the Mode-III fracture, the corresponding stress fields again must be singular, in the plane-strain crack case. The implication of the numerical solutions will be further discussed in the next section.

4.4.1 Determination of the unknown functions $f(t)$, $g(t)$, $\alpha(t)$ and $\beta(t)$

We first retrieve, as a special case of our analysis, the solution of the classical plane-strain crack problem (in which surface effects are neglected) in an attempt

to verify the mathematical model. From [65, 66], we find that

$$\Omega'(z) = \frac{\sigma_{yy}^{\infty} z}{2\sqrt{z^2 - a^2}}, \quad \text{(Mode-I)}, \quad \Omega'(z) = \frac{\sigma_{xy}^{\infty} z}{2\sqrt{z^2 - a^2}}, \quad \text{(Mode-II)},$$

$$\theta'(z) = 0, \text{ for both Mode-I and Mode-II.} \tag{4.61}$$

Therefore, from Eq. (4.61), we derive the differences:

$$\Omega'(z)^{+} - \Omega'(z)^{-} = -\frac{\sigma_{yy}^{\infty} t}{\sqrt{t^2 - a^2}}, \quad -a < t < a, \text{ (Mode-I)},$$

$$\Omega'(z)^{+} - \Omega'(z)^{-} = -\frac{\sigma_{xy}^{\infty} t}{\sqrt{t^2 - a^2}}, \quad -a < t < a, \text{ (Mode-II)}. \tag{4.62}$$

The corresponding solutions for each case are plotted through Figs. (26-27), where the parameters Se_1 and Se_2 vary with respect to the dimensions of the crack.

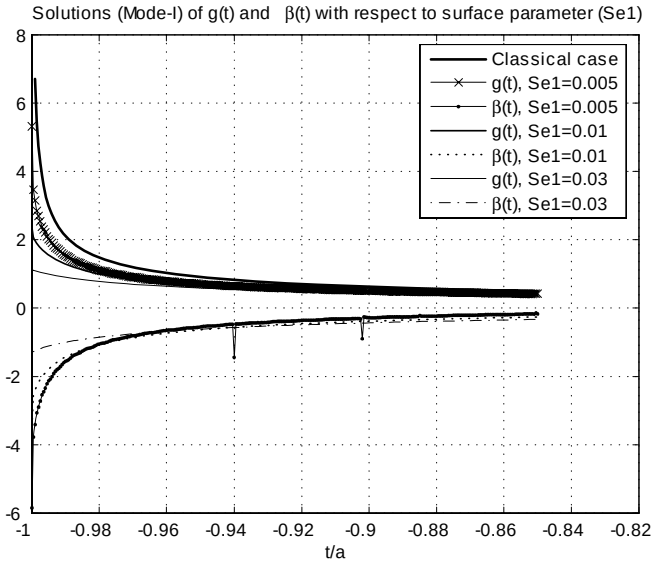

Figure 26: *The solution of* $g(t)$ *and* $\beta(t)$ *(Mode-I), where,* $0.005 < Se_1 < 0.03$, $\sigma_{yy}^{\infty}/\mu = 0.3$.

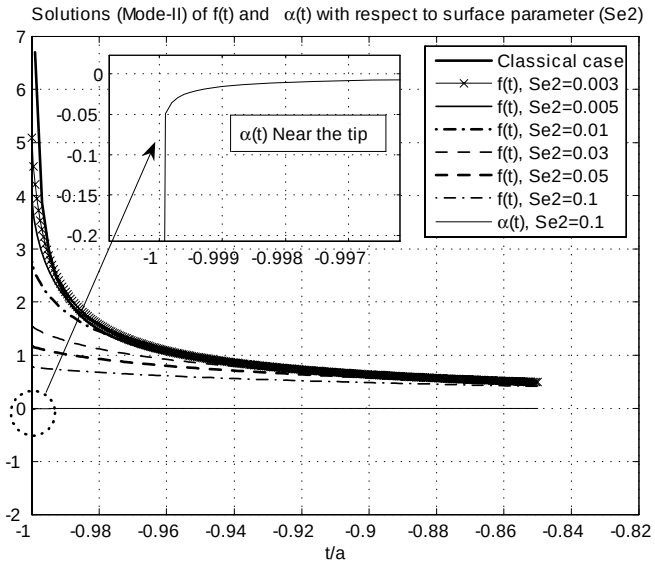

Figure 27: *The solution of* $f(t)$ *and* $\alpha(t)$ *(Mode-II), where,* $0.003 < Se_2 < 0.1,\ \sigma_{xy}^{\infty}/\mu = 0.3$

For the mode-I case, in contrast to the classical case (where $\beta(t) = 0$), we have non-zero solutions for both the functions $g(t)$ and $\beta(t)$ (see, Fig. 26) and both values decrease as the surface effects become significant. This is due mainly to the non-zero contribution of the surface parameters (J_o (related to K_1) and Se_1) implemented in Eq. (4.52). In the case of a mode-II crack, we obtain practically zero distributions for $\alpha(t)$, except in the vicinity of crack tips. The value of $f(t)$, in this case as well, varies with respect to the surface parameter Se_2 (see, Fig. 27) reflecting the effects of surface elasticity. We note here that the solutions presented in Fig. 26 and 27 exhibit strong dependency on surface material properties ($\mu^s,\ \sigma_o,\ \lambda^s$) which may differ depending on the particular materials under consideration. For example, for a material where $\sigma_o >> 0$, the solutions ($\alpha(t)$ and

$f(t)$ in Fig. 27) will closely resemble those in Fig. 26 and vice-versa for a material with sufficiently small J_o ($J_o \approx 0$). Since we currently have very limited sources of surface material properties (See [16]), no quantitative predictions are possible for specific materials. However, the method presented here is sufficiently general to incorporate a wide range of surface parameters in the physical domain. We also note here that the solutions obtained satisfy the imposed natural end conditions ($i.e.(k-1)g(\pm a) + \beta(\pm a) = 0$, $(k-1)f(\pm a) + \alpha(\pm a) = 0$). For example, in the Mode-I case, end values for $g(t)$ and $\beta\,(t)$ are estimated as:

$$g(-1) = 0.8658,\ \beta(-1) = -0.9523,\ \text{when } \sigma_{yy}^{\infty}/\mu = 0.3,\ k = 2.1.$$

The corresponding natural end conditions in this case are given as

$$(k-1)g(\pm a) + \beta(\pm a) = 0$$

which are clearly satisfied by substituting the obtained end values at $t = -1$.

4.4.2 Stress Distributions Near the Crack Tip

Based on the numerical estimations of $\alpha(t)$, $\beta\,(t)$, $f(t)$ and $g(t)$, we can derive a semi-analytic solution for the mode I and mode II cases via Eqs. (4.53-54) and Eqs. (4.58-59), respectively. For example on the $x-$axis, we obtain from Eq. (4.6):

$$\sigma_{yy} - i\sigma_{xy} = 2\Omega'(z) - \theta'\,(z)\,.$$

Therefore, from Eqs. (4.53-54) and Eqs. (4.58-59), the corresponding stress distribution can be expressed as

$$\sigma_{yy} = \frac{1}{\pi}\int_{-a}^{+a} \frac{g(t)}{t-z}dt + \frac{1}{2}\sigma_{yy}^{\infty} - \frac{1}{2\pi}\int_{-a}^{+a} \frac{\beta(t)}{t-z}dt, (\text{Mode-I}), \tag{4.63}$$

$$\sigma_{xy} = \frac{1}{\pi}\int_{-a}^{+a} \frac{f(t)}{t-z}dt + \frac{1}{2}\sigma_{xy}^{\infty} - \frac{1}{2\pi}\int_{-a}^{+a} \frac{\alpha(t)}{t-z}dt, \text{ (Mode-II).} \tag{4.64}$$

By expanding the Cauchy integrals in Eqs. (4.63-4), we have that

$$\begin{aligned} \int_{-a}^{+a} \frac{g(t)}{t-z} &= g(\pm a)\ln r + O(1), \int_{-a}^{+a} \frac{\beta(t)}{t-z} = \beta(\pm a)\ln r + O(1), \\ \int_{-a}^{+a} \frac{f(t)}{t-z} &= f(\pm a)\ln r + O(1), \int_{-a}^{+a} \frac{\alpha(t)}{t-z} = \alpha(\pm a)\ln r + O(1), \end{aligned} \tag{4.65}$$

where $r = |z-a|$. This suggests, together with the bounded end values of $g(t)$, $\beta(t)$, $f(t)$ and $\alpha(t)$, the corresponding stress fields, in the plane crack case, again reduces from a strong square root singularity to a weaker logarithmic singularity (see the results in Figs. 28-29). However, one interesting exceptional case is found in the case of Mode-I fracture when $\sigma_o = 0$. In this case, the corresponding stress distributions continue to exhibit the strong square root singularity at the crack-tips even in the presence of these surface effects. This can be immediately seen from Eq. (4.28b) by setting $\sigma_o = 0$:

$$\frac{2}{\pi}\int_{-a}^{+a} \frac{g(t)}{t-t_o}dt + 2\sigma_{yy}^{\infty} - \frac{1}{\pi}\int_{-a}^{+a} \frac{\beta(t)}{t-t_o}dt = 0.$$

The corresponding solution of this integral equation has been well-studied and indeed demonstrates a strong square root singularity at the crack-tips (see, for example, [65, 66]).

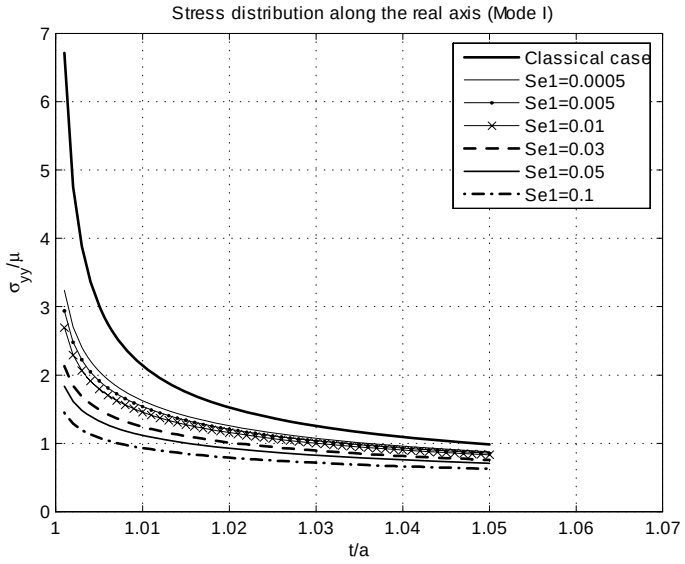

Figure 28: *Stress distribution with respect to surface parameter* (Se_1), $\sigma_{yy}^{\infty}/\mu = 0.3$

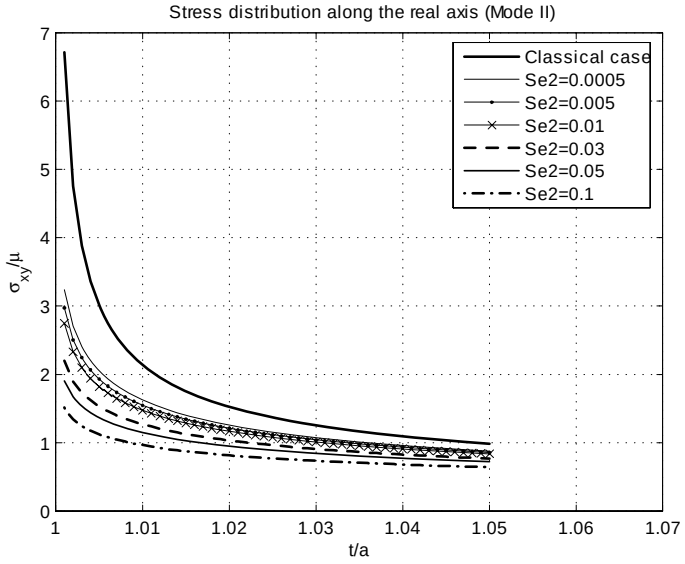

Figure 29: *Stress distribution with respect to surface parameter* (Se_2), $\sigma_{xy}^{\infty}/\mu = 0.3$

As we see from Figs. (28-29), the solutions in both cases (mode-I & mode-II)

reduce to those of the classical case when the surface effects become negligible. Further, the graphs clearly indicate that the surface effects can effectively reduce the corresponding stress distributions. In this regard, since the surface parameters (Se_1, Se_2) are controlled by variations of the crack size, our results also indicate that the corresponding stresses are strongly dependent on crack size. In fact, size dependency of stress fields in materials are the dominant phenomena in the deformations of small scale structures such as nano-inhomogeneities, nano-composite materials and dislocations in sufficiently small-scale structures (see, for example, [16, 44]). We also note here that, in view of Eqs. (4.18-19) and the associated derivations in sections 3.1-3.3, the general solution for the mixed mode problem (mode-I + mode-II) reduces to that of the mode-I and mode-II cases, separately, even when the surface effects are incorporated (see, the compatible results from classical fracture mechanics, [65, 66]).

Finally, it is of interest to ask whether we may choose particular end conditions to achieve bounded stresses of the most significant stress components. For example, in the Mode-I case, the logarithmic singularity in σ_{yy} can be removed when

$$2g(\pm a) = \beta(\pm a) \rightarrow [2g(\pm a) + \beta(\pm a)] \ln r = 0$$

(see Eqs. (4.63) and (4.65)). By finding solutions of the corresponding singular integro differential equations which now involve hyper-singular terms (see Eqs. (4.24a) and (4.25a)). In this respect it is worth emphasizing that in the case of Mode-II fracture with $\sigma_o \neq 0$; only ONE end condition is required at each crack-tip to remove the entire singularity (*i.e.* $2f(\pm a) = \alpha(\pm a)$,see also [84]). However, in these cases, the existence of admissible, bounded solutions is yet to be decided.

4.5 SUMMARY

Through this Chapter, we have considered the plane deformations of a linearly elastic solid in the cases where either a Mode-I or Mode-II crack is present and when the contributions of surface effects are taken into account. Complete semi-analytic solutions are obtained (valid through the entire domain of interest) by solving a series of two coupled Cauchy singular integro-differential equations

It is shown that the incorporation of surface effects reduces the degree of singularity from the classical strong square-root singularity to a weaker logarithmic singularity in the plane case with one exception when surface tension is removed ($\sigma_o = 0$) from the Mode-I fracture system. In this case the corresponding stress fields continue to exhibit the strong square root singularity. The incorporation of surface effects can effectively reduce the corresponding stress distributions and results in elastic responses being size dependent. In addition, we found that the general solution for the mixed mode problem (Mode-I + Mode-II) reduces to those of the mode-I and mode-II cases, separately, even when the surface effects are incorporated. Finally, the analysis of end conditions of the corresponding coupled BVPs reveals that only one end condition can be imposed, at each crack tip, in each case (Mode-I and Mode-II, respectively) except Mode-II fracture case with $\sigma_o = 0$. In this case, not a single end condition can be imposed at each crack tip.

CHAPTER 5

THE EFFECTS OF SURFACE ELASTICITY ON A MODE-III INTERFACE CRACK

5.1 INTRODUCTION

The analysis of the problem of a crack at the interface between dissimilar elastic materials is critical for the understanding of the mechanics and fracture mechanisms of advanced composite materials (for example, laminar and fiber-reinforced composites) where, for example, a high possibility of material debonding and cracking or sliding at the interface exists. Consequently, this problem has been the subject of intense research and discussion in the literature.

Throughout this chapter, we consider anti-plane deformations of a linearly elastic solid consisting of two (perfectly) bonded dissimilar isotropic elastic materials (here represented by two bonded half-spaces) in the presence of a crack along the material interface. The methodology and techniques developed in the previous chapters (in the case of homogeneous crack problems) are further extended to the present case. Most importantly, we project surface properties in a way that each crack face (upper and lower faces) has its own distinct elastic properties which are different from those of each of the bulk materials (see [94]).

Using complex variable methods, we reduce the corresponding problem to a system of coupled Cauchy singular integro-differential equations [65] which is then solved numerically using an adapted collocation technique [77]. This leads to a complete semi-analytic solution valid throughout the entire domain of interest.

We show that the corresponding stress fields again exhibit clear signs of size-dependency and accommodate the results from both the homogeneous crack case and the classical solution when corresponding conditions are imposed. In particular, we show that, among various other interesting phenomena, the stress component (σ_{xz}) demonstrates a discontinuity across the bi-material interface which is in contrast to the classical results from linear elastic fracture mechanics [66, 92].

5.2 ANTI-PLANE INTERFACE CRACK PROBLEM WITH SURFACE EFFECTS

We examine anti-plane deformations of two bonded dissimilar linearly elastic and homogeneous isotropic solids occupying a cylindrical region in $\mathbb{R}^3$ with generators parallel to the $z-$axis of a rectangular Cartesian coordinate system and incorporating a single crack $[-a \leq x \leq a], (y = 0)$ on its interface. We assume that the elastic bi-material cylinder under consideration is infinite in extent and is subjected to uniform remote shear stress $\sigma_{yz} = \sigma_{yz}^{\infty}$ (see, Fig. 30).

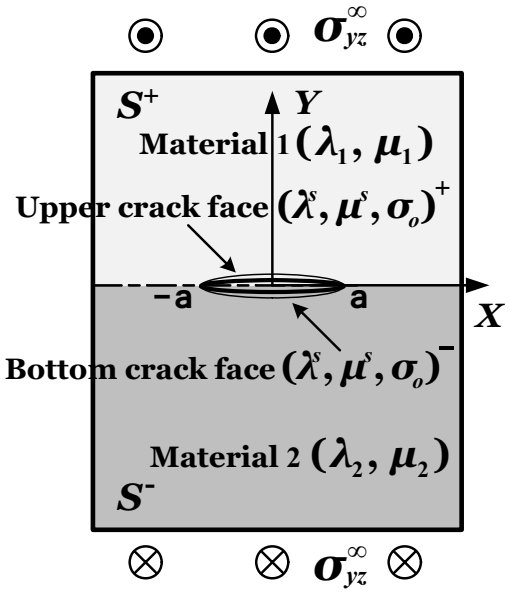

Figure 30: *Schematic of an interface Mode-III crack problem*

5.2.1 Equilibrium Equations and Complex-Variable Formulation

From Eqs. (2.1-2), the equilibrium and constitutive equations describing the deformation of a linearly elastic, homogeneous and isotropic (bulk) solid are given by

$$\sigma_{ij} = \lambda \delta_{ij} \varepsilon_{kk} + 2\mu \varepsilon_{ij}, \tag{5.1a}$$

$$\varepsilon_{ij} = \frac{1}{2}\left(u_{i,j} + u_{j,i}\right). \tag{5.1b}$$

The basic governing equations (including expressions of surface stresses) for an interface Mode-III crack problem are identical to those in the homogeneous Mode-III fracture case since an elastic bi-material can be viewed as a combined set of two distinct elastic materials. Therefore, from Eqs. (3.5-9), we obtain the following for

the equilibrium conditions on the (crack) surface

$$\sigma^s_{xz,x} + [\sigma_{yz}] = 0, \tag{5.2}$$

the expression for the surface stress

$$\sigma^s_{xz} = 2(\mu^s - \sigma_o)\varepsilon_{xz} = \frac{\mu^s - \sigma_o}{\mu}\sigma_{xz}, \because \varepsilon^s_{xz} = \varepsilon_{xz}, \tag{5.3}$$

and complex variable representations of the corresponding displacement and stress components

$$w = \mathrm{Re}[\Omega(z)], \quad \Omega(z) = w(x,y) + i\psi(x,y), \tag{5.4}$$

$$\frac{d\Omega}{dz}(z) = \Omega'(z) = \frac{\partial w}{\partial x} - i\frac{\partial w}{\partial y} = \frac{1}{\mu}\left(\sigma_{xz} - i\sigma_{yz}\right), \tag{5.5}$$

$$\sigma_{yz} = \frac{\mu i}{2}\left[\Omega'(z) - \overline{\Omega'(z)}\right], \quad \sigma_{xz} = \frac{\mu}{2}\left[\Omega'(z) + \overline{\Omega'(z)}\right], \tag{5.6}$$

where $\Omega(z)$ is an analytic function of z in the domain under consideration (in the present case, $S^+ \cup S^- = S$ exterior to the crack as depicted in Fig. 30)

5.2.2 A Traction-free Mode-III Interface Crack Problem in the Presence of Surface Elasticity

Let the upper half-plane ($y > 0$, occupied by *material "1"*) and the lower half-plane ($y < 0$, occupied by *material "2"*) be designated the "+" and "−" sides of the crack, respectively. The elastic properties of *material "1"* and *material "2"* are, in general, different. We further consider the situation where the interface under consideration is perfectly bonded, across which the traction (σ_{yz}) and displacement (w) are continuous (note that σ_{xz} is not necessarily continuous across the interface.). Then the displacements and stresses for the upper and lower half-plane can be expressed as

$$w^{S^+} = \frac{1}{2}\left[\Omega_1(z) + \overline{\Omega_1(z)}\right], \text{ for upper half } \left(S^+,\ y > 0\right), \tag{5.7a}$$

$$w^{S^-} = \frac{1}{2}\left[\Omega_2(z) + \overline{\Omega_2(z)}\right], \text{ for lower half } \left(S^-,\ y<0\right), \tag{5.7b}$$

$$\sigma_{yz}^{S^+} = \frac{\mu_1 i}{2}\left[\Omega_1'(z) - \overline{\Omega_1'(z)}\right],\ \sigma_{xz}^{S^+} = \frac{\mu_1}{2}\left[\Omega_1'(z) + \overline{\Omega_1'(z)}\right], \text{ for upper half } \left(S^+,\ y>0\right), \tag{5.8a}$$

$$\sigma_{yz}^{S^-} = \frac{\mu_2 i}{2}\left[\Omega_2'(z) - \overline{\Omega_2'(z)}\right],\ \sigma_{xz}^{S^-} = \frac{\mu_2}{2}\left[\Omega_2'(z) + \overline{\Omega_2'(z)}\right], \text{ for lower half } \left(S^-,\ y<0\right), \tag{5.8b}$$

where, subscripts "1" and "2" represent the quantities from the upper half (S^+) plane and lower half plane (S^-), respectively. From Eq. (5.2), the boundary conditions on the (crack) surface can be written as;

$$\frac{\partial \sigma_{xz}^s}{\partial x} + (\sigma_{yz})^+ - (\sigma_{yz})^- = 0, \text{ on the upper face,} \tag{5.9a}$$

$$\frac{\partial \sigma_{xz}^s}{\partial x} + (\sigma_{yz})^+ - (\sigma_{yz})^- = 0, \text{ on the lower face,} \tag{5.9b}$$

where, in the case of the present crack problem, the terms $(\sigma_{yz})^-$ in (5.9a) and $(\sigma_{yz})^+$ in (5.9b) are zero, since no material is defined between the upper and lower crack face (material discontinuity along the cut $y = 0, -a < x < a$). In addition, from Eq. (5.3), the surface conditions on either side of the crack face $[-a < x < a], (y = \pm 0)$ can be formulated as follows

$$(\sigma_{yz})^+ = -\frac{\partial \sigma_{xz}^s}{\partial x} = -(\mu^s - \sigma_o)^+ \frac{\partial^2 w^+}{\partial x^2}, \text{ on the upper face,} \tag{5.10a}$$

$$(\sigma_{yz})^- = +\frac{\partial \sigma_{xz}^s}{\partial x} = +(\mu^s - \sigma_o)^- \frac{\partial^2 w^-}{\partial x^2}, \text{ on the lower face,} \tag{5.10b}$$

where, $(\mu^s - \sigma_o)^+ \neq (\mu^s - \sigma_o)^-$, in general. Adding and subtracting Eqs. (5.10 a-b) yields

$$(\sigma_{yz})^+ + (\sigma_{yz})^- = -(\mu^s - \sigma_o)^+ \left(\frac{\partial^2 w^+}{\partial x^2}\right) + (\mu^s - \sigma_o)^- \left(\frac{\partial^2 w^-}{\partial x^2}\right), \tag{5.11a}$$

$$(\sigma_{yz})^+ - (\sigma_{yz})^- = -(\mu^s - \sigma_o)^+ \left(\frac{\partial^2 w^+}{\partial x^2}\right) - (\mu^s - \sigma_o)^- \left(\frac{\partial^2 w^-}{\partial x^2}\right), \tag{5.11b}$$

where, from Eqs. (5.7a-b)

$$\frac{\partial^2 w^+}{\partial x^2} = \frac{1}{2}\left[\Omega_1''(z)^+ + \overline{\Omega_1''(z)}^+\right],\ \frac{\partial^2 w^-}{\partial x^2} = \frac{1}{2}\left[\Omega_2''(z)^- + \overline{\Omega_2''(z)}^-\right]. \tag{5.12}$$

The aforementioned assumptions imply that the displacements and stresses are continuous across the bi-material interface away from the crack $(y = 0, |x| > a,)$. Therefore, we derive from Eqs. (5.7-8) that

$$\mu_1\left[\Omega_1'(z)^+ - \overline{\Omega_1'(z)}^+\right] = \mu_2\left[\Omega_2'(z)^- - \overline{\Omega_2'(z)}^-\right],$$

$$\Omega_1(z)^+ + \overline{\Omega_1(z)}^+ = \Omega_2(z)^- + \overline{\Omega_2(z)}^-,\quad y = 0,\quad x > |a|.$$

By applying the relations $\overline{\Omega_1'(z)}^+ = \overline{\Omega_1'}(z)^-$, on $y = \pm 0$, we have

$$\mu_1\Omega_1'(z)^+ + \mu_2\overline{\Omega_2'}(z)^+ = \mu_2\Omega_2'(z)^- + \mu_1\overline{\Omega_1'}(z)^-, \tag{5.13a}$$

$$\Omega_1(z)^+ - \overline{\Omega_2}(z)^+ = \Omega_2(z)^- - \overline{\Omega_1}(z)^-. \tag{5.13b}$$

Now, in view of Eqs. (5.13a-b), define analytic functions $\theta(z)$ and $\psi(x)$ in the whole plane $(S^+ \cup S^- = S\ )$ cut along $L = -a \le x \le a\ ,\ y = 0$ as

$$\mu_1\Omega_1'(z) + \mu_2\overline{\Omega_2'}(z) = \mu_2\Omega_2'(z) + \mu_1\overline{\Omega_1'}(z) \equiv \theta(z), \tag{5.14a}$$

$$\Omega_1'(z) - \overline{\Omega_2'}(z) = \Omega_2'(z) - \overline{\Omega_1'}(z) \equiv \psi(z). \tag{5.14b}$$

(Again, with the surface energy $\theta(z) \neq 0$, as $w^+ \neq w^-$ on $-a < x < a,\ y = \pm 0$). Therefore, Eq. (5.14a) can be re-written for the upper and lower half planes as

$$\overline{\Omega_2'}(z) \equiv -\frac{\mu_1}{\mu_2}\Omega_1'(z) + \frac{1}{\mu_2}\theta(z),\ \text{for upper half plane } \left(S^+\right), \tag{5.15a}$$

$$\overline{\Omega_1'}(z) \equiv -\frac{\mu_2}{\mu_1}\Omega_2'(z) + \frac{1}{\mu_1}\theta(z),\quad \text{for lower half plane } \left(S^-\right). \tag{5.15b}$$

From (5.15a-b), Eq (5.14b) becomes

$$\Omega_1'(z) = \frac{\mu_2\psi(z)}{\mu_1 + \mu_2} + \frac{1}{\mu_1 + \mu_2}\theta(z),\quad \text{for upper half plane } \left(S^+\right), \tag{5.16a}$$

$$\Omega_2'(z) = \frac{\mu_1 \psi(z)}{\mu_1+\mu_2} + \frac{1}{\mu_1+\mu_2}\theta(z), \text{ for lower half plane } \left(S^-\right). \tag{5.16b}$$

Then, by applying Eqs. (5.15-16), Eq. (5.12) can be re-formulated in terms of $\psi(z)$ and $\theta(z)$ as:

$$\frac{\partial^2 w^+}{\partial x^2} = \frac{1}{2}\left[\frac{\mu_2}{\mu_1+\mu_2}\left(\psi'(z)^+ - \psi'(z)^-\right) + \frac{1}{\mu_1+\mu_2}\left(\theta'(z)^+ + \theta'(z)^-\right)\right], \tag{5.17a}$$

$$\frac{\partial^2 w^-}{\partial x^2} = \frac{1}{2}\left[\frac{\mu_1}{\mu_1+\mu_2}\left(\psi'(z)^- - \psi'(z)^+\right) + \frac{1}{\mu_1+\mu_2}\left(\theta'(z)^+ + \theta'(z)^-\right)\right], \tag{5.17b}$$

By substituting Eqs. (5.17a-b) back into Eqs. (5.11a-b), we have that

$$(\sigma_{yz})^+ + (\sigma_{yz})^- = -\frac{A^s}{\mu_1+\mu_2}\left(\frac{\psi'(z)^+ - \psi'(z)^-}{2}\right) - \frac{B^s}{\mu_1+\mu_2}\left(\frac{\theta'(z)^+ + \theta'(z)^-}{2}\right), \tag{5.18a}$$

$$(\sigma_{yz})^+ - (\sigma_{yz})^- = -\frac{C^s}{\mu_1+\mu_2}\left(\frac{\psi'(z)^+ - \psi'(z)^-}{2}\right) - \frac{D^s}{\mu_1+\mu_2}\left(\frac{\theta'(z)^+ + \theta'(z)^-}{2}\right), \tag{5.18b}$$

where

$$A^s \equiv \mu_2(\mu^s - \sigma_o)^+ + \mu_1(\mu^s - \sigma_o)^-,\ B^s \equiv (\mu^s - \sigma_o)^+ - (\mu^s - \sigma_o)^-,$$
$$C^s \equiv \mu_2(\mu^s - \sigma_o)^+ - \mu_1(\mu^s - \sigma_o)^-,\ D^s \equiv (\mu^s - \sigma_o)^+ + (\mu^s - \sigma_o)^-.$$

In addition, now the left-hand side of Eqs. (5.18a-b) can be expressed via Eqs. (5.8a-b) and (5.15a-b) as;

$$(\sigma_{yz})^+ + (\sigma_{yz})^- = \frac{i}{2}\left[2\mu_1\Omega_1'(z)^+ + 2\mu_2\Omega_2'(z)^- - \left(\theta(z)^+ + \theta(z)^-\right)\right],$$

$$(\sigma_{yz})^+ - (\sigma_{yz})^- = \frac{i}{2}\left[\theta(z)^+ - \theta(z)^-\right].$$

Therefore, we obtain from Eqs. (5.16a-b) that

$$(\sigma_{yz})^+ + (\sigma_{yz})^- = \frac{i}{2}\left[\frac{2\mu_1\mu_2}{\mu_1+\mu_2}\left(\psi(z)^+ + \psi(z)^-\right) + \frac{\mu_1-\mu_2}{\mu_1+\mu_2}\left(\theta(z)^+ - \theta(z)^-\right)\right], \tag{5.19a}$$

$$(\sigma_{yz})^+ - (\sigma_{yz})^- = \frac{i}{2}\left[\theta(z)^+ - \theta(z)^-\right]. \tag{5.19b}$$

Consequently, from Eqs. (5.19a-b), Eqs. (5.18a-b) take the following forms

$$i\left[\frac{2\mu_1\mu_2}{\mu_1+\mu_2}\left(\psi(z)^+ + \psi(z)^-\right) + \frac{\mu_1-\mu_2}{\mu_1+\mu_2}\left(\theta(z)^+ - \theta(z)^-\right)\right] \tag{5.20a}$$
$$= -\frac{A^s}{\mu_1+\mu_2}\left(\psi'(z)^+ - \psi'(z)^-\right) - \frac{B^s}{\mu_1+\mu_2}\left(\theta'(z)^+ + \theta'(z)^-\right),$$

$$i\left[\theta(z)^+ - \theta(z)^-\right] = -\frac{C^s}{\mu_1+\mu_2}\left(\psi'(z)^+ - \psi'(z)^-\right) - \frac{D^s}{\mu_1+\mu_2}\left(\theta'(z)^+ + \theta'(z)^-\right). \tag{5.20b}$$

Next, if we write the unknowns $\psi(z)$ and $\theta(z)$ as Cauchy integrals [65], we have that

$$\psi(z) = \frac{1}{2i\pi}\int_{-a}^{+a}\frac{f(t)}{t-z}dt + \frac{\mu_1+\mu_2}{i\mu_1\mu_2}\left[\sigma_{yz}^{\infty}\right],$$
$$\psi'(z) = \frac{1}{2\pi i}\int_{-a}^{+a}\frac{f(t)\,dt}{(t-z)^2} = -\left[\frac{f(t)}{t-z}\right]_{-a}^{a} + \frac{1}{2\pi i}\int_{-a}^{+a}\frac{f'(t)\,dt}{t-z}, \tag{5.21}$$

where,

$$f(t_o) = \psi(z)^+ - \psi(z)^-.$$

In view of Eqs. (5.20) and (5.21), $\left(\theta(z)^+ - \theta(z)^-\right)$ need to be purely imaginary. Therefore, we express the unknown θ as;

$$\theta(z) = \frac{1}{2i\pi}\int_{-a}^{+a}\frac{i\alpha(t)}{t-z}dt,$$
$$\theta'(z) = \frac{1}{2\pi i}\int_{-a}^{+a}\frac{i\alpha(t)\,dt}{(t-z)^2} = -\left[\frac{i\alpha(t)}{t-z}\right]_{-a}^{a} + \frac{1}{2\pi i}\int_{-a}^{+a}\frac{i\alpha'(t)\,dt}{t-z}, \tag{5.22}$$

where,

$$i\alpha(t_o) = \theta(z)^+ - \theta(z)^-.$$

In addition, the boundary values of on the crack faces can be obtained as (see [65])

$$\psi(z)^+ = \frac{1}{2}f(t_o) + \frac{1}{2i\pi}\int_{-a}^{+a}\frac{f(t)}{t-t_o}dt + \frac{\mu_1+\mu_2}{i\mu_1\mu_2}\left[\sigma_{yz}^{\infty}\right], \tag{5.23a}$$

$$\psi(z)^- = -\frac{1}{2}f(t_o) + \frac{1}{2i\pi}\int_{-a}^{+a}\frac{f(t)}{t-t_o}dt + \frac{\mu_1+\mu_2}{i\mu_1\mu_2}\left[\sigma_{yz}^{\infty}\right]. \tag{5.23b}$$

$$\theta(z)^+ = \frac{1}{2}i\alpha(t_o) + \frac{1}{2i\pi}\int_{-a}^{+a}\frac{i\alpha(t)}{t-t_o}dt, \tag{5.24a}$$

$$\theta(z)^{-} = -\frac{1}{2} i\alpha(t_o) + \frac{1}{2i\pi} \int_{-a}^{+a} \frac{i\alpha(t)}{t - t_o} dt. \tag{5.24b}$$

Finally, from Eqs. (5.20-24), we obtain the following Cauchy singular integro-differential equations for the unknowns $f(t)$ and $\alpha(t),\ t \in (-a, a)$:

$$\begin{aligned} & \frac{2\mu_1\mu_2}{\pi} \int_{-a}^{+a} \frac{f(t)}{t - t_o} dt + 4(\mu_1 + \mu_2) \left[\sigma_{yz}^{\infty}\right] - (\mu_1 - \mu_2)\alpha(t_o) \\ = \ & -A^s f'(t_o) - \frac{B^s}{\pi} \int_{-a}^{+a} \frac{\alpha(t)}{(t - t_o)^2} dt, \end{aligned} \tag{5.25a}$$

$$\alpha(t_o) = \frac{C^s}{\mu_1 + \mu_2} f'(t_o) + \frac{D^s}{\pi(\mu_1 + \mu_2)} \int_{-a}^{+a} \frac{\alpha(t)}{(t - t_o)^2} dt, \tag{5.25b}$$

As in the analysis of the uniqueness results in section (3.23), the natural boundary conditions guaranteeing a unique solution of the BVPs for the anti-plane crack problem are given by

$$\left(w_{,x}^{+} + w_{,x}^{-}\right) w = 0, \text{ at each crack tip.} \tag{5.26}$$

Eq. (5.26) must again be applied for the present BVP. However, in this case, the mechanics of a Mode-III fracture for an interface crack are different in that, in general, $w(\pm a) \neq 0$ at each tip. Consequently, a single end condition (at each crack tip) can be imposed to satisfy equation (5.26). For example, either $f(\pm a) = 0$ or $\alpha(\pm a) = 0$ at each tip. In the following analysis, the admissible end condition is chosen in such a way that the hyper-singular differential equations in (5.25a-b) can be reduced to Cauchy-singular differential equations. More precisely, by imposing $\alpha(\pm a) = 0$ at each crack tip, we obtain from Eqs. (5.21-22) that

$$\theta'(z) = \frac{1}{2\pi i} \int_{-a}^{+a} \frac{i\alpha(t)\, dt}{(t - z)^2} = \frac{1}{2\pi i} \int_{-a}^{+a} \frac{i\alpha'(t)\, dt}{t - z}.$$

Therefore, Eqs. (5.25a-b) are now reduced to the following Cauchy singular integro-differential equations:

$$\begin{aligned} & \frac{2\mu_1\mu_2}{\pi} \int_{-a}^{+a} \frac{f(t)}{t - t_o} dt + 4(\mu_1 + \mu_2) \left[\sigma_{yz}^{\infty}\right] - (\mu_1 - \mu_2)\alpha(t_o) \\ = \ & -A^s f'(t_o) - \frac{B^s}{\pi} \int_{-a}^{+a} \frac{\alpha'(t)}{t - t_o} dt, \end{aligned} \tag{5.27a}$$

$$\alpha(t_o) = \frac{C^s}{\mu_1+\mu_2} f'(t_o) + \frac{D^s}{\pi(\mu_1+\mu_2)} \int_{-a}^{+a} \frac{\alpha'(t)}{t-t_o} dt. \tag{5.27b}$$

5.3 SOLUTION OF SINGULAR INTEGRO-DIFFERENTIAL EQUATIONS BY A COLLOCATION METHOD

The equations appearing in Eqs.(5.27a-b) are coupled first order Cauchy singular-integro differential equations. Although, similar types of equations have been well-studied, classical methods for their solution are not directly applicable here without additional mathematical intervention. In this section, we employ the T^{-1} operator from [92, 93] and a collocation method [77] to analyze the problems mentioned above. By replacing $\alpha(t_o)$ in Eq. (5.27a) and $f'(t_o)$ in Eq. (5.27b) by their counterparts, we derive the following new system of equations;

$$\begin{aligned} &\int_{-a}^{+a} \frac{-\frac{2C^s\mu_1\mu_2}{A^s} f(t) + \left(D^s - \frac{C^sB^s}{A^s}\right)\alpha'(t)}{t-t_o} dt \\ &= \pi\left(\mu_1+\mu_2 - \frac{C^s(\mu_1-\mu_2)}{A^s}\right)\alpha(t_o) + \frac{4\pi C^s(\mu_1+\mu_2)}{A^s}\left[\sigma_{yz}^{\infty}\right]. \end{aligned} \tag{5.28a}$$

$$\begin{aligned} &\int_{-a}^{+a} \frac{-2\mu_1\mu_2 f(t) + \left(\frac{D^s(\mu_1-\mu_2)}{\mu_1+\mu_2} - B^s\right)\alpha'(t)}{t-t_o} dt \\ &= \pi\left(A^s - \frac{C^s(\mu_1-\mu_2)}{\mu_1+\mu_2}\right) f'(t_o) + 4\pi(\mu_1+\mu_2)\left[\sigma_{yz}^{\infty}\right], \end{aligned} \tag{5.28b}$$

Set $\dfrac{t}{a} = x$ in Eqs. (5.28a-b) and obtain

$$\begin{aligned} &\int_{-1}^{+1} \frac{-\frac{2C^s\mu_1\mu_2}{A^s} f(ax) + \left(D^s - \frac{C^sB^s}{A^s}\right)\frac{d\alpha(ax)}{d(ax)}}{a(x-x_o)}(a)\,dx \\ &= \pi\left(\mu_1+\mu_2 - \frac{C^s(\mu_1-\mu_2)}{A^s}\right)\alpha(ax_o) + \frac{4\pi C^s(\mu_1+\mu_2)}{A^s}\left[\sigma_{yz}^{\infty}\right]. \end{aligned} \tag{5.29a}$$

$$\begin{aligned} &\int_{-1}^{+1} \frac{-2\mu_1\mu_2 f(ax) + \left(\frac{D^s(\mu_1-\mu_2)}{\mu_1+\mu_2} - B^s\right)\frac{d\alpha(ax)}{d(ax)}}{a(x-x_o)}(a)\,dx \\ &= \pi\left(A^s - \frac{C^s(\mu_1-\mu_2)}{\mu_1+\mu_2}\right)\frac{df(ax_o)}{d(ax_o)} + 4\pi(\mu_1+\mu_2)\left[\sigma_{yz}^{\infty}\right], \end{aligned} \tag{5.29b}$$

Rewriting $x \to t,\ x_o \to t_o$ and further defining $f(at) = u(t), \alpha(at) = \eta(t)$, from Eqs. (5.29a-b),

$$\begin{aligned}
&\int_{-1}^{+1} \frac{-\frac{2C^s\mu_1\mu_2}{A^s}u(t) + \left(\frac{D^s}{a} - \frac{C^sB^s}{aA^s}\right)\eta'(t)}{t - t_o}dt \\
&= \pi\left(\mu_1 + \mu_2 - \frac{C^s(\mu_1 - \mu_2)}{A^s}\right)\eta(t_o) + \frac{4\pi C^s\left(\mu_1 + \mu_2\right)}{A^s}\left[\sigma_{yz}^{\infty}\right]. \quad (5.30a)
\end{aligned}$$

$$\begin{aligned}
&\int_{-1}^{+1} \frac{-2\mu_1\mu_2u(t) + \left(\frac{D^s(\mu_1 - \mu_2)}{a(\mu_1 + \mu_2)} - \frac{B^s}{a}\right)\eta'(t)}{t - t_o}dt \\
&= \pi\left(\frac{A^s}{a} - \frac{C^s(\mu_1 - \mu_2)}{a\left(\mu_1 + \mu_2\right)}\right)u'(t_o) + 4\pi\left(\mu_1 + \mu_2\right)\left[\sigma_{yz}^{\infty}\right], \quad (5.30b)
\end{aligned}$$

We now utilize the first inverse operator T_{1st}^{-1}defined in the following manner (see [92, 93]) ;

$$T_{1st}^{-1}\psi\left(t\right) = \frac{\sqrt{1 - t_o^2}}{\pi}\int_{-1}^{1}\psi\left(t\right)dt - \frac{\sqrt{1 - t_o^2}}{\pi^2}\int_{-1}^{1}\frac{\psi\left(t\right)}{\left(t - t_o\right)\sqrt{1 - t^2}}dt, \quad t_o \in (-1, 1), \tag{5.31}$$

$$T\left(T^{-1}\psi\right) = \psi,$$

It follows then from Eq. (5.30a) that

$$\begin{aligned}
&-\frac{2C^s\mu_1\mu_2}{A^s}u(t_o) + \left(\frac{D^s}{a} - \frac{C^sB^s}{aA^s}\right)\eta'(t_o) \quad (5.32)\\
&= \frac{\sqrt{1 - t_o^2}}{\pi}\int_{-1}^{1}\left[-\frac{2C^s\mu_1\mu_2}{A^s}u(t) + \left(\frac{D^s}{a} - \frac{C^sB^s}{aA^s}\right)\eta'(t)\right]dt \\
&- \frac{\sqrt{1 - t_o^2}}{\pi}\int_{-1}^{1}\frac{\left(\mu_1 + \mu_2 - \frac{C^s(\mu_1 - \mu_2)}{A^s}\right)\eta(t) + \frac{4C^s(\mu_1 + \mu_2)}{A^s}\left[\sigma_{yz}^{\infty}\right]}{\left(t - t_o\right)\sqrt{1 - t^2}}dt.
\end{aligned}$$

Similarly, by applying the second inverse operator T_{2nd}^{-1} as defined by the relation in [77]

$$T_{2nd}^{-1}\psi\left(t\right) = \frac{1}{\pi\sqrt{1 - t_o^2}}\int_{-1}^{1}\psi\left(t\right)dt - \frac{1}{\pi^2\sqrt{1 - t_o^2}}\int_{-1}^{1}\frac{\sqrt{1 - t^2}\psi\left(t\right)}{t - t_o}dt, \quad t_o \in (-1, 1), \tag{5.33}$$

$$T\left(T^{-1}\psi\right) = \psi,$$

we have from Eq. (5.30b) that

$$\begin{aligned}
&\sqrt{1-t_o^2}\left[-2\mu_1\mu_2 u(t_o)+\left(\frac{D^s(\mu_1-\mu_2)}{a\,(\mu_1+\mu_2)}-\frac{B^s}{a}\right)\eta'(t_o)\right] \\
&=\frac{1}{\pi}\int_{-1}^{1}\left[-2\mu_1\mu_2 u(t)+\left(\frac{D^s(\mu_1-\mu_2)}{a\,(\mu_1+\mu_2)}-\frac{B^s}{a}\right)\eta'(t)\right]dt \\
&-\frac{1}{\pi}\int_{-1}^{1}\frac{\sqrt{1-t^2}}{t-t_o}\left[\left(\frac{A^s}{a}-\frac{C^s(\mu_1-\mu_2)}{a\,(\mu_1+\mu_2)}\right)u'(t)+4\,(\mu_1+\mu_2)\left[\sigma_{yz}^{\infty}\right]\right]dt.
\end{aligned} \tag{5.34}$$

If we assume that the functions u and η have an (approximate) expansion of the form

$$u(t_o)=\sum_{m=0}^{N}a_m T_m\,(t_o)\,,\quad \eta(t_o)=\sum_{m=0}^{N}b_m T_m\,(t_o)\,,\quad m=0,1,2,..., \tag{5.35}$$

where $T_m\,(t_o)$ represents the m th Chebychev polynomial of the first kind. By utilizing properties of the Chebychev polynomials presented in sections 3.3.3 and 4.3.1, the Eqs. (5.32) and (5.34) can then be transformed into the following system of equations

$$\begin{aligned}
&\sum_{m=0}^{N}\left[\begin{array}{c} a_m T_m\,(t_o)\left\{2\mu_1\mu_2\sqrt{1-t_o^2}+m\left(\frac{A^s}{a}-\frac{C^s(\mu_1-\mu_2)}{a(\mu_1+\mu_2)}\right)\right\}-\frac{2\mu_1\mu_2}{\pi}a_m\left(\frac{1+(-1)^m}{1-m^2}\right) \\ +b_m\left(\frac{D^s(\mu_1-\mu_2)}{a(\mu_1+\mu_2)}-\frac{B^s}{a}\right)\left\{\frac{(1-(-1)^m)}{\pi}-\sqrt{1-t_o^2}mU_{m-1}\,(t_o)\right\}\end{array}\right] \\
&=-4t_o\,(\mu_1+\mu_2)\left[\sigma_{yz}^{\infty}\right],
\end{aligned} \tag{5.36}$$

where

$$b_m=\frac{a_m\left(-\frac{2C^s\mu_1\mu_2}{A^s}\right)\left[\frac{\sqrt{1-t_o^2}}{\pi}\left(\frac{1+(-1)^m}{1-m^2}\right)-T_m\,(t_o)\right]}{U_{m-1}\,(t_o)\left\{\left(\frac{D^s}{a}-\frac{C^sB^s}{aA^s}\right)m+\sqrt{1-t_o^2}\left(\mu_1+\mu_2-\frac{C^s(\mu_1-\mu_2)}{A^s}\right)\right\}-\frac{(1-(-1)^m)\sqrt{1-t_o^2}}{\pi}\left(\frac{D^s}{a}-\frac{C^sB^s}{aA^s}\right)}. \tag{5.37}$$

We now select the set of collocation points as given by $t_o=t_{oi}=-\cos(\frac{i\pi}{N})$ for $i=1,2,...,N-1$. In addition, by evaluating Cheychev polynomials of the first kind $T_m(t_{oi})$ and the second kind $U_{m-1}(t_{oi})$ with respect to each collocation point, we find that

$$T_m\left(-\cos\left(\frac{i\pi}{N}\right)\right)=-\cos\left(\frac{im\pi}{N}\right),\quad U_{m-1}\left(-\cos\left(\frac{i\pi}{N}\right)\right)=\frac{\sin\left(\frac{mi\pi}{N}\right)}{\sin\left(\frac{i\pi}{N}\right)}. \tag{5.38}$$

Consequently, in view of Eq. (39), Eqs. (37-38) further reduce to the following system of linear equations

$$\sum_{m=0}^{N}\left[\begin{array}{r} -a_m\cos\left(\frac{im\pi}{N}\right)\left\{2\mu_1\mu_2\sqrt{1-\left(\cos(\frac{i\pi}{N})\right)^2}+m\left(\frac{A^s}{a}-\frac{C^s(\mu_1-\mu_2)}{a(\mu_1+\mu_2)}\right)\right\}-\frac{2\mu_1\mu_2}{\pi}a_m\left(\frac{1+(-1)^m}{1-m^2}\right) \\ +b_m\left(\frac{D^s(\mu_1-\mu_2)}{a(\mu_1+\mu_2)}-\frac{B^s}{a}\right)\left\{\frac{(1-(-1)^m)}{\pi}-\sqrt{1-\left(\cos(\frac{i\pi}{N})\right)^2}m\left(\frac{\sin\left(\frac{mi\pi}{N}\right)}{\sin\left(\frac{i\pi}{N}\right)}\right)\right\}\end{array}\right]$$

$$=4\cos(\frac{i\pi}{N})\left(\mu_1+\mu_2\right)\left[\sigma_{yz}^{\infty}\right], \tag{5.39}$$

where

$$b_m=\mathbf{K}a_m,$$

$$\mathbf{K}=\left(-\frac{2C^s\mu_1\mu_2}{A^s}\right)\left[\frac{\sqrt{1-\left(\cos(\frac{i\pi}{N})\right)^2}}{\pi}\left(\frac{1+(-1)^m}{1-m^2}\right)+\cos\left(\frac{im\pi}{N}\right)\right]$$
$$\times[\frac{\sin\left(\frac{mi\pi}{N}\right)}{\sin\left(\frac{i\pi}{N}\right)}\left\{\left(\frac{D^s}{a}-\frac{C^sB^s}{aA^s}\right)m+\sqrt{1-\left(\cos(\frac{i\pi}{N})\right)^2}\left(\mu_1+\mu_2-\frac{C^s(\mu_1-\mu_2)}{A^s}\right)\right\}$$
$$-\frac{(1-(-1)^m)\sqrt{1-\left(\cos(\frac{i\pi}{N})\right)^2}}{\pi}\left(\frac{D^s}{a}-\frac{C^sB^s}{aA^s}\right)]^{-1} \tag{5.40}$$

or $1\leq i\leq N-1$.

5.4 RESULTS AND DISCUSSION

In this section, the numerical solution of Eqs. (5.39-40) is performed for a range of surface parameters. The listed values are estimated properties of "GaN" obtained from the work of Sharma and Ganti in [16].

$$S_e=\frac{\mu^s-\sigma_o}{a(\mu_1+\mu_2)}: 8.65\times10^{-5}<S_e<0.0865,\quad 10nm<a<10\mu m,$$
$$\mu^s=161.73(J/m^2),\quad \sigma_o=1.3(J/m^2),\quad \mu=168(Gpa). \tag{5.41}$$

Throughout the analysis, we have considered the situation where the material properties of the upper half plane are assumed to be ten times bigger than those

of the lower half plane (i.e. $\mu_1 = 168(Gpa),\ \mu_2 = 16.8(Gpa)$), whereas the surface material properties on upper and lower crack face are set to be equal (i.e. $(\mu^s - \sigma_o)^+ = (\mu^s - \sigma_o)^-$). This is only because, we currently have very limited sources of surface material properties available [16]. However, the method presented here is sufficiently general in that it incorporates the case in which the surface material properties from the upper and lower crack face are different ($(\mu^s - \sigma_o)^+ \neq (\mu^s - \sigma_o)^-$, see Eqs. (5.18a-b) and (5.39-40)) and a wide range of surface parameters in the physical domain.

5.4.1 Comparison with Known Classical Results

We first examine how the solution obtained here, in the presence of surface effects, deviates from the solution of the classical interface anti-plane crack problem. The corresponding analytical solution of the latter problem can be found in [65, 66]:

$$\psi(z) = \left(\frac{\mu_1 + \mu_2}{\mu_1 \mu_2}\right) \frac{-i\sigma_{yz}^{\infty} z}{\sqrt{z^2 - a^2}}.$$

Evaluating $\psi(z)$ at $(-a < t < a)$, we have that

$$\psi(z)^+ = \left(\frac{\mu_1 + \mu_2}{\mu_1 \mu_2}\right) \frac{-i\sigma_{yz}^{\infty} t}{\sqrt{-(a^2 - t^2)}} = \left(\frac{\mu_1 + \mu_2}{\mu_1 \mu_2}\right) \frac{-\sigma_{yz}^{\infty} t}{\sqrt{a^2 - t^2}}, \text{ on the upper face,} \tag{5.42a}$$

$$\psi(z)^- = \left(\frac{\mu_1 + \mu_2}{\mu_1 \mu_2}\right) \frac{i\sigma_{yz}^{\infty} t}{\sqrt{-(a^2 - t^2)}} = \left(\frac{\mu_1 + \mu_2}{\mu_1 \mu_2}\right) \frac{\sigma_{yz}^{\infty} t}{\sqrt{a^2 - t^2}}, \text{ on the lower face.} \tag{5.42b}$$

Then the corresponding difference between the upper and lower faces can be defined from Eqs. (5.21a-b) by

$$\psi(z)^+ - \psi(z)^- = f(t) = \left(\frac{\mu_1 + \mu_2}{\mu_1 \mu_2}\right) \frac{-2\sigma_{yz}^{\infty} t}{\sqrt{a^2 - t^2}}, \quad -a < t < a. \tag{5.43}$$

Also, in the classical case, $\theta(z)$ is found to be zero. Thus, we have that

$$\theta(z)^+ - \theta(z)^- = \alpha(t) = 0. \tag{5.44}$$

Returning to our problem, the values of $f(t)$ can be estimated using Eqs. (5.39-40) and are plotted in Figs. 32 and 34, where the parameter S_e is varied by changing the dimension of the crack (i.e. $20nm < 2a < 20\mu m$). The adopted numerical method performs well ensuring rapid convergence (see Fig. 31).

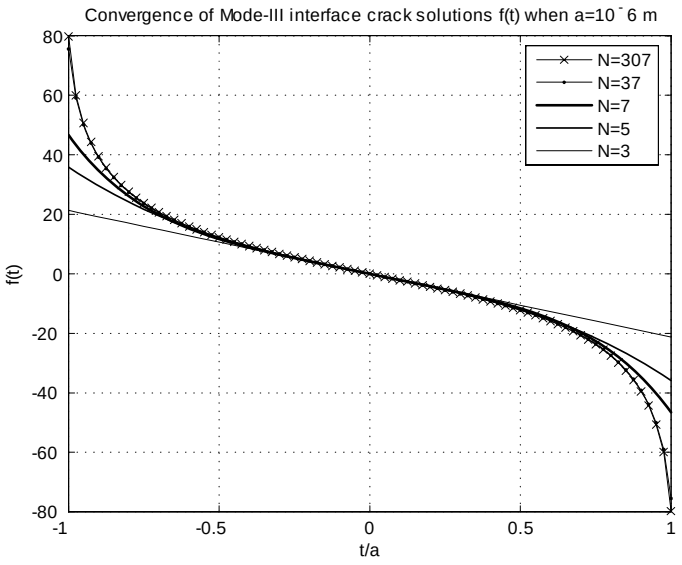

Figure 31: *Convergence of the solution f(t) with respect to number of iterations(N)*

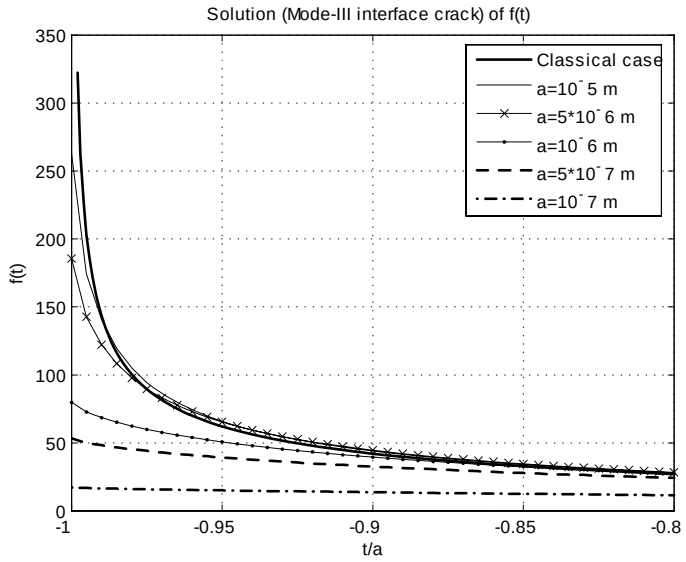

Figure 32: *The solution $f(t)$ (Mode-III interface crack), where* $\frac{\sigma_{yz}^{\infty}}{\mu_1+\mu_2} = 0.1$

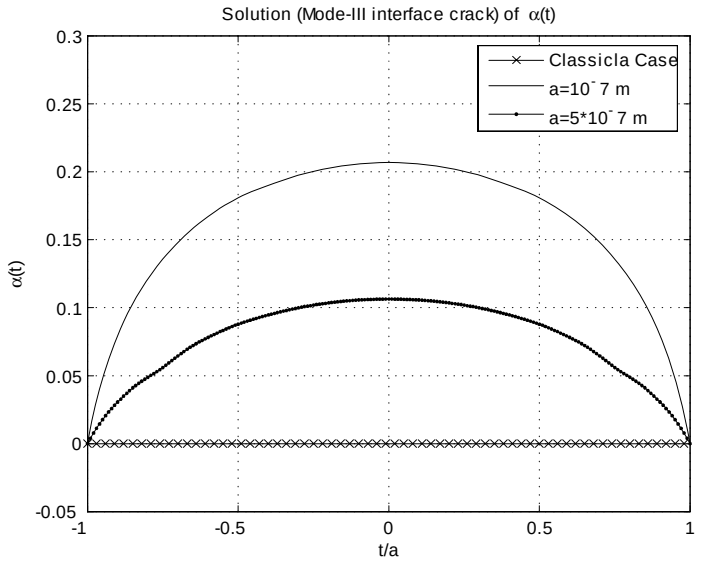

Figure 33: *The solution $\alpha(t)$ (Mode-III interface crack), where* $\frac{\sigma_{yz}^{\infty}}{\mu_1+\mu_2} = 0.1$

Figs. 32-33 clearly indicates that our solution reduces to that of the classical

case as the surface effect becomes negligible. In particular, since we have non-zero values for $f(\pm a) \neq 0$ at the crack tip (see Fig 31-32 and 34), the corresponding stresses (σ_{yz}) must be singular there. We have also found that, in contrast to classical results (see Eq. (5.44)), $\alpha(t)$ has indeed non-zero values (see Fig. 33) resulting in a noticeable contribution to the stress field especially on the real axis. In this respect, the corresponding stresses (σ_{xz}) are finite at the crack tips because $\alpha(t)$ is bounded at these points. These will be the subject of the following section. Finally, our solution accommodates that of the classical result in both single material Mode-III and bi-material Mode-III fractures cases (See Fig. 34).

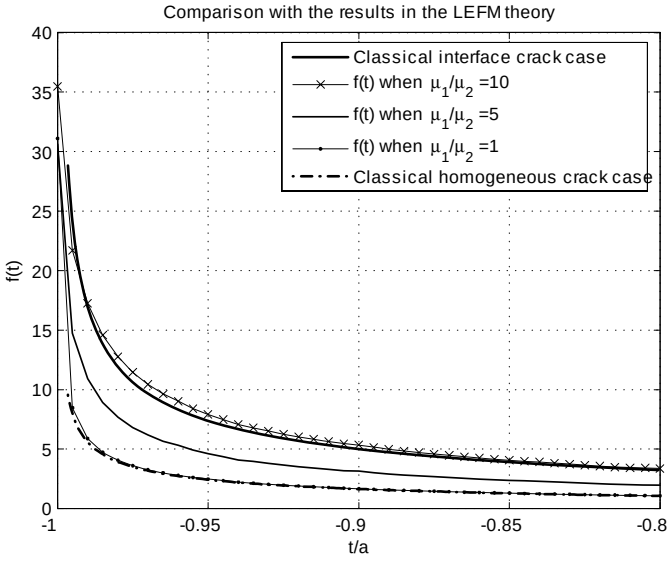

Figure 34: *The solution $f(t)$ with respect to the ratio of μ_1/μ_2 , where $\frac{\sigma_{yz}^{\infty}}{\mu_1+\mu_2} =$* 0.1

5.4.2 Analysis of the Stress Distribution under the Influence of Surface Effects

From Eqs. (5.8a-b) and (5.16a-b), stresses (σ_{yz}) on the upper and lower half plane can be determined by

$$\sigma_{yz}^{S^+} = \frac{\mu_1 i}{2(\mu_1+\mu_2)}\left[\mu_2\psi(z) + \theta(z) - \mu_2\overline{\psi(z)} - \overline{\theta(z)}\right],$$

$$\sigma_{xz}^{S^+} = \frac{\mu_1}{2(\mu_1+\mu_2)}\left[\mu_2\psi(z) + \theta(z) + \mu_2\overline{\psi(z)} + \overline{\theta(z)}\right], \text{ for upper half plane } \left(S^+,\ y>0\right),$$

$$\sigma_{yz}^{S^-} = \frac{\mu_2 i}{2(\mu_1+\mu_2)}\left[\mu_1\psi(z) + \theta(z) - \mu_1\overline{\psi(z)} - \overline{\theta(z)}\right],$$

$$\sigma_{xz}^{S^-} = \frac{\mu_2}{2(\mu_1+\mu_2)}\left[\mu_1\psi(z) + \theta(z) + \mu_1\overline{\psi(z)} + \overline{\theta(z)}\right], \text{ for lower half plane } \left(S^-,\ y<0\right),$$

where, the complex potentials $\psi(t)$ and $\theta(t)$ can be obtained via Eqs. (5.21) and (5.22) with known solutions of $f(t)$ and $\alpha(t)$. We have found that, in contrast to the classical case (where surface effects are completely neglected), the major stress component (σ_{yz}) at the crack tips exhibits a weaker logarithmic singularity rather than the classical strong square root singularity. However, the minor stress component (σ_{xz}), different to those predicted by the classical LEFM theory, is non-zero and remains finite at the crack tips because $\alpha(t)$ is bounded at the tips (i.e. $\alpha(\pm a)=0$). These can be immediately seen by expanding the Cauchy integrals in the corresponding stress expressions. More precisely, We obtain the following expansions at the crack tips

$$\sigma_{yz}^{+} = -\frac{\mu_1}{2}\,\mathrm{Im}\left[\frac{\mu_2}{2i\pi(\mu_1+\mu_2)}\left(f(\pm a)\ln r\right) + \frac{1}{i\mu_1}\left[\sigma_{yz}^{\infty}\right] + \frac{1}{2\pi(\mu_1+\mu_2)}\left(\alpha(\pm a)\ln r\right) + O(1)\right],$$

$$\sigma_{xz}^{+} = \frac{\mu_1}{2}\,\mathrm{Re}\left[\frac{\mu_2}{2i\pi(\mu_1+\mu_2)}\left(f(\pm a)\ln r\right) + \frac{1}{i\mu_1}\left[\sigma_{yz}^{\infty}\right] + \frac{1}{2\pi(\mu_1+\mu_2)}\left(\alpha(\pm a)\ln r\right) + O(1)\right].$$

The above further reduces

$$\sigma_{yz}^{+} = -\frac{\mu_1}{2}\left[\frac{\mu_2}{2\pi(\mu_1+\mu_2)}\left(f(\pm a)\ln r\right) + \frac{1}{\mu_1}\left[\sigma_{yz}^{\infty}\right] + O(1)\right],$$

$$\sigma_{xz}^{+} = \frac{\mu_1}{2}\left[\frac{1}{2\pi(\mu_1+\mu_2)}\left(\alpha(\pm a)\ln r\right) + O(1)\right].$$

Clearly σ_{yz} exhibit a weaker logarithmic singularity, whereas σ_{xz} is finite at the tips, because $f(\pm a) \neq 0$ and $\alpha(\pm a) = 0$, at the crack tips, respectively. More importantly, the results in Figs. 35-36 illustrate the fact that σ_{yz} is continuous across the bi-material interface, whereas σ_{xz} jumps across the interface. The result is in sharp contrast to the classical fracture mechanics solution and due mainly to the non-zero contribution of the complex potential $\theta(z)$ in the presence of the surface effects.

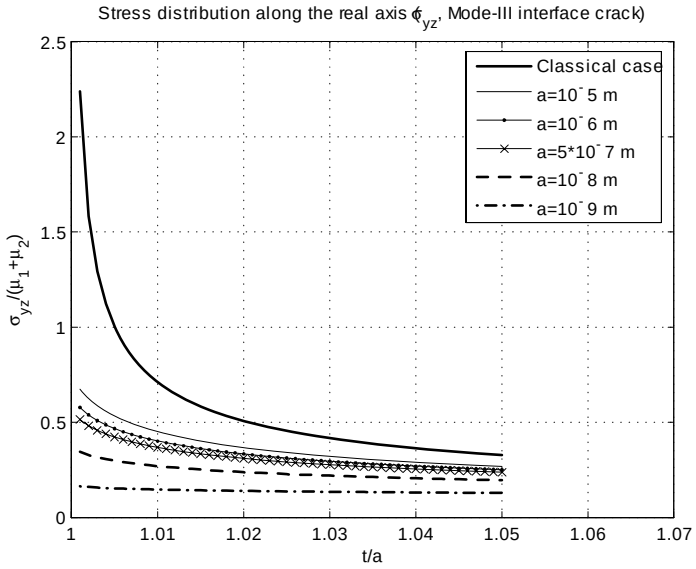

Figure 35: *Stress distribution (σ_{yz}) with respect to surface parameter, where* $\frac{\sigma_{yz}^{\infty}}{\mu_1+\mu_2} = 0.1$

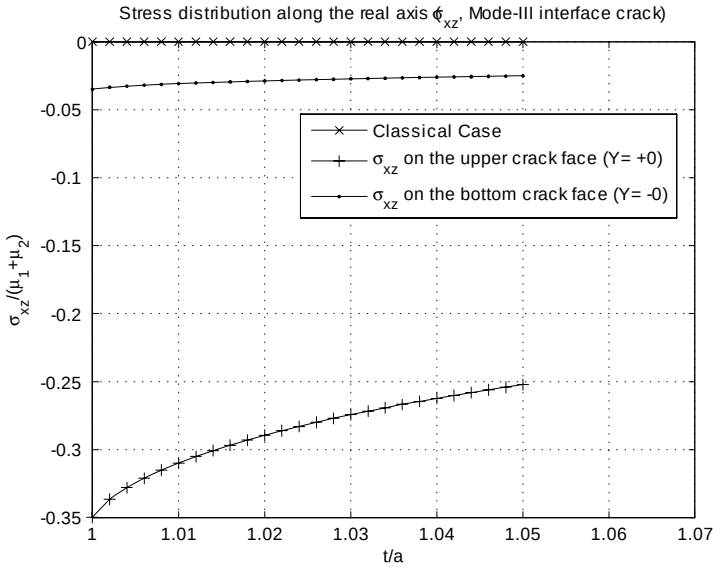

Figure 36: *The jump of stress (σ_{xz}) across the bi-material interface*

Remark 4 *In the theory of linear elastic fracture mechanics, σ_{xz} is continuous across the bi-material interface, since its values are zero on either side of the interface*

$$\sigma_{xz}^{+} = \frac{\mu_1}{2(\mu_1+\mu_2)}\left[\mu_2\psi(z) + \overline{\mu_2\psi(z)}\right] = \sigma_{xz}^{-} = \frac{\mu_2}{2(\mu_1+\mu_2)}\left[\mu_1\psi(z) + \mu_1\overline{\psi(z)}\right] = 0,$$

$$\because \psi(z) = \mathrm{Im},\ on\ \ y = \pm 0,\ x > |a|.$$

However, the interface condition under consideration indicates that traction (σ_{yz}) and displacements (w) are continuous across the interface, yet σ_{xz} are not necessarily continuous. Perhaps, the continuity in stress ($\sigma_{xz}^{+} = \sigma_{xz}^{-}$) indicates the symmetrical nature of the problem in which the solution of Mode-III interface crack problem can be obtained by superposing solutions of two half-plane problems with distinct material properties on either side of the interface. In the case where the surface elasticity is present, the symmetry breaks down due to the effect of surface

mechanics and therefore, the above mentioned statement can no longer be satisfied. In fact, stress (σ_{xz}) on both sides of the interface can be estimated as

$$\sigma_{xz}^{+} = \frac{\mu_1}{2(\mu_1+\mu_2)}\left[\theta(z) + \overline{\theta(z)}\right], \ \text{on } y = 0^{+}, \quad x > |a|,$$

$$\sigma_{xz}^{-} = \frac{\mu_2}{2(\mu_1+\mu_2)}\left[\theta(z) + \overline{\theta(z)}\right], \ \text{on } y = 0^{-}, \quad x > |a|.$$

This clearly indicates that the estimated stresses differ with the material properties ($\mu_1,\ \mu_2$) of the upper and lower half-plane.

Finally, we see from Fig. 35 that stress distributions along the real axis increase when surface effects become negligible and eventually converge to the classical result. Further, since the surface parameter S_e in Eq. (5.41) is controlled by variations in the crack length, our results also indicate that the corresponding stresses are strongly dependent on crack size [16, 44].

5.5 SUMMARY

In this chapter, we have incorporated the effects of surface elasticity into a classical Mode-III interface crack problem arising in the anti-plane shear deformations of a linearly elastic bi-material. It is shown that the major stress component (σ_{yz}) at the crack tips exhibits a weaker logarithmic singularity rather than the classical strong square root singularity, even in the case of an interface crack problem. In particular, we note that the minor stress contributor (σ_{xz}) is finite at the crack tips and jumps across the bi-material interface, in contrast to the classical result from the LEFM theory. It is also again confirmed that, in the case of an interface crack, surface effects, acting as reinforcement, effectively reduce the amount of stresses and lead to the corresponding stress fields being size-dependent.

It is concluded that, in contrast to the homogeneous Mode-III crack problem, a single end condition can be imposed at each crack tip chosen here as $\alpha(\pm a) =$

0 in order to reduce the corresponding systems of integro-differential equations: from hyper-singular to Cauchy singular-integro differential equations. Other choice of end conditions can be made, for example, $f(\pm a) = 0$ at the tips, instead of prescribing $\alpha(\pm a) = 0$. This would result in the major stress components (σ_{yz}) remaining finite (yet σ_{xz} remains unbounded at the crack tips). However this requires solving a system of coupled hyper-singular differential equations which have yet to be studied. The solution and analysis presented in this chapter, are sufficiently general in that, they accommodate the results both obtained from the homogeneous material case (in Chapter. 3) by imposing $\mu_1 = \mu_2$ and $(\mu^s - \sigma_o)^+ = (\mu^s - \sigma_o)^-$, and the classical results, when the surface effects are neglected in the corresponding system.

CHAPTER 6

THE EFFECTS OF SURFACE ELASTICITY ON AN INTERFACE CRACK IN PLANE DEFORMATIONS

6.1 INTRODUCTION

Plane-strain deformations of a linearly elastic bi-material incorporating cracks in its interfacial region has drawn considerable attention from both theoreticians and practitioners in the fields of composite engineering and fracture mechanics. Traditional attempts in the modeling and solution of such problems have incorporated the classical assumptions of LEFM theory which, unfortunately have led to various inconsistencies, for example, the rapid oscillation in both stress and displacement fields in the vicinity of the crack further leading to the possibility of material interpenetration between two dissimilar materials (see, for example, [66, 70]). As discussed earlier, the region near the surface of a solid material experiences local environment changes resulting in the deviation of properties as they approach the boundaries of a bulk material. Consequently, in the case of interface crack problems, a more accurate analysis can be achieved by incorporating a separate description of surface mechanics on either side of the crack surfaces (faces).

In this respect, we examine, throughout this chapter, a bi-material crack-matrix system undergoing plane-strain deformations and subjected to uniform remote tension and in-plane shear in the presence of surface elasticity. More precisely, we formulate governing equations in order to include surface effects onto the surfaces of the interface crack [95] using the Gurtin-Murdoch surface elasticity model [26,

34, 47]. By employing complex variable methods, we reduce the corresponding BVP to a coupled system of singular integro-differential equations. This system is highly complicated in nature so much so that the numerical method adopted in the previous chapters is not immediately applicable. Instead, we introduce an effective, yet simple method (referred to here as a 'direct method') through which the corresponding numerical procedure is simplified immensely. The efficiency and accuracy of the direct method is also cross-checked with the results obtained using the conventional method. A complete semi-analytic solution (valid in the entire domain of interest) is then obtained in both Mode-I and Mode-II fracture cases.

It is shown that, among other various interesting phenomena, the introduction of surface elasticity results in the corresponding stress distribution being size-dependent and leads to logarithmic singular stresses at the crack tips. In particular, we show that the addition of surface mechanics on the faces of the interface crack also eliminates the oscillatory behavior of the corresponding solutions leading to a smooth and non-oscillatory stress distribution within the entire domain under consideration.

6.2 PLANE-STRAIN INTERFACE CRACK PROBLEM WITH SURFACE EFFECTS

We consider plane deformations of a linearly elastic and homogeneous isotropic bi-material solid incorporating a single traction-free (tractions on the crack faces are zero. *i.e.* $\boldsymbol{t}_{yy} = \boldsymbol{t}_{xy} = 0$ on $-a \leq x \leq a,\ y = \pm 0$.) interface crack subjected to uniform remote tension ($\sigma_{yy} = \sigma^{\infty}_{yy}$, Mode-I) and in-plane shear ($\sigma_{xy} = \sigma^{\infty}_{xy}$, Mode-II) stresses (see, Fig. 37).

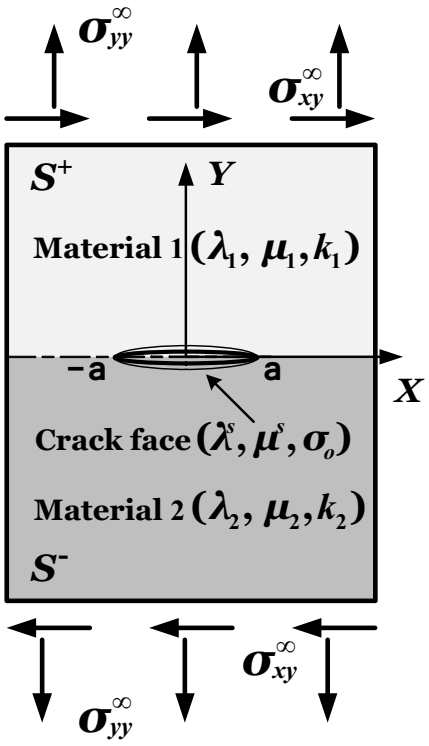

Figure 37: *Schematic of a plane-strain interface crack problem*

6.2.1 Governing Equations and Complex Variable Formulation

The equilibrium and constitutive equations for a linearly elastic, homogeneous isotropic material is given by (See, Eqs. (2.1-2))

$$\sigma_{ij} = \lambda\delta_{ij}\varepsilon_{kk} + 2\mu\varepsilon_{ij}, \tag{6.1a}$$

$$\varepsilon_{ij} = \frac{1}{2}\left(u_{i,j} + u_{j,i}\right). \tag{6.1b}$$

Because the plane-strain deformations of an elastic bi-material solid can be regarded as a combined description of two distinct materials occupying each part of

the bi-material, the governing equations and the corresponding problem settings from the homogeneous Mode-I and Mode-II fracture problems are still valid in the present case. Therefore, in the absence of body forces, the corresponding governing equations of two-dimensional elasticity are given directly from Eqs. (4.3a-b) as:

$$2\mu\left(u+iv\right)=\kappa\Omega(z)-z\overline{\Omega'(z)}-\overline{w\left(z\right)}, \tag{6.2a}$$

$$\sigma_{yy}-i\sigma_{xy}=\Omega'(z)+\overline{\Omega'(z)}+z\overline{\Omega''(z)}+\overline{w'\left(z\right)}, \tag{6.2b}$$

Here $\Omega(z)$ and $w\left(z\right)$ are analytic functions of the complex variable $z=x+iy$ in the cut plane $S^{+}\cup S^{-}=S$ outside the crack (see Fig. 37.) and κ is defined as:

$$\kappa=\frac{\lambda+3\mu}{\lambda+\mu}=3-4\upsilon \text{ (for plane-strain)},$$

where υ is Poisson's ratio taking values in the range $0<\upsilon<\frac{1}{2}$. Thus, κ satisfies the following inequality

$$1<\kappa<3.$$

In addition, from Eqs. (4.7-9), the equilibrium conditions on the crack surface and the expression of the surface stress are given respectively as:

$$\left[\sigma_{yy}-i\sigma_{xy}\right]=i\sigma^{s}_{xx,x}-\sigma_{o}\frac{\partial^{2}\nu}{\partial x^{2}}. \tag{6.3}$$

$$\sigma^{s}_{xx,x}=\frac{\partial\left(\sigma_{o}+\left(2\mu^{s}-\sigma_{o}+\lambda^{s}\right)\frac{\partial u}{\partial x}\right)}{\partial x}=\left(2\mu^{s}-\sigma_{o}+\lambda^{s}\right)\frac{\partial^{2}u}{\partial x^{2}}. \tag{6.4}$$

We note here that the coherency assumption between the surface and the adjoined bulk material is again adopted in the present case so that $\varepsilon^{s}_{xx}=\varepsilon_{xx}$. Finally from Eqs. (6.3-4), we obtain that

$$\left[\sigma_{yy}-i\sigma_{xy}\right]=iJ_{o}\frac{\partial^{2}u}{\partial x^{2}}-\sigma_{o}\frac{\partial^{2}\nu}{\partial x^{2}},\quad\text{where}\quad J_{o}\equiv2\mu^{s}-\sigma_{o}+\lambda^{s}. \tag{6.5}$$

6.2.2 A Traction-free Interface Crack Problem in the Presence of Surface Elasticity

Let us now consider an linearly elastic bi-plane where the upper half-plane ($y > 0$, occupied by *material "1"*) and the lower half-plane ($y < 0$, occupied by *material "2"*) are designated the "$-$" and "$+$" sides of the crack, respectively (see. Fig. 37). We note that the elastic properties of *material "1"* and *material "2"* are, in general, different. Then, from Eqs. (6.2a-b), the displacements and stresses on the upper (S^+) and lower (S^-) regions can be written, respectively, as

$$\begin{aligned} 2\mu_1 \left(u+iv\right)^{S^+} &= \kappa_1 \Omega_1(z) - z\overline{\Omega_1'(z)} - \overline{w_1\left(z\right)}, \\ \left(\sigma_{yy} - i\sigma_{xy}\right)^{S^+} &= \Omega_1'(z) + \overline{\Omega_1'(z)} + z\overline{\Omega_1''(z)} + \overline{w_1'\left(z\right)}, \text{ for upper region } \left(y>0\right). \end{aligned} \tag{6.6a}$$

$$\begin{aligned} 2\mu_2 \left(u+iv\right)^{S^-} &= \kappa_2 \Omega_2(z) - z\overline{\Omega_2'(z)} - \overline{w_2\left(z\right)}, \\ \left(\sigma_{yy} - i\sigma_{xy}\right)^{S^-} &= \Omega_2'(z) + \overline{\Omega_2'(z)} + z\overline{\Omega_2''(z)} + \overline{w_2'\left(z\right)}, \text{ for lower region } \left(y<0\right), \end{aligned} \tag{6.6b}$$

where, again, subscripts "1" and "2" denote the corresponding quantities from the upper and lower regions, respectively. Here, we confine our interest to the situation where the interface ($y = 0, |x| > a,$) under consideration is perfectly bonded, across which the tractions ($\sigma_{yy},\ \sigma_{xy}$) and displacements ($u,\ v$) are continuous. Then, from Eqs. (6.6a-b), the stress continuity condition yields

$$\left[\Omega_1(z) + z\overline{\Omega_1'(z)} + \overline{w_1\left(z\right)}\right]^+ = \left[\Omega_2(z) + z\overline{\Omega_2'(z)} + \overline{w_2\left(z\right)}\right]^- .$$

Noting that $\overline{\Omega_1'(z)}^+ = \overline{\Omega_1}\left(z\right)^-$, on $y = \pm 0$, we have

$$\Omega_1(z)^+ - z\overline{\Omega_2'}(z)^+ - \overline{w_2}\left(z\right)^+ = \Omega_2(z)^- - z\overline{\Omega_1'}(z)^- - \overline{w_1}\left(z\right)^- . \tag{6.7}$$

In view of Eq. (11), we define an analytic function $\theta(z)$ in the entire plane ($S^+ \cup S^- = S$) outside the cut $L = -a \leq x \leq a$, $y = 0$ as:

$$\Omega_1(z) - z\overline{\Omega_2'}(z) - \overline{w_2}(z) = \Omega_2(z) - z\overline{\Omega_1'}(z) - \overline{w_1}(z) \equiv \theta(z). \tag{6.8}$$

Therefore, we obtain

$$w_1(z) = \overline{\Omega_2}(z) - z\Omega_1'(z) - \overline{\theta}(z), \tag{6.9a}$$

$$w_2(z) = \overline{\Omega_1}(z) - z\Omega_2'(z) - \overline{\theta}(z). \tag{6.9b}$$

By substituting Eqs. (6.9a-b) back into Eqs. (6.6a-b), the displacements from the upper and bottom regions can be re-written as:

$$2\mu_1(u+iv)^{S^+} = \kappa_1\Omega_1(z) - \Omega_2(\overline{z}) - (z-\overline{z})\overline{\Omega_1'(z)} + \theta(\overline{z}), \tag{6.10a}$$

$$2\mu_2(u+iv)^{S^-} = \kappa_2\Omega_2(z) - \Omega_1(\overline{z}) - (z-\overline{z})\overline{\Omega_2'(z)} + \theta(\overline{z}). \tag{6.10b}$$

Next, applying the displacement continuity condition, Eqs. (6.10a-b) yield

$$\frac{1}{\mu_1}\left[\kappa_1\Omega_1(z) - \Omega_2(\overline{z}) + \theta(\overline{z})\right]^+ = \frac{1}{\mu_2}\left[\kappa_2\Omega_2(z) - \Omega_1(\overline{z}) + \theta(\overline{z})\right]^-.$$

Since $\Omega_1(\overline{z})^+ = \Omega_1(z)^-$ on $y = \pm 0$, we have

$$(\mu_1 + \mu_2\kappa_1)\Omega_1(z)^+ - \mu_1\theta(z)^+ = (\mu_2 + \mu_1\kappa_2)\Omega_2(z)^- - \mu_2\theta(z)^-. \tag{6.11}$$

From Eq. (6.11), we again define an analytic function $\phi(z)$ in the entire plane ($S^+ \cup S^- = S$) outside the cut region ($L = -a \leq x \leq a$, $y = 0$) as:

$$(\mu_1 + \mu_2\kappa_1)\Omega_1(z) - \mu_1\theta(z) = (\mu_2 + \mu_1\kappa_2)\Omega_2(z) - \mu_2\theta(z) \equiv \phi(z). \tag{6.12}$$

Thus, we find that

$$\Omega_1(z) = \frac{\phi(z) + \mu_1\theta(z)}{(\mu_1 + \mu_2\kappa_1)},\ \Omega_2(z) = \frac{\phi(z) + \mu_2\theta(z)}{(\mu_2 + \mu_1\kappa_2)}. \tag{6.13}$$

In addition, from Eqs. (6.6a-b) and (6.9a-b), we derive expressions for the stresses

$$\left(\sigma_{yy}-i\sigma_{xy}\right)^{S^+}=\Omega_1'\left(z\right)+\Omega_2'\left(\overline{z}\right)+\left(z-\overline{z}\right)\overline{\Omega_1''\left(z\right)}-\theta'\left(\overline{z}\right),$$
$$\text{for upper region } \left(S^+\ ,\ y>0\right), \tag{6.14a}$$

$$\left(\sigma_{yy}-i\sigma_{xy}\right)^{S^-}=\Omega_2'\left(z\right)+\Omega_1'\left(\overline{z}\right)+\left(z-\overline{z}\right)\overline{\Omega_2''\left(z\right)}-\theta'\left(\overline{z}\right),$$
$$\text{for lower region } \left(S^-\ ,\ y<0\right). \tag{6.14b}$$

Consequently, the stress and displacement fields for the upper and lower regions can now be completely described by two complex potentials $(\phi\left(z\right),\ \theta\left(z\right))$ which are analytic in the entire plane $(S^+\cup S^-=S)$ outside the cut $(L=-a\leq x\leq a,$ $y=0\ )$.

Now, from Eq. (6.5), the boundary conditions on the crack faces $(-a<x<a,$ $y=\pm 0)$ can be written as (see Eqs. (4.12-13)):

$$\left(\sigma_{yy}-i\sigma_{xy}\right)^{+}=iJ_o\frac{\partial^2 u^+}{\partial x^2}-\sigma_o\frac{\partial^2 \nu^+}{\partial x^2},$$
$$\left(\sigma_{yy}-i\sigma_{xy}\right)^{-}=-iJ_o\frac{\partial^2 u^-}{\partial x^2}+\sigma_o\frac{\partial^2 \nu^-}{\partial x^2}.$$

In view of Eqs. (6.14a-b), we obtain from the above that

$$\left(\sigma_{yy}-i\sigma_{xy}\right)^{+}=\Omega_1'\left(z\right)^{+}+\Omega_2'\left(z\right)^{-}-\theta'\left(z\right)^{-}=iJ_o\frac{\partial^2 u^+}{\partial x^2}-\sigma_o\frac{\partial^2 \nu^+}{\partial x^2},$$
$$\text{on the upper face, } (y=+0,\ -a<x<a), \tag{6.15a}$$
$$\left(\sigma_{yy}-i\sigma_{xy}\right)^{-}=\Omega_2'\left(z\right)^{-}+\Omega_1'\left(z\right)^{+}-\theta'\left(z\right)^{+},=-iJ_o\frac{\partial^2 u^-}{\partial x^2}+\sigma_o\frac{\partial^2 \nu^-}{\partial x^2},$$
$$\text{on the lower face, } (y=-0,\ -a<x<a). \tag{6.15b}$$

Adding and subtracting Eqs. (6.15a) and (6.15b) yields

$$\theta'\left(z\right)^{+}-\theta'\left(z\right)^{-}=iJ_o\left(\frac{\partial^2 u^+}{\partial x^2}+\frac{\partial^2 u^-}{\partial x^2}\right)-\sigma_o\left(\frac{\partial^2 \nu^+}{\partial x^2}+\frac{\partial^2 \nu^-}{\partial x^2}\right), \tag{6.16a}$$

$$2\left(\Omega_1'(z)^+ + \Omega_2'(z)^-\right) - \left(\theta'(z)^+ + \theta'(z)^-\right)$$
$$= iJ_o\left(\frac{\partial^2 u^+}{\partial x^2} - \frac{\partial^2 u^-}{\partial x^2}\right) - \sigma_o\left(\frac{\partial^2 \nu^+}{\partial x^2} - \frac{\partial^2 \nu^-}{\partial x^2}\right). \tag{6.16b}$$

From (6.13), Eqs. (6.16b) can be re-written as

$$\frac{2\phi'(z)^+}{\mu_1+\mu_2\kappa_1} + \frac{2\phi'(z)^-}{\mu_2+\mu_1\kappa_2} + \left(\frac{\mu_1-\mu_2\kappa_1}{\mu_1+\mu_2\kappa_1}\right)\theta'(z)^+ + \left(\frac{\mu_2-\mu_1\kappa_2}{\mu_2+\mu_1\kappa_2}\right)\theta'(z)^-$$
$$= iJ_o\left(\frac{\partial^2 u^+}{\partial x^2} - \frac{\partial^2 u^-}{\partial x^2}\right) - \sigma_o\left(\frac{\partial^2 \nu^+}{\partial x^2} - \frac{\partial^2 \nu^-}{\partial x^2}\right). \tag{6.17}$$

Now, from Eqs. (6.10a-b), we have that

$$\frac{\partial^2}{\partial x^2}\left(u^+ + iv^+\right) = \frac{1}{2\mu_1}\left(\kappa_1\Omega_1''(z)^+ - \Omega_2''(z)^- + \theta''(z)^-\right), \tag{6.18a}$$

$$\frac{\partial^2}{\partial x^2}\left(u^- + iv^-\right) = \frac{1}{2\mu_2}\left(\kappa_2\Omega_2''(z)^- - \Omega_1''(z)^+ + \theta''(z)^+\right). \tag{6.18b}$$

Adding and subtracting Eqs. (6.15a) and (6.15b) with the further use of Eq. (6.13) gives

$$\frac{\partial^2}{\partial x^2}\left(u^+ + u^- + i\left(v^+ + v^-\right)\right) = \frac{\left(\mu_2\kappa_1-\mu_1\right)\phi''(z)^+}{2\mu_1\mu_2\left(\mu_1+\mu_2\kappa_1\right)}$$
$$+ \frac{\left(\mu_1\kappa_2-\mu_2\right)\phi''(z)^-}{2\mu_1\mu_2\left(\mu_2+\mu_1\kappa_2\right)} + \frac{\kappa_1}{\mu_1+\mu_2\kappa_1}\theta''(z)^+ + \frac{\kappa_2}{\mu_2+\mu_1\kappa_2}\theta''(z)^-, \tag{6.19a}$$

$$\frac{\partial^2}{\partial x^2}\left(u^+ - u^- + i\left(v^+ - v^-\right)\right) = \frac{1}{2\mu_1\mu_2}\left(\phi''(z)^+ - \phi''(z)^-\right). \tag{6.19b}$$

Consequently, from Eqs. (23a-b), Eqs. (20a) and (21) take the following forms

$$\theta'(z)^+ - \theta'(z)^- = iJ_o\,\mathrm{Re}\,\mathcal{P} - \sigma_o\,\mathrm{Im}\,\mathcal{P}, \tag{6.20a}$$

$$\frac{2\phi'(z)^+}{\mu_1+\mu_2\kappa_1} + \frac{2\phi'(z)^-}{\mu_2+\mu_1\kappa_2} + \left(\frac{\mu_1-\mu_2\kappa_1}{\mu_1+\mu_2\kappa_1}\right)\theta'(z)^+ + \left(\frac{\mu_2-\mu_1\kappa_2}{\mu_2+\mu_1\kappa_2}\right)\theta'(z)^-$$
$$= \frac{iJ_o}{2\mu_1\mu_2}\,\mathrm{Re}\left[\phi''(z)^+ - \phi''(z)^-\right] - \frac{\sigma_o}{2\mu_1\mu_2}\,\mathrm{Im}\left[\phi''(z)^+ - \phi''(z)^-\right]. \tag{6.20b}$$

where $\mathcal{P} = [\frac{\left(\mu_2\kappa_1-\mu_1\right)\phi''(z)^+}{2\mu_1\mu_2\left(\mu_1+\mu_2\kappa_1\right)} + \frac{\left(\mu_1\kappa_2-\mu_2\right)\phi''(z)^-}{2\mu_1\mu_2\left(\mu_2+\mu_1\kappa_2\right)} + \frac{\kappa_1}{\mu_1+\mu_2\kappa_1}\theta''(z)^+ + \frac{\kappa_2}{\mu_2+\mu_1\kappa_2}\theta''(z)^-]$.

Next, if we express the unknowns $\phi'(z)$ and $\theta'(z)$ as Cauchy integrals [65], we have that

$$\phi'(z) = \frac{1}{2\pi i}\int_{-a}^{+a}\frac{f(t)+ig(t)}{t-z}dt + \frac{1}{M}(\sigma_{yy}^{\infty} - i\sigma_{xy}^{\infty}),$$
$$\text{where } M = \left(\frac{1}{\mu_1+\mu_2\kappa_1} + \frac{1}{\mu_2+\mu_1\kappa_2}\right), \tag{6.21}$$
$$\phi''(z) = \frac{1}{2\pi i}\int_{-a}^{+a}\frac{f(t)+ig(t)}{(t-z)^2}dt = -\left[\frac{f(t)+ig(t)}{t-z}\right]_{-a}^{+a} + \frac{1}{2\pi i}\int_{-a}^{+a}\frac{f'(t)+ig'(t)}{t-z}dt.$$

$$\theta'(z) = \frac{1}{2\pi i}\int_{-a}^{+a}\frac{\alpha(t)+i\beta(t)}{t-z}dt, \tag{6.22}$$
$$\theta''(z) = \frac{1}{2\pi i}\int_{-a}^{+a}\frac{\alpha(t)+i\beta(t)}{(t-z)^2}dt = -\left[\frac{\alpha(t)+i\beta(t)}{t-z}\right]_{-a}^{+a} + \frac{1}{2\pi i}\int_{-a}^{+a}\frac{\alpha'(t)+i\beta'(t)}{t-z}dt.$$

In addition, the boundary values of $\phi'(z)$ and $\theta'(z)$ on the crack faces ($-a < t_o < a,\ y = \pm 0$) can be found as (see [65]):

$$\phi'(z)^{+} = \frac{1}{2}\left(f(t_o)+ig(t_o)\right) + \frac{1}{2\pi i}\int_{-a}^{+a}\frac{f(t)+ig(t)}{t-t_o}dt + \frac{1}{M}(\sigma_{yy}^{\infty} - i\sigma_{xy}^{\infty}), \tag{6.23a}$$

$$\phi'(z)^{-} = -\frac{1}{2}\left(f(t_o)+ig(t_o)\right) + \frac{1}{2\pi i}\int_{-a}^{+a}\frac{f(t)+ig(t)}{t-t_o}dt + \frac{1}{M}(\sigma_{yy}^{\infty} - i\sigma_{xy}^{\infty}), \tag{6.23b}$$

$$\theta'(z)^{+} = \frac{1}{2}\left(\alpha(t_o)+i\beta(t_o)\right) + \frac{1}{2\pi i}\int_{-a}^{+a}\frac{\alpha(t)+i\beta(t)}{t-t_o}dt, \tag{6.24a}$$

$$\theta'(z)^{-} = -\frac{1}{2}\left(\alpha(t_o)+i\beta(t_o)\right) + \frac{1}{2\pi i}\int_{-a}^{+a}\frac{\alpha(t)+i\beta(t)}{t-t_o}dt. \tag{6.24b}$$

Thus, in view of Eqs. (6.21-6.24), Eqs. (6.20a-b) can be re-written as;

$$\alpha(t_o)+i\beta(t_o) = iJ_o\,\mathrm{Re}\,\mathcal{F} - \sigma_o\,\mathrm{Im}\,\mathcal{F}, \tag{6.25a}$$

$$\begin{aligned}
&\left(f(t_o)+ig(t_o)\right)\left(\frac{1}{\mu_1+\mu_2\kappa_1} - \frac{1}{\mu_2+\mu_1\kappa_2}\right)\\
&+\left(\frac{1}{\mu_1+\mu_2\kappa_1} + \frac{1}{\mu_2+\mu_1\kappa_2}\right)\frac{1}{\pi i}\int_{-a}^{+a}\frac{f(t)+ig(t)}{t-t_o}dt + 2(\sigma_{yy}^{\infty} - i\sigma_{xy}^{\infty})\\
&+\frac{\left(\alpha(t_o)+i\beta(t_o)\right)\left(\kappa_2\mu_1^2 - \kappa_1\mu_2^2\right)}{\left(\mu_1+\mu_2\kappa_1\right)\left(\mu_2+\mu_1\kappa_2\right)}\\
&-\frac{\left(\kappa_1\kappa_2-1\right)\mu_1\mu_2}{\pi i\left(\mu_1+\mu_2\kappa_1\right)\left(\mu_2+\mu_1\kappa_2\right)}\int_{-a}^{+a}\frac{\alpha(t)+i\beta(t)}{t-t_o}dt\\
&=\frac{iJ_o}{2\mu_1\mu_2}\,\mathrm{Re}\left[f'(t_o)+ig'(t_o)\right] - \frac{\sigma_o}{2\mu_1\mu_2}\,\mathrm{Im}\left[f'(t_o)+ig'(t_o)\right].
\end{aligned} \tag{6.25b}$$

Here,

$$\begin{aligned}\mathcal{F} = & \frac{\left(f'(t_o)+ig'(t_o)\right)\left(\kappa_1\mu_2^2-\kappa_2\mu_1^2\right)}{2\mu_1\mu_2\left(\mu_1+\mu_2\kappa_1\right)\left(\mu_2+\mu_1\kappa_2\right)} \\ & + \frac{\left(\kappa_1\kappa_2-1\right)}{\left(\mu_1+\mu_2\kappa_1\right)\left(\mu_2+\mu_1\kappa_2\right)}\left(\frac{1}{2\pi i}\right)\int_{-a}^{+a}\frac{f(t)+ig(t)}{\left(t-t_o\right)^2}dt \\ & + \frac{1}{2}\left(\alpha'(t_o)+i\beta'(t_o)\right)\left\{\frac{\kappa_1}{\mu_1+\mu_2\kappa_1}-\frac{\kappa_2}{\mu_2+\mu_1\kappa_2}\right\}+ \\ & \left\{\frac{\kappa_1}{\mu_1+\mu_2\kappa_1}+\frac{\kappa_2}{\mu_2+\mu_1\kappa_2}\right\}\frac{1}{2\pi i}\int_{-a}^{+a}\frac{\alpha(t)+i\beta(t)}{\left(t-t_o\right)^2}dt.\end{aligned}$$

Finally, by separating the real and imaginary parts of Eqs. (6.25a-b), we obtain the following coupled first-order Cauchy singular integro-differential equations for the unknowns $f\left(t\right),\ g\left(t\right),\ \alpha\left(t\right)$ and $\beta\left(t\right)$:

$$\begin{aligned}\alpha(t_o) = & -g'(t_o)\frac{\sigma_o\left(\kappa_1\mu_2^2-\kappa_2\mu_1^2\right)}{2\mu_1\mu_2\left(\mu_1+\mu_2\kappa_1\right)\left(\mu_2+\mu_1\kappa_2\right)} \\ & + \frac{\sigma_o\left(\kappa_1\kappa_2-1\right)}{2\pi\left(\mu_1+\mu_2\kappa_1\right)\left(\mu_2+\mu_1\kappa_2\right)}\int_{-a}^{+a}\frac{f(t)}{\left(t-t_o\right)^2}dt \\ & - \beta'(t_o)\frac{\sigma_o}{2}\left(\frac{\kappa_1}{\mu_1+\kappa_1\mu_2}-\frac{\kappa_2}{\mu_2+\kappa_2\mu_1}\right) \\ & + \frac{\sigma_o}{2\pi}\left(\frac{\kappa_1}{\mu_1+\kappa_1\mu_2}+\frac{\kappa_2}{\mu_2+\kappa_2\mu_1}\right)\int_{-a}^{+a}\frac{\alpha(t)}{\left(t-t_o\right)^2}dt, \qquad (6.26a)\end{aligned}$$

$$\begin{aligned}& - g(t_o)\left(\frac{1}{\mu_1+\mu_2\kappa_1}-\frac{1}{\mu_2+\mu_1\kappa_2}\right) \\ & + \left(\frac{1}{\mu_1+\mu_2\kappa_1}+\frac{1}{\mu_2+\mu_1\kappa_2}\right)\frac{1}{\pi}\int_{-a}^{+a}\frac{f(t)}{t-t_o}dt \\ & - \frac{\beta(t_o)\left(\kappa_2\mu_1^2-\kappa_1\mu_2^2\right)}{\left(\mu_1+\mu_2\kappa_1\right)\left(\mu_2+\mu_1\kappa_2\right)} - \frac{\left(\kappa_1\kappa_2-1\right)\mu_1\mu_2}{\pi\left(\mu_1+\mu_2\kappa_1\right)\left(\mu_2+\mu_1\kappa_2\right)}\int_{-a}^{+a}\frac{\alpha(t)}{t-t_o}dt \\ & = -\frac{J_o}{2\mu_1\mu_2}f'(t_o) - 2\sigma_{xy}^{\infty} \qquad (6.26b)\end{aligned}$$

$$\beta(t_o) = f'(t_o)\frac{J_o\left(\kappa_1\mu_2^2 - \kappa_2\mu_1^2\right)}{2\mu_1\mu_2\left(\mu_1+\mu_2\kappa_1\right)\left(\mu_2+\mu_1\kappa_2\right)} + \frac{J_o\left(\kappa_1\kappa_2-1\right)}{2\pi\left(\mu_1+\mu_2\kappa_1\right)\left(\mu_2+\mu_1\kappa_2\right)}\int_{-a}^{+a}\frac{g(t)}{\left(t-t_o\right)^2}dt + \alpha'(t_o)\frac{J_o}{2}\left(\frac{\kappa_1}{\mu_1+\kappa_1\mu_2} - \frac{\kappa_2}{\mu_2+\kappa_2\mu_1}\right) + \frac{J_o}{2\pi}\left(\frac{\kappa_1}{\mu_1+\kappa_1\mu_2} + \frac{\kappa_2}{\mu_2+\kappa_2\mu_1}\right)\int_{-a}^{+a}\frac{\beta(t)}{\left(t-t_o\right)^2}dt, \tag{6.26c}$$

$$f(t_o)\left(\frac{1}{\mu_1+\mu_2\kappa_1} - \frac{1}{\mu_2+\mu_1\kappa_2}\right) + \left(\frac{1}{\mu_1+\mu_2\kappa_1} + \frac{1}{\mu_2+\mu_1\kappa_2}\right)\frac{1}{\pi}\int_{-a}^{+a}\frac{g(t)}{t-t_o}dt + \frac{\alpha(t_o)\left(\kappa_2\mu_1^2-\kappa_1\mu_2^2\right)}{\left(\mu_1+\mu_2\kappa_1\right)\left(\mu_2+\mu_1\kappa_2\right)} - \frac{\left(\kappa_1\kappa_2-1\right)\mu_1\mu_2}{\pi\left(\mu_1+\mu_2\kappa_1\right)\left(\mu_2+\mu_1\kappa_2\right)}\int_{-a}^{+a}\frac{\beta(t)}{t-t_o}dt = -\frac{\sigma_o}{2\mu_1\mu_2}g'(t_o) - 2\sigma_{yy}^{\infty} \tag{6.26d}$$

Similar to the analysis of the uniqueness results in section 4.24, the natural boundary conditions ensuring a unique solution of the BVPs for the plane-strain interface crack problems are given by

$$\left(u_{,x}^{+} + u_{,x}^{-}\right)u = 0,\ \sigma_o\left(v_{,x}^{+} + v_{,x}^{-}\right)v = 0,\ \text{at each tip } (z = \pm a). \tag{6.27}$$

It is clear from Eq. (6.27) that the maximum number of admissible end conditions in the case of a plane interface crack problem is *two* since, in general, u and v are non-zero at the crack tips ($z = \pm a$). However, one interesting exception is found when $\sigma_o = 0$. In this case, the surface elasticity affects only the equilibrium equation in the x direction, and not that in the y direction. In other words, the second expression of Eq. (6.27) is automatically satisfied and therefore, only *one* end condition can be imposed when $\sigma_o = 0$.

6.3 COUPLED SINGULAR INTEGRO-DIFFERENTIAL EQUATIONS

The equations in Eqs. (6.26a-d) comprise a coupled system of singular-integro differential equations. Solutions of the coprresponding simplified version (non-coupled and Cauchy singular) of such equations have been well established in the literature (see, for example, [77,83,91]). In chapters 4-5, we extended the methods used by the aforementioned authors to the case of a coupled system (two unknowns with two coupled equations) and provided complete semi-analytic solutions. However, the methods used (we refer to the methods here as 'conventional methods') involved substantial 'pre-treatment' of the equations via either regularization (see, for example, [83]) or the so-called 'T^{-1} transformation' ([77]), resulting in a highly complicated system of equations. The pre-treatment is necessary in order to introduce a weight function (e.g. $\sqrt{1-t^2}$) in the corresponding mathematical analysis. Unfortunately, given the additional complications presented in Eqs (6.26a-d) (four unknowns with four coupled equations), it is extremely challenging (and numerically expensive) to solve the corresponding coupled system of differential equations by using conventional methods.

In the following analysis, we directly introduce a weight function without employing the T^{-1} transform (we refer to the method as the 'direct method'). The direct method will simplify the corresponding mathematical and numerical process immensely, since it does not involve additional mathematical pre-treatment. In this respect, a Mode-III fracture case is re-solved using both methods (the direct method and conventional method) to determine whether the direct method indeed produces successful results in comparison to those from the conventional method.

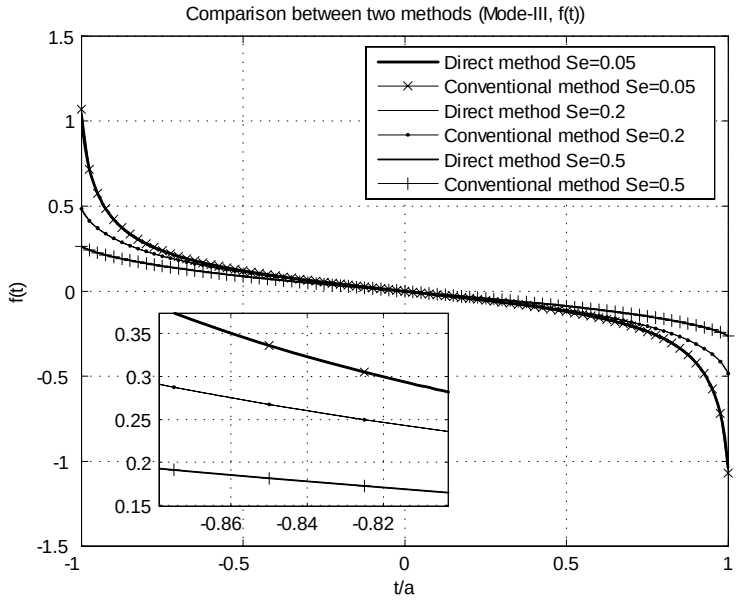

Figure 38: *Comparison of the results (Mode-III, $f(t)$) using the direct and conventional method*

It is clear from Fig. 41 that the direct method produces successful results (in fact, results obtained from both methods are almost identical) and guarantees fast convergence (within 30 iterations). We note here that it is still possible to solve the Eqs. (6.26a-d) by using the conventional method. However, that will only complicate the mathematical procedure and require massive computational resources.

6.3.1 Mode-II ($\sigma_{yy}^{\infty} = 0, \quad \sigma_{xy}^{\infty} \neq 0$) case

By setting $t/a = t$ in Eqs. (6.26a-d) and further defining the unknown functions as (see chapters 4-5 for more details)

$$f(at) = f(t), \; g(at) = g(t), \; \alpha(at) = \alpha(t), \; \beta(at) = \beta(t),$$

we obtain from Eqs. (6.26a-b) that

$$\alpha(t_o) = g'(t_o)\left(\frac{C_s\sigma_o}{2a\mu_1\mu_2}\right) + \frac{D_s\sigma_o}{2a\pi}\int_{-1}^{+1}\frac{f(t)}{(t-t_o)^2}dt - \beta'(t_o)\left(\frac{F_s\sigma_o}{2a}\right) + \left(\frac{E_s\sigma_o}{2a\pi}\right)\int_{-1}^{+1}\frac{\alpha(t)}{(t-t_o)^2}dt, \tag{6.28a}$$

$$-A_s g(t_o) + \frac{B_s}{\pi}\int_{-1}^{+1}\frac{f(t)}{t-t_o}dt - C_s\beta(t_o) - \frac{D_s\mu_1\mu_2}{\pi}\int_{-1}^{+1}\frac{\alpha(t)}{t-t_o}dt = -\left(\frac{J_o}{2a\mu_1\mu_2}\right)f'(t_o) - 2\sigma_{xy}^{\infty}, \tag{6.28b}$$

$$\beta(t_o) = -\left(\frac{C_s J_o}{2a\mu_1\mu_2}\right)f'(t_o) + \frac{D_s J_o}{2a\pi}\int_{-1}^{+1}\frac{g(t)}{(t-t_o)^2}dt + \alpha'(t_o)\left(\frac{F_s J_o}{2a}\right) + \left(\frac{E_s J_o}{2a\pi}\right)\int_{-1}^{+1}\frac{\beta(t)}{(t-t_o)^2}dt, \tag{6.28c}$$

$$A_s f(t_o) + \frac{B_s}{\pi}\int_{-1}^{+1}\frac{g(t)}{t-t_o}dt + C_s\alpha(t_o) - \frac{D_s\mu_1\mu_2}{\pi}\int_{-1}^{+1}\frac{\beta(t)}{t-t_o}dt = -\left(\frac{\sigma_o}{2a\mu_1\mu_2}\right)g'(t_o), \tag{6.28d}$$

where,

$$\left(\frac{1}{\mu_1+\mu_2\kappa_1} - \frac{1}{\mu_2+\mu_1\kappa_2}\right) = A_s, \left(\frac{1}{\mu_1+\mu_2\kappa_1} + \frac{1}{\mu_2+\mu_1\kappa_2}\right) = B_s,$$

$$\frac{(\kappa_2\mu_1^2 - \kappa_1\mu_2^2)}{(\mu_1+\kappa_1\mu_2)(\mu_2+\kappa_2\mu_1)} = C_s, \frac{(\kappa_1\kappa_2 - 1)}{(\mu_1+\kappa_1\mu_2)(\mu_2+\kappa_2\mu_1)} = D_s,$$

$$\left(\frac{\kappa_1}{\mu_1+\kappa_1\mu_2} + \frac{\kappa_2}{\mu_2+\kappa_2\mu_1}\right) = E_s, \left(\frac{\kappa_1}{\mu_1+\kappa_1\mu_2} - \frac{\kappa_2}{\mu_2+\kappa_2\mu_1}\right) = F_s.$$

If we assume that surface tension (σ_o) is equal to zero based on the fact that its contribution to the system is practically negligible (see Fig. 27 and the corresponding discussion), Eqs. (6.28a-d) now reduce to;

$$\alpha(t_o) = 0 \tag{6.29}$$

$$-A_s g(t_o) + \frac{B_s}{\pi}\int_{-1}^{+1}\frac{f(t)}{t-t_o}dt + 2\sigma_{xy}^{\infty} - C_s\beta(t_o) = -\left(\frac{J_o}{2a\mu_1\mu_2}\right)f'(t_o), \tag{6.30}$$

$$\beta(t_o) = -\left(\frac{C_s J_o}{2a\mu_1\mu_2}\right) f'(t_o) + \frac{D_s J_o}{2a\pi}\int_{-1}^{+1}\frac{g(t)}{(t-t_o)^2}dt + \left(\frac{E_s J_o}{2a\pi}\right)\int_{-1}^{+1}\frac{\beta(t)}{(t-t_o)^2}dt, \tag{6.31}$$

$$A_s f(t_o) + \frac{B_s}{\pi}\int_{-1}^{+1}\frac{g(t)}{t-t_o}dt - \frac{D_s\mu_1\mu_2}{\pi}\int_{-1}^{+1}\frac{\beta(t)}{t-t_o}dt = 0. \tag{6.32}$$

By taking the derivative with respect to "t_o", Eq. (6.32) becomes

$$f'(t_o) = -\frac{B_s}{A_s\pi}\int_{-1}^{+1}\frac{g(t)}{(t-t_o)^2}dt + \frac{D_s\mu_1\mu_2}{A_s\pi}\int_{-1}^{+1}\frac{\beta(t)}{(t-t_o)^2}dt. \tag{6.33}$$

Substituting Eq. (6.33) into Eq. (6.31) yields

$$\beta(t_o) = \frac{J_o}{2a\pi}\int_{-1}^{+1}\frac{\left(\frac{B_sC_s}{A_s\mu_1\mu_2}+D_s\right)g(t)}{(t-t_o)^2}dt + \frac{J_o}{2a\pi}\int_{-1}^{+1}\frac{\left(-\frac{C_sD_s}{A_s}+E_s\right)\beta(t)}{(t-t_o)^2}dt. \tag{6.34}$$

As discussed in earlier sections, a single end condition can be imposed in the present case (when $\sigma_o = 0$). In this respect, we choose the admissible end condition in such a way that the hyper-singular terms in Eq. (6.34) are reduced to Cauchy-singular. More precisely, by imposing the following condition

$$\left(\frac{B_sC_s}{A_s\mu_1\mu_2}+D_s\right)g(t) + \left(-\frac{C_sD_s}{A_s}+E_s\right)\beta(t) = 0,$$

at each crack tip, we obtain from Eq (6.34) and the above that

$$\begin{aligned}\beta(t_o) &= \frac{J_o}{2a\pi}\left[\left(\frac{B_sC_s}{A_s\mu_1\mu_2}+D_s\right)g'(t) + \left(-\frac{C_sD_s}{A_s}+E_s\right)\beta'(t)\right]_{-a}^{+a} \\ &\quad + \frac{J_o}{2a\pi}\int_{-1}^{+1}\frac{\left(\frac{B_sC_s}{A_s\mu_1\mu_2}+D_s\right)g'(t)}{t-t_o}dt + \frac{J_o}{2a\pi}\int_{-1}^{+1}\frac{\left(-\frac{C_sD_s}{A_s}+E_s\right)\beta'(t)}{t-t_o}dt \\ &= \frac{J_o}{2a\pi}\int_{-1}^{+1}\frac{\left(\frac{B_sC_s}{A_s\mu_1\mu_2}+D_s\right)g'(t)}{t-t_o}dt + \frac{J_o}{2a\pi}\int_{-1}^{+1}\frac{\left(-\frac{C_sD_s}{A_s}+E_s\right)\beta'(t)}{t-t_o}dt.\end{aligned}$$

Consequently, Eq. (6.34) reduces to

$$\begin{aligned}
&\beta(t_o) \\
= \; & \frac{J_o}{2a\pi}\int_{-1}^{+1}\frac{\left(\frac{B_sC_s}{A_s\mu_1\mu_2}+D_s\right)g'(t)}{t-t_o}dt+\frac{J_o}{2a\pi}\int_{-1}^{+1}\frac{\left(-\frac{C_sD_s}{A_s}+E_s\right)\beta'(t)}{t-t_o}dt
\end{aligned} \tag{6.35}$$

Now, motivated by the numerical analysis in [96], that we propose approximations for solutions in the form

$$\begin{aligned}
f(t) &\approx f_N(t)=\sum_{m=0}^{N}\frac{1}{\sqrt{1-t^2}}a_mT_m(t), \\
g(t) &\approx g_N(t)=\sum_{m=0}^{N}\sqrt{1-t^2}b_mU_{m-1}(t), \\
\beta(t) &\approx \beta_N(t)=\sum_{m=0}^{N}\sqrt{1-t^2}C_mU_{m-1}(t), \quad m=0,1,2,...,
\end{aligned} \tag{6.36}$$

where $T_m(t)$ and $U_m(t)$ represent the m th Chebychev polynomial of the first kind and second kind, respectively. In addition, the Chebychev polynomials have the following properties:

$$\frac{dT_m(t)}{dt}=mU_{m-1}(t), \quad \frac{dU_m(t)}{dt}=\frac{(m+1)T_{m+1}(t)-tU_m(t)}{t^2-1} \tag{6.37}$$

Therefore, from Eqs. (6.36-37), we find that

$$f'_N(t)=\sum_{m=0}^{N}a_m\left[\frac{tT_m(t)}{(1-t^2)^{3/2}}+\frac{mU_{m-1}(t)}{\sqrt{1-t^2}}\right], \tag{6.38a}$$

$$g'_N(t)=\sum_{m=0}^{N}-\frac{mb_mT_m(t)}{\sqrt{1-t^2}}, \; \beta'_N(t)=\sum_{m=0}^{N}-\frac{mC_mT_m(t)}{\sqrt{1-t^2}}. \tag{6.38b}$$

Next, in view of Eqs. (6.36) and (6.38b), Eq. (6.35) becomes

$$\begin{aligned}
&\sum_{m=0}^{N}\sqrt{1-t_o^2}C_mU_{m-1}(t_o)=\sum_{m=0}^{N}\frac{J_o}{2a\pi}[\int_{-1}^{+1}\frac{-mb_mT_m(t)\left(\frac{B_sC_s}{A_s\mu_1\mu_2}+D_s\right)}{\sqrt{1-t^2}(t-t_o)}dt \\
&+\int_{-1}^{+1}\frac{-mC_mT_m(t)\left(-\frac{C_sD_s}{A_s}+E_s\right)}{\sqrt{1-t^2}(t-t_o)}dt].
\end{aligned} \tag{6.39}$$

By utilizing the following properties of the Chebychev polynomials [91]:

$$\int_{-1}^{1} \frac{T_m(t)}{(t-t_o)\sqrt{1-t^2}} dt = \pi U_{m-1}(t_o), \tag{6.40}$$

Eq. (6.39) reduces to

$$\sum_{m=0}^{N} \sqrt{1-t_o^2} C_m U_{m-1}(t_o) = \sum_{m=0}^{N} \frac{J_o}{2a} [\left(\frac{B_s C_s}{A_s \mu_1 \mu_2} + D_s\right)(-m) b_m U_{m-1}(t_o)$$
$$+ \left(-\frac{C_s D_s}{A_s} + E_s\right)(-m) C_m U_{m-1}(t_o)].$$

From the above, we derive the relation between a_m and b_m as:

$$C_m = b_m \frac{-m J_o \left(\frac{B_s C_s}{\mu_1 \mu_2} + A_s D_s\right)}{2a A_s \sqrt{1-t_o^2} + m J_o (A_s E_s - C_s D_s)}. \tag{6.41}$$

Similarly, from Eq. (6.36), Eq. (6.32) becomes

$$\sum_{m=0}^{N} \left[\frac{a_m T_m(t_o)}{\sqrt{1-t_o^2}} + \frac{B_s}{A_s \pi} \int_{-1}^{+1} \frac{\sqrt{1-t^2} b_m U_{m-1}(t)}{t-t_o} dt\right]$$
$$= \sum_{m=0}^{N} \left[\frac{D_s \mu_1 \mu_2}{A_s \pi} \int_{-1}^{+1} \frac{\sqrt{1-t^2} C_m U_{m-1}(t)}{t-t_o} dt\right] \tag{6.42}$$

Again, the Chebychev polynomials have the following properties [91]:

$$\int_{-1}^{1} \frac{\sqrt{1-t^2} U_{m-1}(t)}{t-t_o} dt = -\pi T_m(t_o). \tag{6.43}$$

Therefore, Eq. (6.42) reduces to

$$\sum_{m=0}^{N} T_m(t_o) \left[\frac{a_m}{\sqrt{1-t_o^2}} - b_m \frac{B_s}{A_s} + C_m \frac{D_s \mu_1 \mu_2}{A_s}\right] = 0.$$

In view of Eq. (6.41), the above yields

$$b_m = a_m \frac{A_s \left(2a A_s + \frac{1}{\sqrt{1-t_o^2}} (-C_s D_s + A_s E_s) m J_o\right)}{B_s \left\{2a A_s \sqrt{1-t_o^2} + m J_o (-C_s D_s + A_s E_s)\right\} + m J_o (D_s \mu_1 \mu_2) \left(\frac{B_s C_s}{\mu_1 \mu_2} + A_s D_s\right)}. \tag{6.44}$$

In addition, by using Eq. (6.44), Eq. (6.41) can be re-written as

$$C_m = a_m \frac{-\frac{1}{\sqrt{1-t_o^2}}\left(\frac{B_s C_s}{\mu_1\mu_2} + A_s D_s\right) m J_o A_s}{B_s\left\{2aA_s\sqrt{1-t_o^2} + mJ_o\left(-C_s D_s + A_s E_s\right)\right\} + mJ_o D_s \mu_1\mu_2\left(\frac{B_s C_s}{\mu_1\mu_2} + A_s D_s\right)}. \tag{6.45}$$

Finally, with the successive use of Eqs (6.36), (6.38a) and (6.40), we have from Eq. (6.30) that

$$\begin{aligned}
&\sum_{m=0}^{N}[a_m U_{m-1}(t_o)\left(B_s + \frac{J_o m}{2a\mu_1\mu_2\sqrt{1-t_o^2}}\right) \\
&+ a_m \frac{J_o t_o T_m(t_o)}{2a\mu_1\mu_2\left(1-t_o^2\right)^{3/2}} - \sqrt{1-t_o^2}U_{m-1}(t_o)\left(A_s b_m + C_s C_m\right)] \\
&= -2\sigma_{xy}^{\infty}.
\end{aligned} \tag{6.46}$$

We now select the set of collocation points as given by $t_o = t_{oi} = -\cos(\frac{i\pi}{N})$ for $i = 1, 2, ..., N-1$. Further, by evaluating $T_m(t_{oi})$ and $U_{m-1}(t_{oi})$ with respect to each collocation points, we find that

$$T_m\left(-\cos\left(\frac{i\pi}{N}\right)\right) = -\cos\left(\frac{im\pi}{N}\right), U_{m-1}\left(-\cos\left(\frac{i\pi}{N}\right)\right) = \frac{\sin\left(\frac{mi\pi}{N}\right)}{\sin\left(\frac{i\pi}{N}\right)}. \tag{6.47}$$

Then, from Eq. (6.47) together with Eqs. (6.44-45), Eq. (6.46) further reduces to the following system of linear equations

$$\begin{aligned}
&\sum_{m=0}^{N}[-a_m \sin\left(\frac{mi\pi}{N}\right)\left(B_s + \frac{J_o m}{2a\mu_1\mu_2\sin\left(\frac{i\pi}{N}\right)}\right) \\
&- a_m \frac{J_o\cos(\frac{i\pi}{N})\cos\left(\frac{im\pi}{N}\right)}{2a\mu_1\mu_2\sin^2\left(\frac{i\pi}{N}\right)} + a_m\left(K_m^{II}A_s + H_m^{II}C_s\right)\sin\left(\frac{i\pi}{N}\right)\sin\left(\frac{mi\pi}{N}\right)] \\
&= 2\sigma_{xy}^{\infty}\sin\left(\frac{i\pi}{N}\right).
\end{aligned} \tag{6.48}$$

where

$$b_m = a_m K_m^{II},\ C_m = a_m H_m^{II},$$

$$K_m^{II} \equiv \frac{A_s\left(2aA_s + \frac{1}{\sin\left(\frac{i\pi}{N}\right)}\left(-C_s D_s + A_s E_s\right) m J_o\right)}{B_s\left\{2aA_s\sin\left(\frac{i\pi}{N}\right) + mJ_o\left(-C_s D_s + A_s E_s\right)\right\} + mJ_o\left(D_s\mu_1\mu_2\right)\left(\frac{B_s C_s}{\mu_1\mu_2} + A_s D_s\right)},$$

$$H_m^{II} \equiv \frac{-\frac{1}{\sin\left(\frac{i\pi}{N}\right)}\left(\frac{B_sC_s}{\mu_1\mu_2}+A_sD_s\right)mJ_oA_s}{B_s\left\{2aA_s\sin\left(\frac{i\pi}{N}\right)+mJ_o\left(-C_sD_s+A_sE_s\right)\right\}+mJ_oD_s\mu_1\mu_2\left(\frac{B_sC_s}{\mu_1\mu_2}+A_sD_s\right)}.$$

Consequently, the solution of the coupled Eqs. (6.30-32) is now reduced to the solution of the system of equations Eq. (6.48) for the unknown constants a_m, b_m and c_m. The latter can be obtained by using any of the existing numerical software packages (e.g. Matlab, Maple, NAG, etc.).

6.3.2 Mode-I ($\sigma_{yy}^{\infty} \neq 0, \quad \sigma_{xy}^{\infty} = 0$) case

For the Mode-I case, we have from Eqs. (6.28a-d) that when $\sigma_o = 0$

$$-A_sg(t_o)+\frac{B_s}{\pi}\int_{-1}^{+1}\frac{f(t)}{t-t_o}dt-C_s\beta(t_o)=-\left(\frac{J_o}{2a\mu_1\mu_2}\right)f'(t_o), \tag{6.49}$$

$$\begin{aligned}\beta(t_o) = &-\left(\frac{C_sJ_o}{2a\mu_1\mu_2}\right)f'(t_o)\\ &+\frac{D_sJ_o}{2a\pi}\int_{-1}^{+1}\frac{g(t)}{(t-t_o)^2}dt+\left(\frac{E_sJ_o}{2a\pi}\right)\int_{-1}^{+1}\frac{\beta(t)}{(t-t_o)^2}dt,\end{aligned} \tag{6.50}$$

$$A_sf(t_o)+\frac{B_s}{\pi}\int_{-1}^{+1}\frac{g(t)}{t-t_o}dt+2\sigma_{yy}^{\infty}-\frac{D_s\mu_1\mu_2}{\pi}\int_{-1}^{+1}\frac{\beta(t)}{t-t_o}dt=0. \tag{6.51}$$

From Eqs. (6.49-50), we obtain

$$\begin{aligned}&\frac{B_sC_s}{\pi}\int_{-1}^{+1}\frac{f(t)}{t-t_o}dt+\frac{D_sJ_o}{2a\pi}\int_{-1}^{+1}\frac{g'(t)}{t-t_o}dt+\frac{E_sJ_o}{2a\pi}\int_{-1}^{+1}\frac{\beta'(t)}{t-t_o}dt\\ &=A_sC_sg(t_o)+\beta(t_o)\left(1+C_s^2\right).\end{aligned} \tag{6.52}$$

In addition, taking derivatives with respect to t_0 in Eq. (6.51) yields

$$f'(t_o)=-\frac{B_s}{A_s\pi}\int_{-a}^{+a}\frac{g(t)}{(t-t_o)^2}dt+\frac{D_s\mu_1\mu_2}{A_s\pi}\int_{-a}^{+a}\frac{\beta(t)}{(t-t_o)^2}dt.$$

Substituting the above into Eq. (6.50), we have that

$$\begin{aligned}&\frac{J_o}{2a\pi}\int_{-1}^{+1}\frac{\left(\frac{B_sC_s}{A_s\mu_1\mu_2}+D_s\right)g(t)}{(t-t_o)^2}dt+\frac{J_o}{2a\pi}\int_{-1}^{+1}\frac{\left(E_s-\frac{C_sD_s}{A_s}\right)\beta(t)}{(t-t_o)^2}dt\\ &=-\beta(t_o).\end{aligned} \tag{6.53}$$

Since we imposed the following natural end condition

$$\left(\frac{B_sC_s}{A_s\mu_1\mu_2}+D_s\right)g(\pm a)+\left(-\frac{C_sD_s}{A_s}+E_s\right)\beta(\pm a)=0, \tag{6.54}$$

Eq. (6.53) becomes

$$\begin{aligned}&\frac{J_o}{2a\pi}\int_{-1}^{+1}\frac{\left(\frac{B_sC_s}{A_s\mu_1\mu_2}+D_s\right)g'(t)}{t-t_o}dt+\frac{J_o}{2a\pi}\int_{-1}^{+1}\frac{\left(E_s-\frac{C_sD_s}{A_s}\right)\beta'(t)}{t-t_o}dt\\&=-\beta(t_o).\end{aligned} \tag{6.55}$$

With successive use of Eqs. (6.36), (6.38b) and (6.40), Eqs. (6.52) and (6.55) reduce to

$$\begin{aligned}&\sum_{m=0}^{N}U_{m-1}(t_o)\,[-\frac{J_om}{2a}\left(\frac{B_sC_s}{A_s\mu_1\mu_2}+D_s\right)b_m\\&-C_m\left\{\frac{J_om}{2a}\left(E_s-\frac{C_sD_s}{A_s}\right)+\sqrt{1-t^2}\right\}]\\&=0,\end{aligned}$$

$$\begin{aligned}&\sum_{m=0}^{N}U_{m-1}(t_o)\,[-b_m\left(A_sC_s\sqrt{1-t_o^2}+\frac{D_sJ_om}{2a}\right)\\&-C_m\left\{\sqrt{1-t_o^2}\left(1+C_s^2\right)+\frac{E_sJ_om}{2a}\right\}+a_mB_sC_s]\\&=0.\end{aligned}$$

herefore, we establish the following relations for $a_m,\ b_m$ and C_m as

$$C_m\left[\sqrt{1-t^2}+\frac{J_om}{2a}\left(E_s-\frac{C_sD_s}{A_s}\right)\right]=b_m\left(-\frac{J_om}{2a}\right)\left(\frac{B_sC_s}{A_s\mu_1\mu_2}+D_s\right). \tag{6.56}$$

$$\begin{aligned}a_m=&\frac{b_m}{B_sC_s}\left(A_sC_s\sqrt{1-t_o^2}+\frac{D_sJ_om}{2a}\right)\\&+\frac{C_m}{B_sC_s}\left\{\sqrt{1-t_o^2}\left(1+C_s^2\right)+\frac{E_sJ_om}{2a}\right\}.\end{aligned} \tag{6.57}$$

In view of Eqs. (6.36) and (6.43), Eq. (6.51) can be re-written as :

$$\sum_{m=0}^{N}\left[a_m\frac{A_sT_m(t_o)}{\sqrt{1-t_o^2}}-b_mB_sT_m(t_o)+C_mD_s\mu_1\mu_2T_m(t_o)\right]=-2\sigma_{yy}^{\infty}. \tag{6.58}$$

Finally, by utilizing the same collocation technique as in the Mode-II case, Eqs. (6.56-58) can be transformed into the following systems of linear equations

$$\sum_{m=0}^{N}[-a_m A_s \cos\left(\frac{im\pi}{N}\right) + a_m K_m^I B_s \cos\left(\frac{im\pi}{N}\right)\sin\left(\frac{i\pi}{N}\right)$$
$$- a_m H_m^I K_m^I D_s \mu_1\mu_2 \cos\left(\frac{im\pi}{N}\right)\sin\left(\frac{i\pi}{N}\right)]$$
$$= -2\sigma_{yy}^{\infty}\sin\left(\frac{i\pi}{N}\right), \tag{6.59}$$

where

$$b_m = a_m K_m^I,\ C_m = H_m^I b_m = a_m H_m^I K_m^I,$$
$$K_m^I = \frac{B_s C_s}{\left(A_s C_s \sin\left(\frac{i\pi}{N}\right) + \frac{D_s J_o m}{2}\right) + H_m^I\left\{\sin\left(\frac{i\pi}{N}\right)(1+C_s^2) + \frac{E_s J_o m}{2}\right\}},$$
$$H_m^I = \frac{-\frac{J_o m}{2}\left(\frac{B_s C_s}{\mu_1\mu_2} + A_s D_s\right)}{A_s \sin\left(\frac{i\pi}{N}\right) + \frac{J_o m}{2}\left(A_s E_s - C_s D_s\right)}.$$

Therefore, by solving the above equations (Eq. 6.59), the unknowns a_m, b_m and c_m can be completely determined in the Mode-I case.

6.4 RESULTS AND DISCUSSION

In this section, the numerical solution of Eqs. (49-50) and Eq. (59) is derived for the two cases when a crack is subjected to a uniform remote in-plane shear (mode -II crack problem) and a uniform remote tension (mode-I crack problem), respectively. Throughout the analysis, we adopt the same range of surface parameters used previously (Sharma and Ganti [16]).

$$Se = \frac{J_o}{a} : 16\times 10^8 \le Se \le 16\times 10^{10},$$
$$\mu^s = 161.73(J/m^2), \quad \sigma_o = 1.3(J/m^2),\ J_o = 400(J/m^2),$$
$$168\times 10^7(Pa) \le \mu_1, \mu_2 \le 168\times 10^9(Pa),\ 2.3 \le \kappa_1, \kappa_2 \le 2.7\ . \tag{6.60}$$

For practical purposes, we do not present numerical results here for the most general cases when the surface material properties corresponding to the upper and lower faces of the crack are distinct (although the model fully incorporates this general case for a range of surface parameters). Instead, we simplify the numerical calculations by assuming that the upper and lower crack faces have identical surface properties but the bulk materials remain distinct. This is certainly sufficient to illustrate the effect of surface elasticity on the behaviour of this bi-material particularly in the vicinity of the crack.

6.4.1 Functions $f(t)$, $g(t)$, and $\beta(t)$

To verify our model we consider the special case of a homogeneous material (material properties from the upper and bottom regions coincide) containing a crack and reproduce the classical solutions from the LEFM theory (see, for example, [65,66]) followed by the solutions to the corresponding problems which incorporate surface effects (see Chapter. 4). For a single material crack, we find that

$$f(t) = \Omega'(z)^{+} - \Omega'(z)^{-} = -\frac{\sigma_{xy}^{\infty} t}{\sqrt{t^2 - a^2}},\ g(t) = \beta(t) = 0,\ -a < t < a,$$

(classical LEFM, Mode-II),

$$f(t) = \text{Non-zero bounded solution (see.Fig. 39)},\ g(t) = \beta(t) = 0,$$

(single material crack with surface effects, Mode-II).

In the present case, the unknown functions can be obtained subsequently as:

$$f_N(t) = \sum_{m=0}^{N} \frac{1}{\sqrt{1-t^2}} a_m T_m(t),$$

$$g_N(t) = \sum_{m=0}^{N} \sqrt{1-t^2} b_m U_{m-1}(t) = \sum_{m=0}^{N} \sqrt{1-t^2} a_m K_m^{II} U_{m-1}(t),$$

$$\beta_N(t) = \sum_{m=0}^{N} \sqrt{1-t^2} C_m U_{m-1}(t) = \sum_{m=0}^{N} \sqrt{1-t^2} a_m H_m^{II} U_{m-1}(t),\ \text{for}\ -1 < t < 1.$$

and the unknown constants a_m can be determined from Eqs. (6.48). The corresponding solutions for each case are plotted through Figs. (39-41).

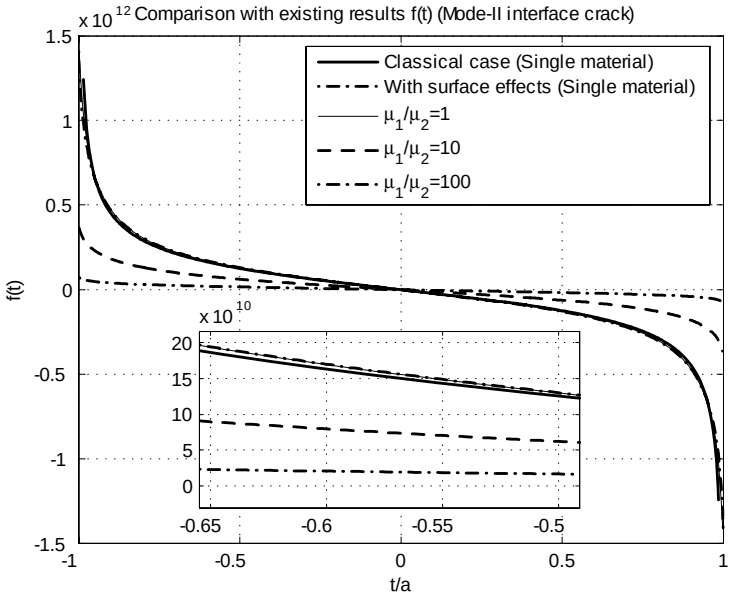

Figure 39: *The solution of* $f(t)$ *(Mode-II interface fracture), where* $\sigma_{xy}^{\infty}/\mu_1 = 0.37$

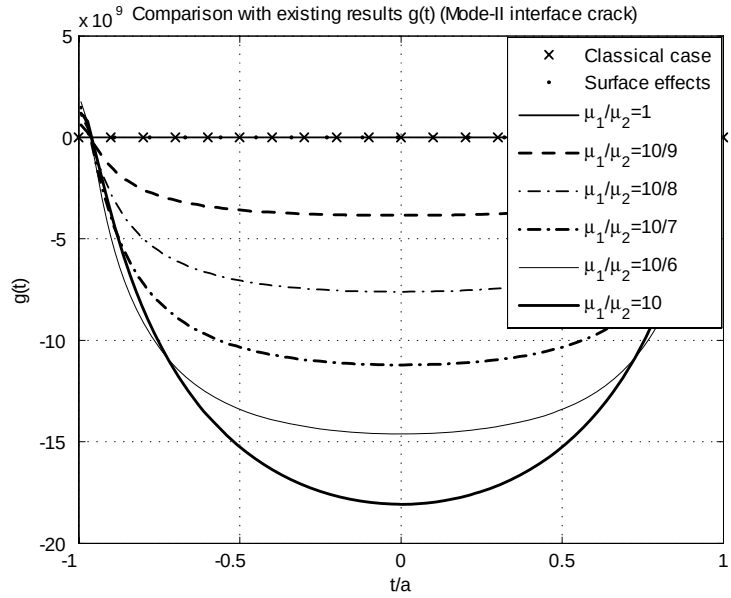

Figure 40: *The solution of $g(t)$ (Mode-II interface fracture), where $\sigma_{xy}^{\infty}/\mu_1 = 0.37$*

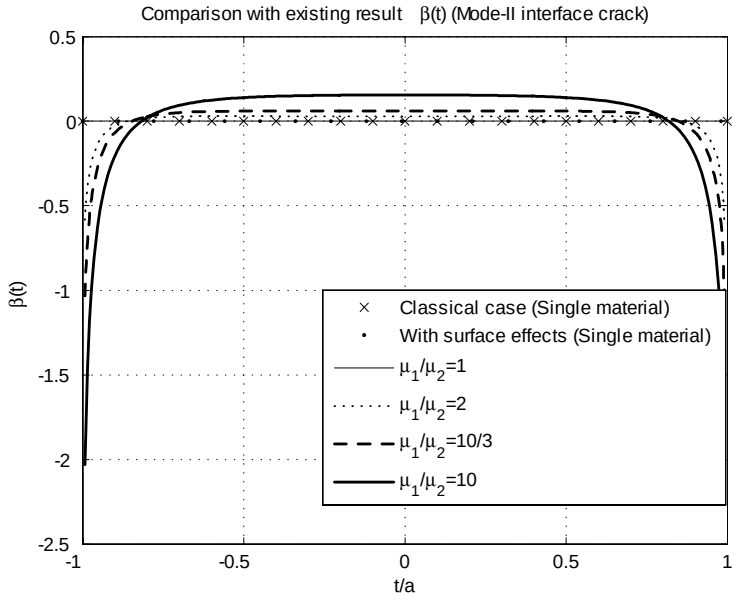

Figure 41: *The solution of $\beta(t)$ (Mode-II interface fracture), where $\sigma_{xy}^{\infty}/\mu_1 = 0.37$*

The results clearly illustrate that our solutions reduce to the classical results obtained from the literature, as the material properties of the two regions coincide. More specifically, the estimated value of $f(t)$ increases until it reaches the value obtained from the cases corresponding to a crack in a homogeneous material. The solutions of $g(t)$ and $\beta\,(t)$ decrease to zero which is compatible with existing results. This also can be directly shown from Eqs. (6.28) and (6.48) i.e. , by setting $\mu_1 = \mu_2 = \mu$ and $\kappa_1 = \kappa_2 = \kappa$, we have

$$\left(\frac{1}{\mu+\mu\kappa} - \frac{1}{\mu+\mu\kappa}\right) = A_s = 0,\ \frac{(\kappa\mu^2 - \kappa\mu^2)}{(\mu+\kappa\mu)\,(\mu+\kappa\mu)} = C_s = 0,$$

which yields $K_m^{II} = H_m^{II} = 0$. Therefore, we find

$$f_N(t) = \sum_{m=0}^{N} \frac{1}{\sqrt{1-t^2}} a_m T_m(t) \ \text{(Non-zero)},$$
$$g_N(t) = \sum_{m=0}^{N} \sqrt{1-t^2} b_m U_{m-1}(t) = \sum_{m=0}^{N} \sqrt{1-t^2} a_m \boldsymbol{K}_m^{II} U_{m-1}(t) = 0,$$
$$\beta_N(t) = \sum_{m=0}^{N} \sqrt{1-t^2} C_m U_{m-1}(t) = \sum_{m=0}^{N} \sqrt{1-t^2} a_m \boldsymbol{H}_m^{II} U_{m-1}(t) = 0.$$

Similar analyses can be performed for the Mode-I case illustrating analogous results. In this case, we have non-zero $g(t)$ and $f(t) = \beta(t) = 0$. In addition, our solutions in Figs. 39-41 also demonstrate the apparent presence of mixed mode crack tip fields regardless of the type of applied loading. We also note here that the solutions obtained satisfy the imposed natural end condition:

$$\left(\frac{B_s C_s}{A_s \mu_1 \mu_2} + D_s\right) g(\pm a) + \left(-\frac{C_s D_s}{A_s} + E_s\right) \beta(\pm a) = 0.$$

For example, in the Mode-II case, end values for $g(t)$, $f(t)$ and $\beta(t)$ are estimated as:

$$g(-1) = 1.1932 \times 10^9, \ \beta(-1) = -2.0289,$$

when, $\sigma_{xy}^{\infty}/\mu_1 = 0.37$, $\mu_1 = 168 \times 10^9$ and $\mu_2 = 168 \times 10^8$. Therefore, the corresponding natural end conditions in this case can be calculated as

$$\left(\frac{B_s C_s}{A_s \mu_1 \mu_2} + D_s\right) 1.1932 \times 10^9 + \left(-\frac{C_s D_s}{A_s} + E_s\right) (-2.0289) = 9.851\,4 \times 10^{-13} \approx 0,$$

which is clearly satisfied. Finally, the results in Figs. 39-41 indicate that solutions ($f(t)$, $g(t)$ and $\beta(t)$) have non-zero finite values at the crack tips leading to the corresponding stress fields being weakly singular, in fact logarithmic. We will discuss more about this point shortly after the next section.

6.4.2 Oscillatory Singularity

The solutions of interface crack problems in the context of LEFM show rapid oscillation in both the stress and displacement fields, and indicate the possibility of material interpenetration which is, of course, physically inadmissible (see, for example, [66,70]). The oscillatory behavior have previously been avoided by either imposing mathematical restrictions at the crack tips [97,98] or by considering some special classes of nonlinear materials (see, for example, [99]). The aforementioned results have been the subject of intense discussion in the literature.

In the present case, we have found that the oscillatory singularities can also be eliminated with the incorporation of surface effects. The graphs in Figs. 42-43 clearly indicate that the oscillatory phenomena gradually decays as the effect of surface elasticity increases. In other words, the stress fields obtained from the present solution no longer oscillate. The results hold true for both Mode-I and Mode-II cases (see the non-oscillatory solutions through Figs. 44-47). In addition, our solution from both fracture cases (Mode-I and Mode-II) varies with respect to the surface parameter Se reflecting the contributions of surface elasticity.

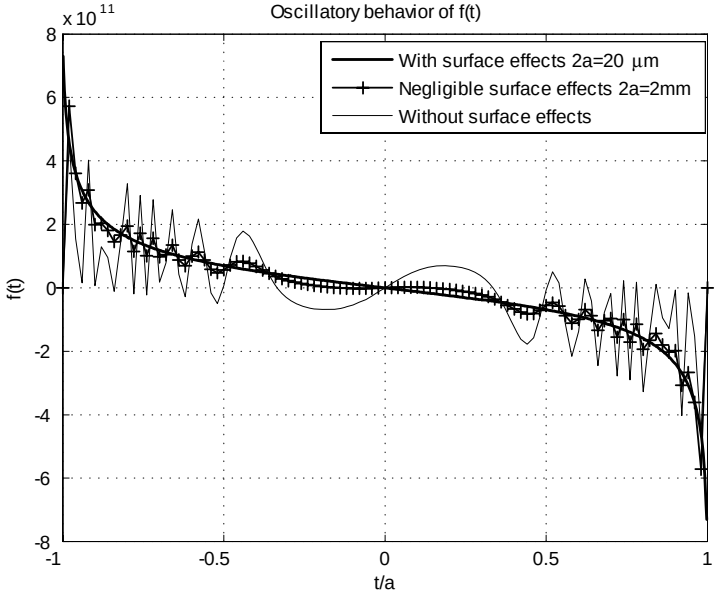

Figure 42: *Removal of oscillatory singularity $f(t)$(Mode-II interface fracture)*

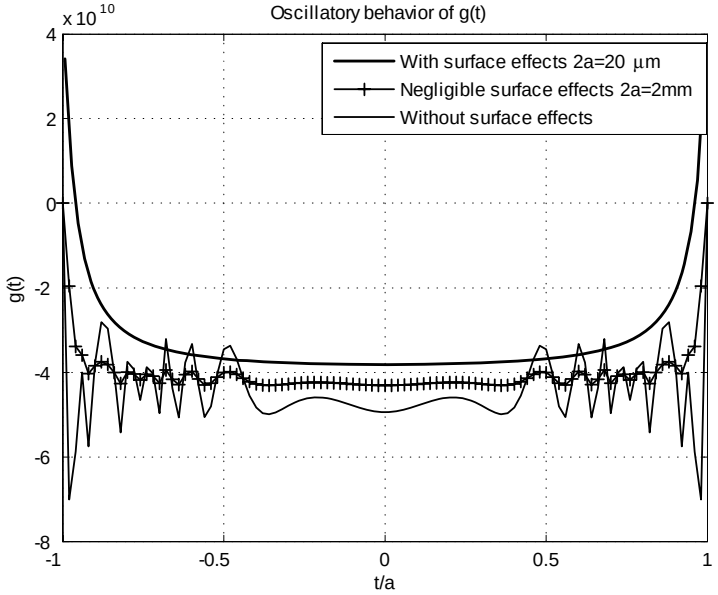

Figure 43: *Removal of oscillatory singularity $g(t)$(Mode-II interface fracture)*

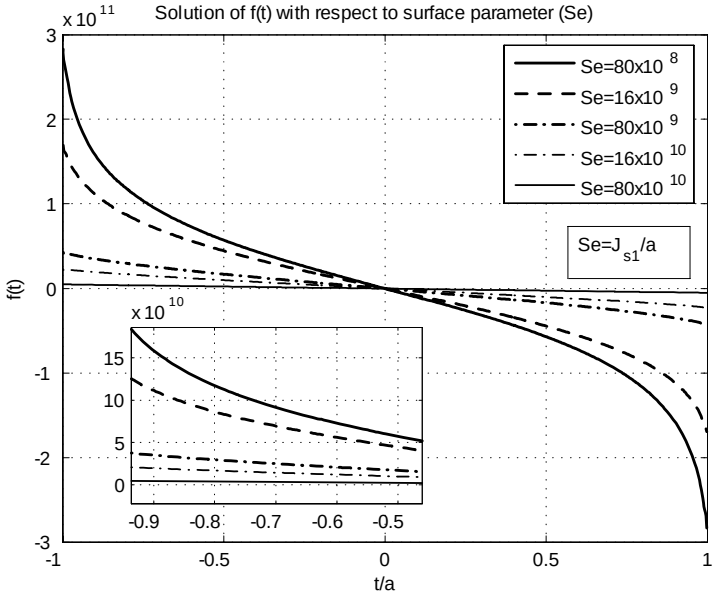

Figure 44: *The solution of $f(t)$ with respect to surface parameter (Mode-II interface fracture), where $\sigma_{xy}^{\infty}/\mu_1 = 0.37$*

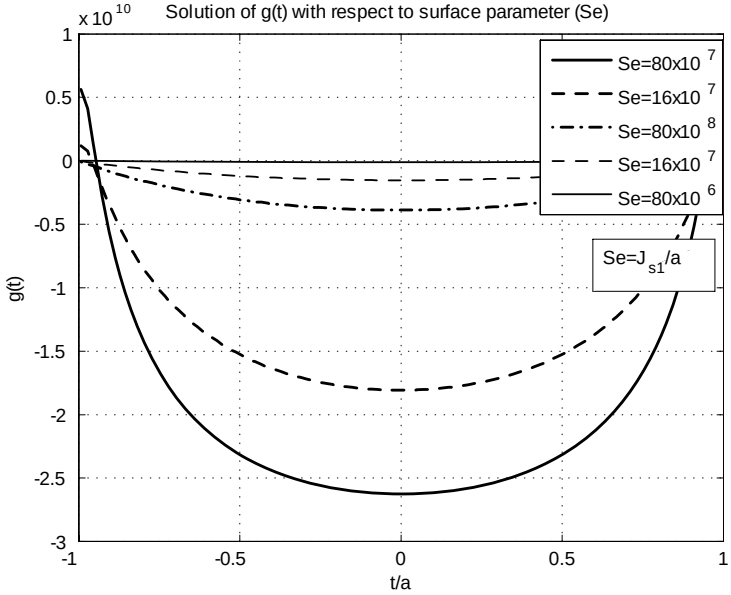

Figure 45: *The solution of $g(t)$ with respect to surface parameter (Mode-II in-*

terface fracture), where $\sigma_{xy}^{\infty}/\mu_1 = 0.37$

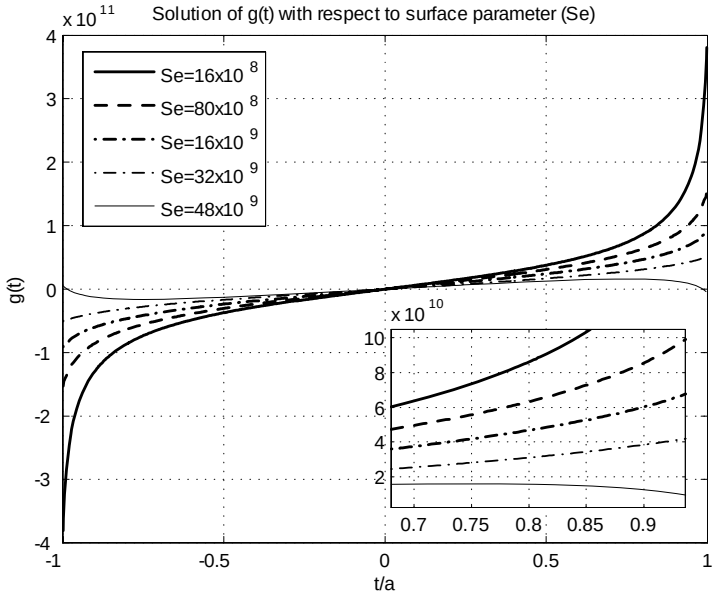

Figure 46: *The solution of* $g(t)$ *with respect to surface parameter (Mode-I interface fracture), where* $\sigma_{yy}^{\infty}/\mu_1 = 0.37$

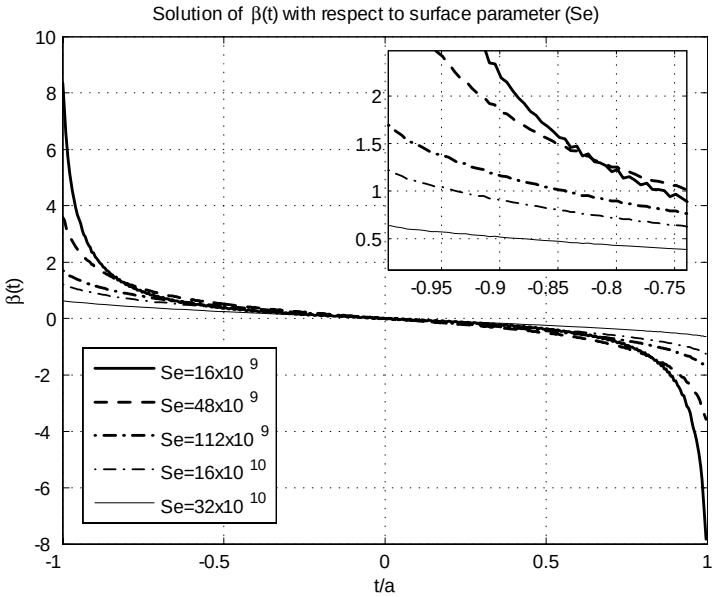

Figure 47: *The solution of* $\beta(t)$ *with respect to surface parameter (Mode-I interface fracture), where* $\sigma_{yy}^{\infty}/\mu_1 = 0.37$

Finally, based on the numerical estimations of $g(t)$, $f(t)$, $\alpha(t)$ and $\beta(t)$, the stresses on the real axis can be estimated. More precisely, we have from Eqs. (6.13) and (6.14a) that

$$(\sigma_{yy} - i\sigma_{xy}) = \left(\frac{1}{\mu_1 + \mu_2\kappa_1} + \frac{1}{\mu_2 + \mu_1\kappa_2}\right)\phi'(z)$$
$$+\frac{\mu_1 + \mu_2 - \mu_1\mu_2\kappa_1\kappa_2}{(\mu_1 + \mu_2\kappa_1)(\mu_2 + \mu_1\kappa_2)}\theta'(z) \equiv B_s\phi'(z) + X_s\theta'(z). \tag{6.61}$$

In view of Eqs. (6.21-22), Eq. (6.61) can be re-written as:

$$(\sigma_{yy} - i\sigma_{xy}) = \frac{B_s}{2\pi i}\int_{-1}^{+1}\frac{f(t) + ig(t)}{t - z}dt + (\sigma_{yy}^{\infty} - i\sigma_{xy}^{\infty}) + \frac{X_s}{2\pi i}\int_{-1}^{+1}\frac{\alpha(t) + i\beta(t)}{t - z}dt,$$

By separating real and imaginary parts, the above yields

$$\sigma_{yy} = \frac{B_s}{2\pi}\int_{-1}^{+1}\frac{g(t)}{t - z}dt + \frac{X_s}{2\pi}\int_{-1}^{+1}\frac{\beta(t)}{t - z}dt + \sigma_{yy}^{\infty}, \tag{6.62a}$$

$$\sigma_{xy} = \frac{B_s}{2\pi}\int_{-1}^{+1}\frac{f(t)}{t - z}dt + \frac{X_s}{2\pi}\int_{-1}^{+1}\frac{\alpha(t)}{t - z}dt + \sigma_{xy}^{\infty}. \tag{6.62b}$$

Therefore, the stress field can be completely determined with given $g(t)$, $f(t)$, $\alpha(t)$ and $\beta(t)$. For example, in the mode-II case, we find from Eq. (6.62a-b) that

$$\sigma_{yy} = \frac{B_s}{2\pi}\int_{-1}^{+1}\frac{g(t)}{t - z}dt + \frac{X_s}{2\pi}\int_{-1}^{+1}\frac{\beta(t)}{t - z}dt, \sigma_{xy} = \frac{B_s}{2\pi}\int_{-1}^{+1}\frac{f(t)}{t - z}dt + \sigma_{xy}^{\infty}. \tag{6.63}$$

In particular, by expanding the Cauchy integrals in Eq. (6.63), we obtain the following expressions at the crack tips ($t = \pm a$)

$$\begin{aligned}\sigma_{yy} &= \frac{B_s}{2\pi}g(\pm a)\ln r + \frac{X_s}{2\pi}\beta(\pm a)\ln r + O(1),\\ \sigma_{xy} &= \frac{B_s}{2\pi}f(\pm a)\ln r + \sigma_{xy}^{\infty} + O(1),\end{aligned}$$

which clearly indicate that the corresponding stress fields, in the plane interface crack case (For both Mode-I and Mode-II fractures), exhibit a weaker logarithmic

singularity at the crack tips with non-zero finite values of solutions ($g(t)$, $f(t)$ and $\beta(t)$, see Figs. 39-41 and 44-47) at these points. Examples of estimated stresses are illustrated through Figs. 48-49 with respect to varying surface parameters. The results recognize the fact that surface effects, acting basically in the same way as a reinforcement, can effectively reduce the corresponding stress fields (materials get stiffer as surface effects increase). In addition, since the surface parameters Se are controlled by variations of the crack size, our results also indicate that the corresponding stresses are strongly dependent on crack size. In fact, size dependency of stress fields in materials are the dominant phenomena in the deformations of small scale structures such as the nano-inhomogeneity, nano-composite materials and dislocations in small-scale structures (see, for example, [16, 44]).

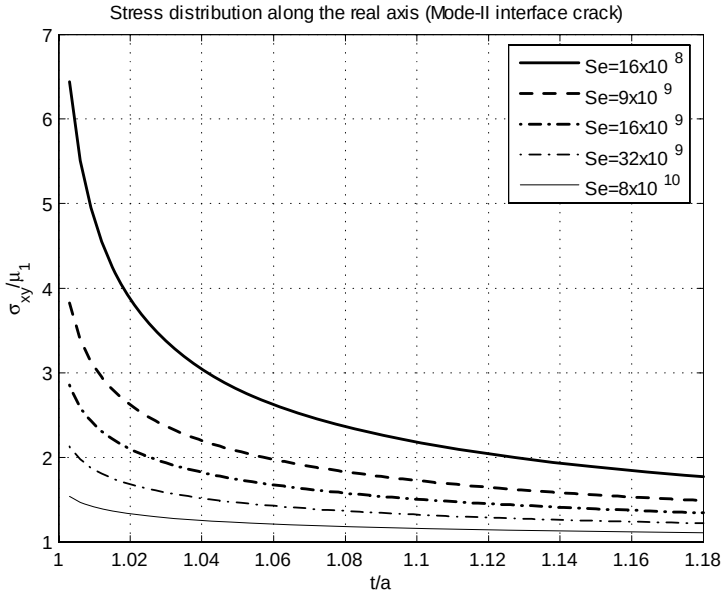

Figure 48: *Stress distribution with respect to surface parameter (Mode-II interface crack), where* $\sigma_{xy}^{\infty}/\mu_1 = 0.37$

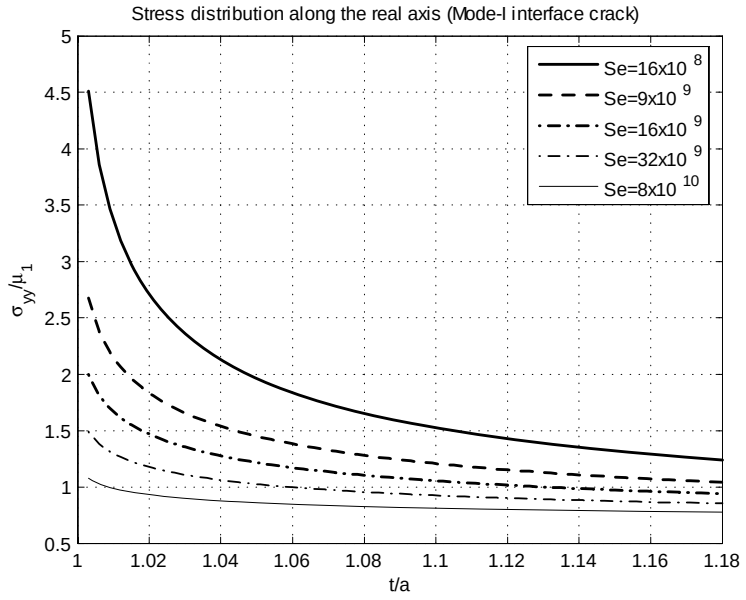

Figure 49: *Stress distribution with respect to surface parameter (Mode-I interface crack), where* $\sigma_{yy}^{\infty}/\mu_1 = 0.37$

6.5 SUMMARY

In this chapter, we have considered, in the presence of surface elasticity, a traction-free crack between two dissimilar linearly elastic isotropic homogeneous materials undergoing plane deformations. The bi-material is subjected either to remote tension (mode-I) or in-plane shear (mode-II). The surface mechanics is incorporated in both faces of an interface crack using a version of the continuum based surface/interface model of Gurtin and Murdoch. Complex variable methods are used to obtain a semi-analytic solution valid throughout the entire domain of interest by reducing the problem to a system of coupled Cauchy singular integro-differential equations which is solved numerically. In this respect, the direct method is adopted

avoiding additional mathematical pre-treatment and massive computational resources in the corresponding analysis.

In contrast to the homogeneous plane crack problem, *two* natural end conditions can be imposed in the case of an interface plane fracture. However, it is found that the number of admissible end conditions further reduces to *one* when surface tension is removed from the system (i.e. $\sigma_o = 0$). In the corresponding analysis, we chose an end condition in a way that the degree of singularity of the obtained system of differential equations reduces from hyper-singular to Cauchy singular. Our numerical analysis results also indicate that the imposed end condition is well satisfied.

It is shown that our analysis predicts weakly logarithmic singular stresses at the crack tips and the corresponding stress fields to be size-dependent. In particular, we note that, in contrast to classical LEFM results, the incorporation of surface effects effectively removes the oscillatory behavior of the solution leading to smooth and non-oscillatory stress distributions in the vicinity of the crack tips. Further, the corresponding stress fields derived in our analysis demonstrate the apparent presence of mixed mode crack tip fields regardless of the type of applied loading and the amount of stresses decrease as the surface effects become significant. Finally, the solutions obtained from our analysis are sufficiently general in that they actually reduce to the results from both the homogeneous plane-strain fracture case (in Chapter. 4) by setting $\mu_1 = \mu_2$ and $\kappa_1 = \kappa_2$ and the classical LEFM results, when the surface effects are neglected in the corresponding bulk-crack system.

CHAPTER 7

CONCLUSIONS AND FUTURE WORK

7.1 CONCLUSIONS

In this dissertation, we address a series of crack problems from the classical theory of Linear Elastic Fracture Mechanics (LEFM) with the renewed realization of the role of surface elasticity. The general deformations and stress analysis of an elastic solid incorporating a crack is of fundamental importance in the understanding of failure and fracture mechanisms of engineering materials. Traditional prediction models and solutions from the classical assumptions of LEFM theory, unfortunately have led to various inconsistencies such as the prediction of a strong square root stress singularity at the crack tips and, in the case of interface fracture, the rapid oscillation in both stress and displacement fields in the vicinity of the crack further leading to the possibility of material interpenetration between two dissimilar materials.

The primary objective of the present study is to resolve the above mentioned contradictory results from the classical LEFM theory and provide a more accurate description for the corresponding bulk-crack systems. In this respect, we focus on the fact that the region near the surface of a solid material experiences local environmental changes resulting in the deviation of properties as they approach the boundaries of a bulk material. Such effects (surface effects) become significant, when a high surface to volume ratio is present at the small scale. This further suggests that a more comprehensive and accurate modeling and analysis of a bulk-crack system would include a separate description of surface elasticity on both sides

of crack surfaces (faces). In the present study, we have incorporated the effects of surface elasticity into the analysis of bulk-crack systems using a version of the Gurtin-Murdoch (curvature-independent) surface elasticity model. It is assumed that the crack (including its crack tips) is 'surrounded' by a negligibly thin elastic membrane (with elastic properties different from those of the surrounding bulk material) firmly attached to the bulk material without slipping. In the mathematical modeling, we regarded a crack as an interval of the x-axis ($y = 0$, $-a < x < a$) on a typical complex $x - y$ plane in $\mathbb{R}^2$. We then imposed the properties of the surface layer onto the boundaries of a crack (upper ($y = +0$) and bottom ($y = -0$) faces of the crack).

The analysis of our mathematical model involves the use of complex variable methods and the theory of Cauchy integrals to reduce the corresponding (highly non-standard) BVP to a series of hyper-singular integro-differential equations. By imposing appropriately chosen natural end conditions, the corresponding hyper-singular integro-differential equations are further deduced to Cauchy-singular forms. The latter is solved using adapted numerical techniques (e.g. collocation method and Chebyshev polynomials) leading to a complete (within the entire domain of interest) semi-analytic solution from which we derived various interesting results of each corresponding crack problem discussed through Chapters 3-6.

Chapter 3 addresses and analyzes the effects of surface elasticity in a classical Mode-III crack problem arising in the anti-plane shear deformations of a linearly elastic homogeneous isotropic solid. Since only a single scalar displacement field in the axial direction is needed in the description of anti-plane shear motion, the anti-plane problem offers the advantages of exploring various possible scenarios arising in the mechanics of materials, yet still maintains a relatively simple mathematical

setting. This also corresponds with our motivation to preferentially challenge a Mode-III fracture problem in the presence of surface elasticity.

It is shown that the introduction of the effects of surface elasticity results in the reduction of the stress singularity at the crack tip from the strong square root singularity to a weaker logarithmic singularity. In particular, the corresponding stresses derived from our analysis exhibit clear signs of size-dependency and do indeed accommodate those in the classical LEFM solutions when the surface effects are removed from the corresponding bulk-crack system. The uniqueness theorem of the corresponding BVP is also examined leading to the conclusion that either a traction $(w^{+}_{,x} + w^{-}_{,x})$ or displacement (w) condition is required at each crack tip to uniquely determine a solution. However, in Mode-III fracture, since $w = 0$ (displacement condition) is automatically prescribed at each crack tip, the solution can be uniquely determined without imposing any extra end conditions.

Problems regarding a mode-III crack subjected to non-uniform surface tractions are also considered in this chapter. In this respect, we have obtained a complete numerical solution when the crack faces are subjected to arbitrary surface tractions characterized by stress functions described by general polynomials of degree n. In addition, it is found that, from the particular case of our general solution (when the crack faces are subjected to uniform traction), the decomposition theory in classical elasticity still holds true when surface elasticity is taken into account on both crack faces. This result is important particularly in that, when used in conjunction with the general methodology presented in this chapter, they essentially lead to the solutions of a class of problems in which the surface traction is characterized by a much wider and more practically realistic class of functions.

Through Chapter 4, we have examined the plane deformations of a linearly elastic solid in the cases where either a Mode-I or Mode-II crack is present and

when the contributions of surface effects are taken into account. Problems involving plane deformations of an elastic solid provide direct physical relevance to those in real-world problems. However, the governing equations describing the in-plane motion are much more complicated in comparison to those from anti-plane shear deformations since two scalar fields are necessary in order to fully describe the plane deformations. With additional complexity induced by the effects of surface elasticity, the corresponding plane-strain crack problem results in solving highly non-standard (and coupled) hyper-singular integro-differential equations. By imposing carefully chosen admissible end conditions, the hyper-singular terms in the corresponding differential equations are reduced to Cauchy singular form. We then numerically solved the reduced system of coupled integro-differential equations and obtained complete semi-analytic solutions valid throughout the entire domain of interest. It is also confirmed that the obtained solutions well satisfy the imposed end conditions.

Based on the solutions obtained through the analysis in this chapter, we have demonstrated that the incorporation of surface effects reduces the degree of singularity from the classical strong square root singularity to a weaker logarithmic singularity in the plane case with one exception when surface tension is removed ($\sigma_o = 0$) from the Mode-I fracture system. In this case the corresponding stress fields continue to exhibit the strong square root singularity even in the presence of surface elasticity. In particular, the incorporation of surface effects can effectively reduce the corresponding stress distributions and result in elastic responses being size-dependent. It is also shown that the natural boundary conditions of the corresponding BVP admit only a single condition at each crack tip, in each case (Mode-I and Mode-II, respectively) with the exception of the Mode-II fracture case when ($\sigma_o = 0$). In the Mode-II fracture, not a single end condition can be imposed

at each crack tip. Finally, we note that the general solution for the mixed mode problem (Mode-I + Mode-II) reduces to those of the Mode-I and Mode-II cases, separately, even when the surface effects are incorporated.

In Chapter 5, we have incorporated the effects of surface elasticity into a classical Mode-III interface crack problem arising in the anti-plane shear deformations of a linearly elastic bi-material. The analysis of an interface crack between two dissimilar elastic materials is of fundamental importance in the understanding of the mechanics and fracture mechanisms of advanced composite materials (for example, laminar and fiber-reinforced composites) where, for example, a high possibility of material debonding and cracking or sliding at the interface exists. The main objective of this chapter is to examine the effects of surface elasticity on two distinguished faces of the interface crack. In this respect, we projected surface properties in a way that each crack face (upper and lower faces) has its own distinct elastic properties which are different from those of each of the bulk materials.

Using complex variable methods and adequately chosen end conditions, we again reduce the corresponding problem to a system of coupled Cauchy singular integro-differential equations which is then solved numerically using an adapted collocation technique. We have demonstrated that the corresponding stress distributions again exhibit clear signs of size-dependency and accommodate the results from both the homogeneous crack case and the classical solution when corresponding conditions are imposed. In particular, it is shown that that the major stress component (σ_{yz}) at the crack tips exhibits a weaker logarithmic singularity rather than the classical strong square root singularity, even in the case of an interface crack problem. It is also found that the minor stress contributor (σ_{xz}) is finite at the crack tips and more importantly, jumps across the bi-material interface, in contrast to the classical result from the LEFM theory.

In regard to the natural admissible boundary conditions, a single end condition can be imposed at each crack tip in contrast to the homogeneous Mode-III crack problem. In this study, we have chosen the end condition to reduce the corresponding systems of integro-differential equations: from hyper-singular to Cauchy singular-integro differential equations. This further leads to the boundedness of the minor stress contributor (σ_{xz}). In this respect, other choice of end conditions can be made, for example, $f(\pm a) = 0$ at the tips (instead of prescribing $\alpha(\pm a) = 0$) in an attempt to obtain bounded major stress component (σ_{yz}) remaining σ_{xz} infinite at the crack tip. However this involves solving a system of coupled hyper-singular differential equations which have yet to be studied. Finally, it is noted that the solution and analysis presented in this chapter, are sufficiently general in that, they accommodate the results both obtained from the homogeneous material case by imposing $\mu_1 = \mu_2$ and $(\mu^s - \sigma_o)^+ = (\mu^s - \sigma_o)^-$, and the classical results, when the surface effects are neglected in the corresponding bulk-crack system.

Plane-strain deformation of a linearly elastic bi-material incorporating cracks in its interfacial region is, perhaps, the most comprehensive description of a bulk-crack system which involves all the complex nature of the mechanics of fracture. The classical prediction models of such crack problems from the theory of LEFM often produce results quite apart from real world phenomena such as the rapid oscillation in both stress and displacement fields near the crack tip leading to the possibility of material interpenetration between two adjoined dissimilar materials. Chapter 6 addresses the above mentioned inconsistencies and considers, in the presence of surface elasticity, a bi-material crack-matrix system undergoing plane-strain deformations and subjected to uniform remote tension and in-plane shear. More specifically, we refine governing equations to include surface effects on both faces of the interface crack using Gurtin-Murdoch (curvature-independent)

surface elasticity model. To this end, a system of coupled Cauchy-singular integro-differential equations is obtained using Complex variable methods and the theory of Cauchy integrals which is highly complicated in nature (four unknowns with four coupled integro-differential equations). Instead of using conventional numerical method adopted in Chapters 3-5, we introduced an effective, yet simple method (referred to in this study as a 'direct method') through which we obtained a complete semi-analytic solution for both Mode-I and Mode-II fracture cases.

In contrast to the homogeneous plane-strain fracture case, two natural admissible conditions can be imposed at each crack tip in the case of an interface plane-strain crack problem. However, it is found that the number of admissible end conditions further reduces to one when surface tension is removed from the corresponding system (i.e. $\sigma_o = 0$). In this study, we chose an end condition in a way that the hyper-singular terms in the obtained system of differential equations reduce to Cauchy singular form. The corresponding numerical analysis results also indicate that the imposed end condition is well-satisfied. It is shown that, among other various interesting phenomena, our analysis predicts weakly logarithmic singular stresses at the crack tips and the corresponding stress fields to be size-dependent. In particular, we note that, in contrast to classical LEFM results, the incorporation of surface effects effectively removes the oscillatory behavior of the solution leading to smooth and non-oscillatory stress distributions within the entire domain of interest. Further, the corresponding stress fields derived in our analysis demonstrate the apparent presence of mixed mode crack tip fields regardless of the type of applied loading and the amount of stresses decrease as the surface effects become significant. Finally, the solutions obtained from our analysis are sufficiently general in that they accommodate the results from both the homogeneous plane-strain fracture case (in Chapter. 4) by setting $\mu_1 = \mu_2$ and

$\kappa_1 = \kappa_2$ and the classical LEFM results, when the surface effects are neglected in the corresponding bulk-crack system.

We expect that the results obtained in this dissertation will advance the understanding of the role of surface mechanics in the mechanics and mechanisms of fracture of engineering materials subjected to various types of applied loading. In particular, the complete solutions obtained through Chapters 3-6 with respect to various possible scenarios provide physical relevance to corresponding real world problems and therefore will enhance future design and analysis of mechanical systems, particularly at the nano/micro scale where surface effects are known to be significant. Finally, the corresponding modeling and development in regard to the implementation of the theory of surface elasticity into the description of a matrix-crack system will serve as a guideline for further studies in this subject, for example, the analysis of the effects of a second-order (curvature-dependent) theory of surface elasticity in LEFM.

7.2 FUTURE WORK

The most important extension of our work includes the incorporation of a higher-order (e.g. curvature-dependent) theory of surface elasticity with the possibility of the complete removal of stress singularities at crack tips. It is shown in this dissertation that the effects of first-order surface elasticity lead, in most cases, to the reduction of the classical strong square root singularity of LEFM to a weaker logarithmic singularity. Although, the degree of singularity is reduced, our model was not able to predict finite stresses at the crack tips. This is mainly because the necessary and sufficient requirements for bounded stresses at the crack tip cannot be satisfied within the present (a first-order) description. More precisely, the maximum number of admissible end conditions is limited in each case of crack problems.

Therefore, imposing, in addition, any further end-point conditions overdetermines the corresponding BVPs. For example, in the homogeneous plane-strain fracture case (Mode-I and Mode-II), stress components on the real axis (outside of a crack, $y=0$, $x>|a|$) are given by

$$\begin{aligned}
\sigma_{xx}+\sigma_{yy} &= 4\,\mathrm{Re}\left[\Omega'(z)\right]=2\,\mathrm{Re}\left[\frac{1}{\pi i}\int_{-a}^{+a}\frac{f(t)+ig(t)}{t-z}dt+\sigma_{yy}^{\infty}-i\sigma_{xy}^{\infty}\right],\\
\sigma_{yy}-i\sigma_{xy} &= \left[2\Omega'(z)-\theta'(z)\right]\\
&= \left[\frac{1}{\pi i}\int_{-a}^{+a}\frac{f(t)+ig(t)}{t-z}dt+\sigma_{yy}^{\infty}-i\sigma_{xy}^{\infty}-\frac{1}{2\pi i}\int_{-a}^{+a}\frac{\alpha(t)+i\beta(t)}{t-z}dt\right].
\end{aligned}$$

The Cauchy integrals in the above equation can be expanded near the crack tip (for example $z=\pm a$) to give

$$\begin{aligned}
\sigma_{xx}+\sigma_{yy} &= \frac{2}{\pi}g(\pm a)\ln r+\sigma_{yy}^{\infty}+O(1),\\
\sigma_{yy}-i\sigma_{xy} &= \frac{1}{2\pi i}\left[2(f(\pm a)+ig(\pm a))-\alpha(\pm a)-i\beta(\pm a)\right]\ln r+\sigma_{yy}^{\infty}-i\sigma_{xy}^{\infty}+O(1),
\end{aligned}$$

where $r=|z-a|$. Therefore, the necessary and sufficient conditions for the all stress components to be bounded at the crack tips are that the expressions in the above equation admit no logarithmic singularity. In other words, the following *three* conditions must be satisfied at each crack tip

$$g(\pm a)=0,\quad \beta(\pm a)=0\ \ and\ \ \ 2f(\pm a)=\alpha(\pm a).$$

Since $f(t)=\alpha(t)=0$ for Mode-I case and $g(t)=\beta(t)=0$ for Mode-II case (see Chapter. 4), the above combined mode conditions can also be rewritten as

$$\begin{aligned}
&g(\pm a)=0,\ \beta(\pm a)=0\ \ \text{for Mode-I case,}\\
&2f(\pm a)=\alpha(\pm a)\ \ \text{for Mode-II case,}
\end{aligned}\tag{7.1}$$

respectively. However, only a single natural boundary condition is admissible in the case of homogeneous Mode-I and Mode-II fracture within the description of the first-order theory of surface elasticity. Consequently, the corresponding solution

cannot satisfy bounded stresses at the crack tips with the stress singularity reduced to logarithmic form.

In this respect, in [51] the authors demonstrated that the Steigmann–Ogden theory of surface elasticity (curvature-dependent surface energy) [32,33] produces a more accurate description, particularly when a system is subjected to wrinkling and bending deformation modes. In particular, since a curvature-dependent (second-order) theory of surface elasticity includes additional descriptions of bending effects, correspondingly more degrees of freedom can be admitted at the boundaries of systems. In the case of a bulk-crack system, this means that additional end conditions can be imposed, on top of the natural boundary conditions, and thus may satisfy necessary and sufficient conditions for bounded stresses. In fact, by using curvature-dependent theory, in [52] the authors obtained a system of Fredholm integral equations, in the case of interface plane-strain crack problem. They, then show that (although, the actual solutions of the corresponding differential equations are not presented) the expected form of solutions leads to bounded stresses at crack tips. Consequently, it will be very interesting to readdress the problems considered in the present work, whether the incorporation of a curvature-dependent (second-order) theory of surface elasticity indeed admits finite stresses at the crack tips.

Another interesting extension of the present work is to examine, within the description of a first-order surface elasticity, whether we may choose particular end conditions (other than used in the present work) to achieve boundedness of the most significant stress components. For example, in the Mode-I fracture case, it is clear from Eq. (4.63) that the logarithmic singularity in σ_{yy} can be removed when $2g(t) = \beta(t)$ at each crack tip ($t = \pm a$), with σ_{xx} remaining singular. i.e.

$$(2g(\pm a) - \beta(\pm a)) \ln r = 0, \text{ when } 2g(\pm a) = \beta(\pm a).$$

However, this now involves solving a system of coupled hyper-singular integro-differential equations (instead of Cauchy singular) since the corresponding hyper-singular terms can be reduced to Cauchy singular form only when $(k-1)g(\pm a) + \beta(\pm a) = 0$, one which we give up in order to impose $2g(\pm a) = \beta(\pm a)$ at the crack tips (note that, in this case, only a *single* end condition is allowed within the first-order description). In this respect, it is worth emphasizing that for a Mode-II fracture with $\sigma_o \neq 0$, only *one* end condition is required at each crack tip to remove the *entire* singularity (See. Eq. (7.1)). The determination of the existence of admissible, bounded solutions of the corresponding non-standard hyper-singular integro-differential equations will be the key of this practice.

BIBLIOGRAPHY

[1] Gurtin, M. E.: The linear theory of elasticity, in Handbuch der Physik 6a(2), Springer-Verlag(1972)

[2] Gurtin, M. E.: An introduction to continuum mechanics, Academic press (1981)

[3] Ogden, R. W.:Non-linear elastic deformations, ellis Horwood (1984)

[4] Trudell, C., Noll, W.: The none-linear field theories of mechanics, in Handbuch der Physik 3(3), Springer-Verlag (1965)

[5] Timoshenko, S. P., Goodier, J. N.: Theory of elasticity. McGraw-Hill. London (1982)

[6] Wang, C. T.: Applied elasticity. McGraw Hill Inc. New York (1953)

[7] Chen, Y. X., Dorgan, B. L., Mcllroy, D. N., Aston, D. E.: On the importance of boundary conditions of nanomechanical bending behavior and elastic modulus determination of silver nanowires. J. Appl. Phys. 100, 104301 (2006)

[8] Mai, W. J., Wang, Z. L.; Quantifying the elastic deformation behavior of bridged nanobelt. Appl. Phys. Lett. 89, 073112 (2006)

[9] Tabib-Azar, M., Nassirou, M., Wang, R., Sharma, S., Kamins, T. I.: Mechanical properties of self-welded silicon nanobridges. Appl. Phys. Lett. 87, 113102 (2005)

[10] Chen, C. Q., Shi, Y., Zhang, S., Zhu., J., Yan, Y. J.: Size Dependence of Young's Modulus in ZnO Nanowires. Phys. Rev. Lett. 96, 075505 (2006)

[11] Ni, H., Li, X. D.: Young's modulus of ZnO nanobelts measured using atomic force microscopy and nanoindentation techniques.Nanotechnology, 17, 3591 (2006)

[12] Adam, N.K.: The Physics and Chemistry of Surfaces, 3rd edn. Oxford University Press, London (1941)

[13] Adamson, A.W.: Physical Chemistry of Surfaces. Interscience, New York/London (1967)

[14] Suzuki, T., Endo, H., Shibayama, M.: Analysis of surface structure and hydrogen/deuterium exchange of colloidal silica suspension by contrast-variation small-angle neutron scattering. Langmuir 24, 4537–4543 (2008)

[15] Sugiyama, A., Taguchi, Y., Nagaoka, S., Nakajima, A.: Size-dependent magnetic properties of naked andligand-capped nickel nanoparticles. Chem. Phys. Lett. 485, 129–132 (2010)

[16] Sharma, P., Ganti, S.: Size-dependent Eshelby's tensor for embedded nano-inclusions incorporating surface/interface energies. ASME J. Appl. Mech. 71(5), 663–671 (2004)

[17] Miller, R. E., Shenoy, V. B.: Size-dependent elastic properties of nanosized structural elements. Nano technology. 11, 139-147 (2000)

[18] Zhou, L. G., Huang ,H.: Are surfaces elastically softer or stiffer?. Appl. Phys. Lett. 84, 1940-1941 (2004)

[19] Poncharal, P., Wang, Z., Ugarte, D., Deheer, W.: Electrostatic deflections and electromechanical resonances of carbon nanotubes. Science. 283, 1513-1516 (1999)

[20] Rose, K. C., Wang, J., Hutchinson, J. W., Lieber, C.: Nanoplate mechanics: dramatic decrease in Young's modulus unpublished (2000)

[21] Wong, E., Sheehan, P. E., Lieber C. M.: Nanobeam mechanics: elasticity, strength and toughness of nanorods and nanotubes. Science 277, 1971-1975 (1997)

[22] Jing, G. Y., Duan, H. L., Sun, X. M., Zhang, Z. S., Xu, J., Li, Y. D., Whang, J. X., Yu, D. P.L: Surface effects on elastic properties of silver nanowires: Contact atomic-force microscopy. Phys. Rev. B 73, 235409 (2006)

[23] Cuenot, S., Freigny, C., Demoustier-Champagne, S., Nysten, B.:Surface tension effect on the mechanical properties of nanomaterials measured by atomic force microscopyPhys. Rev. B 69, 165410 (2004)

[24] Gibbs, J.W.: The Scientific Papers of J. Willard Gibbs, vol I. Longmans Green, London. (1906)

[25] Orowan, E.: Surface energy and surface tension in solids and fluids. Proc, Roy. Soc. A. 316, 473-491(1970)

[26] Gurtin, M. E., Murdoch, A. I.: A continuum theory of elastic material surfaces. Arch. Ration. Mech. Anal. 57(4), 291-323 (1975)

[27] Gurtin, M. E., Murdoch, A. I.: Surface stress in solids, Int. J. Solids struct. 14, 431-440 (1978)

[28] Cahn, J.W., Larche' F.: Surface stress and chemical equilibrium of small crystals- II. solid particles embedded in a solid matrix. Acta Metall. 30, 51–56 (1982)

[29] Benveniste, Y., Aboudi, J.: Continuum model for fiber reinforced materials with debonding. Int. J. Solid. struct 20(11-12), 935-951 (1984)

[30] Thomson, R., Chuang, T. J.: The role of surface stress in fracture. Acta Metall. 34(6), 1133-1143 (1986)

[31] Cammarata, R.C.: Surface and interface stress effects in thin films. Progress. Surf. Science. 46, 1–38 (1994)

[32] Steigmann, D. J., Ogden, R.W.: Plane deformations of elastic solids with intrinsic boundary elasticity. Proc. R. Soc. Lond. A. 453, 853–877 (1997)

[33] Steigmann, D. J., Ogden, R.W.: A necessary condition for energy-minimizing plane deformations of elastic solids with intrinsic boundary elasticity. Math. Mech. Solids. 2, 3–16 (1997)

[34] Gurtin, M. E., Weissmuller, J., Larche, F.: A general theory of curved deformable interface in solids at equilibrium. Philos. Mag. A. 78(5), 1093-1109 (1998)

[35] Wang, G.F., Wang, T.J.: Deformation around nanosized elliptical hole with surface effect. Appl. Phys. Lett. 89, 161901 (2006)

[36] Buehler, M. J., Abraham, F.F., Gao, H. J.: Hyperelasticity governs dynamic fracture at a critical length scale, Nature London . 426, 141-146 (2003)

[37] Buehler, M. J., Gao, H. J., Huang, Y. G.: Continuum and atomistic studies of the near-crack field of a rapidly propagating crack in a harmonic lattice, Theor. Appl. Fract. Mech. 41, 21-42.(2004)

[38] Buehler, M. J., Gao, H. J.: Dynamical fracture instabilities due to local hyperelasticity at crack Tips, Nature London . 439, 307-310 (2006)

[39] Abraham, F.F., Broughton, J. Q., Bernstein, N., Kaxiras, E.: Spanning the continuum to quantum length scales in a dynamic simulation of brittle fracture, Europhys. Lett. 44, 783-787.(1998)

[40] Shenoy, V.B.: Size-dependent rigidities of nanosized torsional elements, Int. J. Solids Struct. 39, 4039-4052 (2002)

[41] Chuang, T. J.: Effects of surface tension on the toughness class. J. American. Ceram. Soc. 70(3), 160-164 (1987)

[42] Wu, C. H.: The effect of surface stress on the configurational equilibrium of voids and cracks. J. Mech. Physics. Solids. 47, 2469-2492 (1999)

[43] Wu, C. H., Wang, M. L.: The effect of crack-tip point loads on fracture. J. Mech. Physics. Solids. 48, 2283–2296 (2000)

[44] Tian, L., Rajapakse, R. K. N. D.: Analytical solution of size-dependent elastic field of a nano-scale circular inhomogeneity. ASME J. Appl. Mech. 74(3) 568-574 (2007)

[45] Tian, L., Rajapakse, R. K. N. D.: Elastic field of an isotropic matrix with a nanoscale elliptical inhomogeneity. Int. J. Solids. Struct. 44, 7988–8005 (2007)

[46] Zhi, Y., Liying, J.: Surface effects on the electromechanicalcoupling and bending behaviours of piezoelectric nanowires. J. Phys. D: Appl. Phys. 44, 075404 (6pp) (2011)

[47] Ru, C-Q.: Simple geometrical explanation of Gurtin-Murdoch model of surface elasticity with clarification of its related versions. Sci. China. 53(3), 536-544 (2010)

[48] Duan, H. L., Wang, J., Huang, Z. P., Karhaloo, B. L.: Size-dependent effective elastic constants of solids containing nano-inhomogeneities with interface stress, J. Mech. Phys. Solids, 53(7), 1574-1596 (2005)

[49] Ogden, R.W., Steigmann, D. J., Haughton, D.M.: Effect of elastic surface coating on the finite deformation and bifurcation of a pressurized circular annulus. J. Elasticity. 47(2),121-145 (1997)

[50] Schiavone, P., Ru, C-Q.: Integral equation methods in plane strain elasticity with boundary reinforcement. Proc, Royal Soc. London A. 454, 2223 (1998)

[51] Chhapadia, P., Mohammadi, P., Sharma, P.: Curvature-dependent surface energy and implications for nanostructures. J. Mech. Phys. Solids, 59, 2103-2115 (2011)

[52] Sendova, T., Walton, J. R.: The effect of surface tension in modeling interfacial fracture. AIP Conf. Proc. 1301, 291-300 (2010)

[53] Brennan, J. J.: Interfacial Chemistry and Bonding in Fiber Reinforced Glass and Class-Ceramic Matrix Composites, Ceramic Microstructures and Role of Interface. J. A. Pask and A. G. Evans Eds. Plenum Press, New York (1988)

[54] Kim, J. O., Bau, H. H.: A Study of the Fiber-Matrix Interface in Composite Materials. ASME. J. Appl. Mech. 59, S163-S165 (1992)

[55] Achenbach, J. D., Zhu, H.: Effect of Interphases on Micro and Macro mechanical Behavior of Hexagonal-Array Fiber Composites. ASME J. Appl. Mech. 57, 956-963 (1990)

[56] Ghahremani, F.: Effect of Grain Boundary Sliding on Anelasticity of Polycrystals. Int. J. Solids. Sturct. 16,825-845 (1980)

[57] Hashin, Z.: The Spherical Inclusion with Imperfect Interface. ASEM. J. Appl. Mech. 58, 444-449 (1991)

[58] Knowles, J. K., Sternberg, E.: On the singularity induced by certain mixed boundary value problems in linearized and nonlinear elastostatics. Int. J. Solid. Struct. 11, 1173-1201(1975)

[59] Ru, C. Q.: On Complex-Variable Formulation for Finite Plane Elastostatics of Harmonic Materials. Acta Mech. 156, 219-234 (2002)

[60] Bigoni, D., Serkove S. K., Valentini, M., Movechan, A. B.: Asymptotic Model of Dilute Composite with Imperfectly Bonded Inclusions. Int. J. Solids. Struct. **35**, 3239-3258 (1998)

[61] Lipton, R., Vernescu B.: Variational Methods, Size Effects and External Microstructures for Elastic Composite with Imperfect Interface. Math. Models. Method. Appl. Sci. 5, 1139-1173 (1995)

[62] Steif, P. S., Hoysan, S. F.: An Energy Method for Calculating the Stiffness of Aligned Short-Fiber Composites. Mech. Mat. **6,** 197-210 (1987)

[63] Weissmuller, J., Cahn,J.W.: Mean stresses in microstructure due to interface stresses: a generalization of a capillary equation for solids. Acta Materialia. 45, 1899-1906 (1997)

[64] Rottman, C.: Landau theory of coherent interphase interface. Physical Review B. 38, 12031-12034 (1988)

[65] Muskhelishvili, N. I.: Some basic problems of the mathematical theory of elasticity. P. Noordhof, Groningen, The Netherlands (1953)

[66] England, A. H.: Complex Variable Methods in Elasticity. John Wiley & Sons Ltd. London (1971)

[67] Sih, G. C.: Boundary Problems for Longitudinal Shear Cracks. Dev. Theor. Appl. Mech., 2, pp. 117–130 (1965)

[68] Chiang, C. R.: Slightly curved cracks in antiplane strain. Int. J. Fract. 32, R63-66 (1987)

[69] Sih, G. C.: Stress distribution internal crack tips for longitudinal shear problems. J. Appl. Mech. 32(1), 51-58 (1965)

[70] Rice, J. R., Sih, G. C.: Plane problems of cracks in dissimilar media. J. Appl. Mech. 32, 418-423 (1965)

[71] Hoagland, R. G., Daw, M. S., and Hirth, J. P.: Some Aspects of Forces and Fields in Atomic Models of Crack Tips. J. Mater. Res., 6, pp. 2565–2571 (1991)

[72] Wu, C.H., Wang, M.L.: Configurational equilibrium of circular-arc cracks with surface stress. Int. J. Solids Struct. 38, 4279–4292 (2001)

[73] Gill, S.P.A.: The effect of surface-stress on the concentration of stress at nanoscale surface flaws. Int. J. Solids Struct. 44, 7500–7509 (2007)

[74] Wang, G.-F., Feng, X.-Q., Wang, T.-J., Gao, W.: Surface Effects on the Near-Tip Stresses for Mode-I and Mode-III Cracks. ASME J. Appl. Mech., 75, 1–5 (2008)

[75] Brown, J. W., Churchill, R. V.: Complex variables and applications. McGraw Hill Inc. New York (1976)

[76] Ervin, V.J., Stephan, E.P.: Collocation with Chebyshev polynomials for a hypersingular integral equationon an interval. J. Comput. Appl. Math. 43, 221–229 (1992)

[77] Chakrabarti, A., Hamsapriye: Numerical solution of a singular integro-differential equation. Z. Agnew. Math. Mech. 79(4), 233–241 (1999)

[78] Horgan, C. O.: Anti-plane shear deformations in linear and nonlinear solid mechanics. SIAM Review, 37 (1), 53-81 (1995)

[79] Kim, C. I., Schiavone, P. and Ru, C-Q.: The effects of surface elasticity on an elastic solid with mode-III crack: complete solution. ASME J. Appl. Mech. 77, 021011-1-021011-7 (2010)

[80] Kim, C. I., Schiavone, P. and Ru, C-Q.: Analysis of a mode-III crack in the presence of surface elasticity and a prescribed non-uniform surface traction. Z. angew. Math. Phys. 61(3), 555–564 (2010)

[81] Lengyel, T.: Analysis of Displacement in an Elastic Solid with a Mode-III Crack in the Presence of Surface Elasticity. M.Sc. Thesis. University of Alberta (2011)

[82] Ioakimidis, N.I.: A natural interpolation formula for Prandtl's singular integrodifferential equation. Int. J. Num. Meth. Fluids, 4, 283 - 290 (1984)

[83] Frankel, J. I.: A Galerkin solution to a regularized Cauchy singular integro-differential equation. Quart. Appl. Math. LIII (2), 245 - 258 (1995)

[84] Kim, C. I., Schiavone, P. and Ru, C-Q.: A clarification of the role of crack-tip conditions in linear elasticity with surface effects. Math. Mech. Solids. (Accepted for publication Dec. 14. 2011)

[85] Lu, N. C., Cheng J., Cheng, Y. H.: A dynamic model of bridging fiber pull-out of composite materials. Mehc. Research Communications. 32, 1-14 (2005)

[86] Lu, N. C., Cheng J., Cheng, Y. H.: An asymmetrical self-similar dynamic crack model of bridging fiber pull-out in unidirectional composite materials. Int. J. Communicational Methods in Eng. Sci. Mech. 9, 171-179 (2008)

[87] Gorbatickh, L., Nuller, B., Kachanov M.: Sliding on cracks with non-uniform frictional characteristics. Int. J. Solids & struct. 38, 7501-7524 (2001)

[88] Gorbatickh, L., Nuller, B., Kachanov M.: Non-uniform frictional sliding under cyclic loading with frictional characteristics changing in the process of sliding. Int. J. Solids & struct. 39, 89-104 (2002)

[89] Gorbatickh, L.: Mathematical and computational aspects of nonuniform frictional slip modeling. J. Computational & Appl. Mech. 168, 215-224 (2004)

[90] Kim, C. I., Schiavone, P., Ru, C-Q.: Analysis of Plane-Strain Crack Problems (Mode I and Mode II) in the Presence of Surface Elasticity. J. Elasticity. 104(1), 397–420 (2011)

[91] Kaya, A.C., Erdogan, F.: On the solution of integral equations with a generalized Cauchy kernel. Quart. Appl. Math. XLV(3), 455 - 469 (1987)

[92] Gakhov, F.D.: Boundary value problems. Pergamon Press. Oxford (1963)

[93] Chakrabarti, A., George, A.J.: Solution of a singular integral equation involving two intervals arising in the theory of water waves. Appl. Math. Lett. 7(5), 43-47 (1994)

[94] Kim, C. I., Schiavone, P. and Ru, C-Q.: The effect of surface elasticity on a mode-III Interface Crack. Arch. Mech. 63(3), 267–286 (2011)

[95] Kim, C. I., Schiavone, P. and Ru, C-Q.: Effect of surface elasticity on an interface crack in plane deformations. Proc. Roy. Soc. London A. 467, 3530–3549 (2011)

[96] Ilyin, V. A. Numerical Methods of Electro-physics. Nauka, Moscow (1985)

[97] Atkinson, C.: On stress singularities and interfaces in linear elastic fracture mechanics. Int. J. Fracture. 13, 807-820 (1977)

[98] Comninou, M.: The interface crack. J. Appl. Mech. 44, 631-636 (1977)

[99] Knowles, J. K, Sternberg, E.: Large deformations near a tip of an interface crack between two neo-Hookean sheets. J. Elasticity 13, 257-293 (1983)